Charles University

Faculty of Science

Study programme: Biology

Branch of study: Genetics, Molecular Biology and Virology

Bc. Daniel Žucha

Practical aspects of single-cell RT-qPCR experiments

Praktické aspekty analýzy jednotlivých buněk pomocí RT-qPCR

Diploma thesis

Supervisor: Ing. Lukáš Valihrach, Ph.D.

Prague, 2020

Prehlásenie

Prehlasujem, že som záverečnú prácu spracoval samostatne a že som uviedol všetky použité informačné zdroje a literatúru. Táto práca ani jej podstatná časť nebola predložená k získaniu iného alebo rovnakého akademického titulu.

V Prahe, 25.5.2020

Acknowledgement

I would like to express my sincerest gratitude to Ing. Lukáš Valihrach Ph.D., who has been a continuous support both in terms of science and companionship. I value him for his open-mindedness, patience, curious scientific mind and honesty, what gave me enough room to explore my capabilities. I am also very thankful to Ing. Peter Androvič, in whom I see great scientist and friend in one person. Lastly, I would like to thank my beloved relatives, my dear girlfriend and the closest friends for their continuous support and enthusiasm that kept pushing me onwards.

This research was funded by grants P303-19-02046S, CZ.1.05/1.1.00/02.0109 and RVO 86652036, which were obtained by the Institute of Biotechnology CAS and the Institute of Experimental Medicine CAS.

Abstract

Recent breakthroughs in the RNA quantification of single cells are rapidly transforming the view on biology and medicine. Flexibility and sensitivity of reverse transcription quantitative PCR (RT-qPCR) make it an ideal method for quantification of single-cell material, but its limits had not been yet fully explored.

In this thesis, various factors influencing RT-qPCR performance in single-cell application have been assessed, including conditions of sample collection and processing, importance of quality control, performance of reverse transcription, preamplification and role of qPCR assays. We showed that prolonged time for single cell collection as well as repeated freeze-thaw cycles had negligible effect on RT-qPCR data quality. Direct lysis routinely applied for RNA extraction from single cells may be scaled up to 256 cells. The comprehensive comparison of 11 reverse transcriptases in low RNA input conditions identified 2 best-performing enzymes. Decrease in preamplification volume as well as poor primer design resulted in the loss of sensitivity. Finally, the established workflow has been applied to profile gene expression of astrocytes in mouse model of amyotrophic lateral sclerosis (ALS) identifying important components of ALS-induced changes to astrocyte transcriptome.

Altogether, the thesis represents a complete set of recommendations for performing single-cell RT-qPCR experiments based on the provided literature, experimental results and practical notes. It can serve as a guide to secure high experimental performance, analysis power and savings on experimental costs.

Keywords: single cell, reverse transcription, preamplification, quantitative PCR, amyotrophic lateral sclerosis, astrocytes

Abstrakt

Prelomové objavy spojené s kvantifikáciou RNA z jednotlivých buniek menia aktuálny pohľad na biológiu a medicínu. Vhodnou metódou pre ich analýzu je modifikovateľná a vysoko senzitívna metóda reverznej transkripcie a kvantitatívnej PCR (RT-qPCR), ktorej limitácie však neboli doposiaľ plne preskúmané v kontexte tak nízkych množstiev vstupného materiálu.

Táto práca sa zameriava na objasnenie vplyvu rôznorodých faktorov, ktoré by mohli ovplyvniť správnosť fungovania RT-qPCR, zahrňujúc podmienky pre zber vzoriek a ich spracovanie, kontroly kvality, výkonnosť reverznej transkripcie, preamplifikácie a rolu qPCR esejí. Naše výsledky ukazujú, že predĺžené časy pri zbere buniek ako aj opakované zmrazovanie a rozmrazovanie vzoriek malo zanedbateľný dopad na kvalitu RT-qPCR dát. Priama lýza buniek, bežne využívaná pri extrakcii RNA z jednotlivých buniek, je taktiež vhodná pre vzorky obsahujúce až 256 buniek. Porovnanie 11 revererzných transkriptáz s minimálnym množstvom vstupného materiálu identifikovalo 2 enzýmy s nadštandardným výkonom. Zníženie reakčného objemu preamplifikácie či neoptimálny dizajn primerov viedol k zníženiu senzitivity reakcie. Na záver bola optimalizovaná RT-qPCR použitá k profilovaniu génovej expresie astrocytov v myšom modeli amyotrofickej laterálnej sklerózy (ALS), ktorou sme identifikovali ALS-indukované zmeny v astrocytárnom transkriptóme.

Táto práca ponúka obsiahly zoznam doporučení pre analýzu jednotlivých buniek metódou RT-qPCR, ktoré sú založené na literatúre, experimentálnych výsledkoch a praktických poznatkoch. Práca môže slúžiť ako návod na zaistenie vysokej účinnosti experimentov, zvýšenej sily analýzy či zníženie experimentálnych nákladov.

Kľúčové slová: jednotlivé bunky, reverzná transkripcia, preamplifikácia, kvantitatívna PCR, amyotrofická laterálna skleróza, astrocyty

Abbreviations

ALS - amyotrophic lateral sclerosis, AMV - Avian Myeloblastosis Virus, BSA - bovine serum albumin, cDNA - complementary DNA, CNS - central nervous system, Cq - cycle of quantification, CV - coefficient of variation, ΔCq - Cq difference, ERCC - External RNA Controls Consortium, GFAP - glial fibrillary acidic protein, FACS - fluorescence-activated cell sorting, GSP - gene specific primers, IPC - interplate calibrator, LCM - laser capture microdissection, LoD - Limit of Detection, LoQ - Limit of Quantification, MIQE - Minimum Information for publication of Quantitative real-time PCR experiments, MMLV - Moloney Murine Leukemia Virus, NFW - nuclease free water, NGS - Next Generation Sequencing, PC - principal component, PCA - principal component analysis, PCR - polymerase chain reaction, preAMP – preamplification, qPCR - real-time quantitative PCR, RDA - redundancy analysis, RNAse – ribonuclease, RNA-Seq - RNA-Sequencing, RQ - relative quantities, RT - reverse transcription, RTase - reverse transcriptase, RT-qPCR - reverse transcription qPCR, R^2 - coefficient of determination, scRNA-Seq - single-cell RNA-Seq, scRT-qPCR - single-cell RT-qPCR, Tukey HSD - Tukey post-hoc multiple comparison test, UMI - unique molecular identifiers

Table of Contents

1 Introduction

Eukaryotic organisms are complex machineries balancing the constant intake of information delivered by stimuli of both external and internal origin. The stimuli are received, processed and responded to via intricate network of organs and tissues that are adapted to decompose the signal into a fine-tuned web of cellular response elements. Deeper knowledge of these systems does not only extend the understanding of the surroundings, but it is also essential for progress of high-end medical treatments.

Analyte sampling from whole tissues of interest provides insights into the major changes that occur within the region of interest. These samples are generally easy to obtain, store, process and their analysis is financially viable. However, such samples do not contain the information on the cell-type composition, possibly missing out on the fine characteristics that are unique to different cell types.

Increase in the analysis resolution can be achieved by the single-cell profiling. When compared to tissue samples, distinctive cell-type patterns are evident, providing valuable knowledge of the exact cellular state. Main concerns associated with the single-cell analysis are collection of the individual cells; minute amounts of the processed analyte ready for quantification; substantial data noise arising from the variability of the individual cells and experimental costs.

Responses to the environmental stimuli are lucidly inscribed in the cell's genome, transcriptome and/or proteome. However, the explicit informativeness is corrupted by the variability inherent to the single-cell data, primarily arising from the limiting analyte quantity or stochastic nature of biological systems at lower scales (e.g. transcription bursts). These factors emphasize the utility of highly precise methods, such as quantitative real-time PCR (qPCR).

Quantification of different nucleic acids (or protein) with qPCR requires an *a priori* step of generating DNA molecule. Reverse transcription (RT) generates complementary DNA (cDNA) to the RNA molecule by utilizing reverse transcriptase (RTase) enzyme. Selection for RNA of interest is delivered by the complexity of RT priming. RT has been previously noted for its variability, contributing with undesired uncertainty, what is especially unwanted for the already

variable single-cell biology. qPCR is well-positioned candidate for single-cell analysis, as its extensive optimizations have made it highly sensitive and reproducible tool of quantification. The throughput of single-cell experiments can be increased by the platform substitution to the Next Generation Sequencing (NGS). NGS offers quantification of cell's whole transcriptome, although then the experiments become more expensive and laborious, in both the laboratory and data analysis sections. In many instances, NGS protocols make use of RT and PCR amplification, making the reverse-transcription quantitative PCR (RT-qPCR) workflow improvements often interchangeably applicable.

Scope of this diploma thesis is to highlight caveats of single-cell workflow analysis, concerning the sample handling, RT, preamplification, qPCR and data analysis. Subsequently, reader should be capable of conducting his own single-cell experiment based on the informed decisions, knowledgeable of potential hindrances in light of the presented literature and conducted measurements.

2 Literature overview

It has been well over 35 years now that polymerase chain reaction (PCR), developed by Kary Mullis, has seen light of the world (Mullis *et al.*, 1986). It has not been long after that the sensitivity of this method was showcased on single cells (Li *et al.*, 1988), prophesying its utility for decades to come. However, the single-cell variability was not noted until qPCR was introduced (Higuchi *et al.*, 1993), enabling the exploration of differential gene expression. qPCR's fine-tuning increased method's precision and throughput (Nolan, Hands and Bustin, 2006; Tichopad *et al.*, 2009; Ståhlberg and Kubista, 2014; Svec *et al.*, 2015; Millington *et al.*, 2019), making it a superior analytical tool of nucleic acid quantification. In continuation, development of multimodal approaches, where quantification of RNA, DNA and protein from a single cell is coupled, empowers the analysis (Ståhlberg *et al.*, 2012; Darmanis *et al.*, 2016).

Major step in the throughput is delivered by evermore popular whole transcriptome sequencing (Saliba *et al.*, 2014; Kolodziejczyk *et al.*, 2015; Svensson *et al.*, 2017; Ziegenhain *et al.*, 2017). Despite the undisputable advantages of sequencing, RT-qPCR still provides unprecedented precision, simplicity of work and lower costs. Broadly saying, RT-qPCR is finely suited for exploration of several selected genes, whereas RNA-Sequencing (RNA-Seq) provides much needed broader view on the cell's transcriptomic landscape and is better suited for discrimination of novel cell types (Kelley *et al.*, 2018; Chen, Lake and Zhang, 2019; Batiuk *et al.*, 2020). The methodological and practical aspects inherent to these two methods allow for direct comparison and interchangeability of suggested improvements (Kroneis *et al.*, 2017), which are also to be seen within this diploma thesis.

Understanding of individual cellular functionality rapidly gained popularity in the investigation of complex tissues, such as cells of nervous system or cancer diseases (Chung *et al.*, 2017; Kelley *et al.*, 2018; Batiuk *et al.*, 2020), or single cells that exist individually and express unique molecular patterns (circulating tumor cells, peripheral blood mononuclear cells) (Zhu *et al.*, 2017; Newman *et al.*, 2019). Single-cell profiling is associated with inherent variation. Major defined contributors are: i) Cell type, ii) Microenvironment, iii) Cell state dependence and iv) Temporal variations in cell's transcriptome dynamics (Kubista, Dreyer-Lamm and Ståhlberg, 2018). The uncertainty that surrounds single-cell experiments can be minimized with sufficient

documentation. A set of guidelines - Minimum Information for publication of Quantitative real-time PCR experiments (MIQE) – was produced to ensure that the proposed observations are a true result of the biological questioning (Bustin *et al.*, 2009, Stahlberg & Kubista, 2017). MIQE encourage good experimental practice and provide common solid ground. Detailed workflow enlistment is essential for disclosure of technical drawbacks, particularly for single-cell sample preparation, collection and then RT, as these steps were previously indicated as main contributors of technical variability (Bengtsson *et al.*, 2008; Tichopad *et al.*, 2009; Bustin *et al.*, 2015; Hodne and Weltzien, 2015; Ståhlberg and Kubista, 2018).

2.1 Sample preparation and cell collection

Sample preparation and cell collection are possibly the most challenging steps of the single-cell RT-qPCR (scRT-qPCR) workflow. The unique complexity of different tissues has led to development of organism and tissue-specific dissociation protocols (*Worthington tissue dissociation guide*). At this time, the full extent of changes in the gene expression profiles that are attributable to the dissociation remain unknown. Some functional genes were identified to be readily influenced by dissociation, such as immediate early response (*Fos*, *Jun*) or heat-shock protein genes (Van Den Brink *et al.*, 2017). Although the protocol of Zeng *et al.* (2014) declares to have minimal impact, its generalized applicability and claims has not been fully explored yet. The extent of available protocols combined with unknown aftereffects plays an important role in cross-validation of the results, emphasizing the importance of rigorous documentation requested by the MIQE guidelines.

There are varying approaches on how to collect cells, favorizing different aspects of cell-type-specific accessibility depending on their abundancy, morphology or spatial position within the tissue. Well-established methods are fluorescent-activated cell sorting (FACS), micromanipulation and laser capture microdissection (LCM). Considering that cell-collection runs in sub-optimal conditions, collection speed can be looked upon as the major factor inducing the change of gene expression profiles. Therefore, the eminent efficiency of FACS (thousands of cells in a short time) coupled with collection of live cells could be viewed on as the most optimal option (Ståhlberg and Kubista, 2014). FACS is also suited for finding rare cell types for the cases when larger amounts of the starting material are available. What gives FACS on its effectiveness,

also takes away on the quality control as it does not allow direct visual inspection of cell morphology (Ståhlberg and Kubista, 2014). Oppositely, micromanipulation allows to inspect quality of the aspirated cells for the cost of increased processing time. Its gentle handling also leads to collection of less stressed and live cells. Amount of the input material (number of cells) can be also kept at minimum. Low inputs equally stand true for LCM, with cells being collected predominantly fixated (Walch *et al.*, 2001), but collection of live cells is also possible (Podgorny, 2013). However, fixation has detrimental effects on the intactness of RNA, already introducing severe bias at early steps (Aggerholm-Pedersen *et al.*, 2014; Ståhlberg and Kubista, 2018). On the strong side, LCM retains valuable information on the cell's spatial position within the tissue, communicating biologically relevant clues which would be otherwise lost upon dissociation. Similarly, tissues difficult to dissociate can be readily processed by LCM.

Novel single-cell collection procedures commonly rely on the extension of the workflow – combining the cell collection with downstream steps (RT-qPCR or RNA-Seq). For high-throughput methods, this also often comes with end-to-end solution, including bioinformatics and data visualization (Chromium Software Suite by 10x Genomics, SeqGeq Analysis Software by Illumina). In comparison, low-throughput methods focus on the selection of high-quality relevant cells, minimizing the experimental costs and allow for customization to desired downstream analysis. The current leader in single-cell collection coupled with direct analysis is Chromium System (10x Genomics) with its scalable platform, able to profile millions of cells (Zheng *et al.*, 2017). Using fine-tuned microfluidics, a cell from the suspension is encapsulated within a droplet with a gel bead containing barcoded oligonucleotides and RT reagents. First, cDNA is synthetized inside the droplet, then the droplets are pooled, dissolved and cDNA libraries containing unique molecular identifiers (UMI) (barcodes monitoring for the PCR amplification bias) are readied. Superior advantage of this instrumentation is the capability to analyze various modalities/analytes (genome, transcriptome, chromatin accessibility, immune profiling) with a single instrument. For continuation, extensive overview of available single-cell collection and analysis methods is summarized in Valihrach *et al.* (2018).

On the practical side of cell collection, the cell of the interest is not always successfully transferred into the collection vessel. Simply, cells happen to be misclassified, what is

accountable to the sophistication of the selection procedure. Another frequently arising problem is that the cell may be sorted onto the side of the well, not ending up in the lysis buffer and drying out, eventually leading to degradation of the analyte. To prevent processing of the unwanted material, low-throughput qPCR measurement of biologically relevant marker genes is routinely performed on the preamplified cDNA material, preceding the high-throughput qPCR measurements. This quality control step assesses analyte's quality and determines the biological categorization. The performance of this step is presented in the *5.3 Quality control of the collected single cells* section.

Collectively, single-cell collection underscores the importance of quick, effective, high-throughput and gentle single-cell collection approaches in the aim of preservation native gene expression profiles (Valihrach *et al.*, 2018). Latest steps forward ensure not only improved technical parameters, but also simplify the workflow and data analysis, making the single-cell approach accessible to wider range of researchers and clinicians, granting them powerful tool to uncover yet undiscovered truths.

2.2 RNA extraction

The extraction of nucleic acids when the whole tissues are analyzed requires use of strong chaotropic agents (e.g. guanidine thiocynate) that help to release and protect the extracted analyte. The extraction process also involves later purification and washing steps, as these agents would interfere with the chemistry of downstream applications. Washing steps are however known to lead to analyte losses, what is not feasible for a single-cell material counting the total transcript counts in tens or hundreds of thousands copies, with the vast majority of genes actually represented just by few single transcripts (Ståhlberg, Rusnakova and Kubista, 2013; Svec *et al.*, 2013; Marinov *et al.*, 2014).

Considering these factors, analyte extraction for single-cell material can utilize a different condition – hypotonic environment of the lysis buffer. The cell lysis then occurs through osmosis. Upon cell's membrane rupture, the contents are immediately diluted, slowing down RNA degradation by the intracellular ribonucleases. To maximize the prevention of RNA degradation, the added reagent should fulfill roles of: i) making the mRNA accessible for RT and

ii) maintain mRNA integrity. Among the myriad of tested direct lysis conditions, Svec *et al.* (2013) had identified solution of 1 mg/ml bovine serum albumin (BSA) as an optional lysis buffer. BSA has shown to deliver high yields and retain RNA stable even throughout repeated freeze-thaw cycles or during short-term storage at room temperature. These enhancing properties are thought to stem from its carrier effect (adsorption to the surfaces of reaction chamber, preventing the nucleic acid from binding) or through its stabilizing effect, similar to its role in the blood pH maintenance (Svec *et al.*, 2013).

RNA is released simultaneously with the genomic DNA, which being present in two copies may contribute to some confounding false positive results. Nonetheless, DNase treatment is not commonly applied to single cells. Treating the samples with DNase would compromise factors of greater importance – reaction volumes are needed to be kept low, RNA concentrations high and avoid washing steps that lead to analyte losses (Dzamba *et al.*, 2016). The problem of genomic DNA background can be surpassed by careful design of PCR assay primer pairs, extending past the exon-exon junction (see *2.5 QPCR* section) (Ståhlberg and Bengtsson, 2010; Dzamba *et al.*, 2016).

2.3 Reverse transcription

RT is the first critical enzymatic reaction in the single-cell workflow, as any RNA molecule that fails to be converted into cDNA is inevitably excluded and will not be reported downstream. Such risk greatly increases when dealing with minute amounts of the input material, following properties of the Poisson distribution (Ståhlberg and Kubista, 2014; Andersson *et al.*, 2015). Because of this, any improvement on the sensitivity, efficiency or reproducibility ensures more reliable presentation of the cellular transcriptome. Major caveat is that RT is known to vary substantially in the aforementioned parameters. Main contributing factors are: i) Priming strategy, ii) RTase, iii) Additives/inhibitors and iv) Reaction temperature profile (Ståhlberg and Kubista, 2018). Uncertainty provided by the RT step calls for its detailed investigation to clarify its weak points.

2.3.1 Primers

Primers, short stretches of nucleotides, are essential to cDNA synthesis; RTase requires the unique conformation of double-stranded DNA/RNA hybrid helix in order to synthetize the complementary DNA sequence. In routine RT-qPCR applications, three primer types can be used: i) random primers (random hexamers), ii) oligo(dT)s or iii) gene specific primers (GSP). None of the priming strategies can be generalized for all applications, as they differ in the range of targeted molecules, the efficiency of priming or the length of the synthetized product. Random hexamers prime any matching sequence – mRNA, rRNA, non-coding RNA or genomic DNA. Given the nature of probability, longer RNAs are targeted more often - proportionally to their length. This potentially leads to distorted representation of the cell's transcriptome in the cDNA counts. The unevenness is rooted in the use of RTases lacking RNase H activity, what increases their efficiency but at the same time it allows a single RNA molecule to be repeatedly reverse transcribed (Schwaber, Andersen and Nielsen, 2019). Oligo(dT)'s major advantage is selection for polyadenylated transcripts, an aspect greatly leveraged in the production of sequencing libraries or scenarios when depletion for abundant rRNA is not feasible due to low material content (single cells). This selection property makes oligo(dT)s the most frequently used priming strategy for RNA-Seq application. For scRT-qPCR purposes, random hexamers and oligo(dT)s can be used collectively to supplement mutual downsides (Ståhlberg and Bengtsson, 2010). Use of gene-specific primers is usually evaded in single-cell analysis, as the optimization of RT with multiple primers at limiting concentrations would pose doubts on the reaction sensitivity and the efficiency of cost- and time-optimization.

Primer concentration is equally important parameter in the discussion of priming strategy performance. Increase in the primer concentration was shown to even double the yield (Schwaber et al., 2019), but this effect plateaus at certain level, differently for individual priming strategies (Miranda & Steward, 2017). Despite the unquestionable advantage of increased efficiency, higher primer concentration comes in hand with production of unspecific products or overrepresentation of longer transcripts (see above – random hexamers), leading to complications in the analysis or increased experimental costs (RNA-Seq). Because of these reasons, Bagnoli et al. (2018) investigated optimization by a decrease in the primer

concentration in single-cell RNA-Seq (scRNA-Seq). As he reports, primer concentration decrease by 80 % from the concentration recommended by the RTase manufacturer did not affect the experiment's quality and reduced the costs.

2.3.2 Reverse transcriptase

An essential component of the reaction is the enzyme carrying out the synthesis of DNA strand complementary to the RNA transcript. RTase is known to be the leading contributor to the reaction outcome (Ståhlberg, 2004; Levesque-Sergerie *et al.*, 2007; Okello *et al.*, 2010; Sieber *et al.*, 2010; Lindén, Ranta and Pohjanvirta, 2012). The most sought after RTase performance parameters are sensitivity, efficiency, accuracy and reproducibility. The sensitivity encompasses reliable capture of rare transcripts; the efficiency describes the reaction yield; the accuracy ensures consistent efficiency for varying concentrations of the input material and the reproducibility interprets the variability of its performance. Quality of these metrics is a decisive parameter in the realm of single-cell analysis, being that for particular genes the count of individual RNA molecules is on median between ~3 and ~100 copies per cell (~100 copies for protein-coding, ~10 for splicing regulators and only ~3 for transcription factors) (Marinov *et al.*, 2014), unsuccessful capture of every RNA transcript substantially distorts the exploration of the true cellular state (Bengtsson *et al.*, 2008).

For *in vitro* applications, the most commonly used RTases are derivatives of Avian Myeloblastosis Virus (AMV) or Moloney Murine Leukemia Virus (MMLV) ancestor. However, AMV-derived RTases were repeatedly outclassed by its MMLV-derived counterparts (Ståhlberg *et al.*, 2004; Okello *et al.*, 2010; Sieber *et al.*, 2010; Lindén, Ranta and Pohjanvirta, 2012). Proposed explanation assumes that monomeric structure of MMLV is more suitable for introduction of amino acid point-mutations, such as loss of RNase H function, enhanced processivity, fidelity, terminal transferase activity or resistance to inhibitors (Baranauskas *et al.*, 2012; Konishi, Yasukawa and Inouye, 2012).

Nonetheless, the quality of particular RTase is determined by the measurable metrics of its performance. The most commonly discussed metric is reaction yield, describing the conversion rate of RNA to cDNA. Literature have predominantly covered the results for bulk or

tissue samples (Ståhlberg, 2004; Levesque-Sergerie *et al.*, 2007; Schwaber, Andersen and Nielsen, 2019), whereas the metrics for single cells are left almost undiscussed (Schwaber, Andersen and Nielsen, 2019). RT yield is often regarded as gene-dependent (Bustin and Nolan, 2004; Ståhlberg, 2004; Ståhlberg *et al.*, 2004; Lindén, Ranta and Pohjanvirta, 2012; Schwaber, Andersen and Nielsen, 2019) and does not necessarily decrease for less abundant transcripts. Besides the biological phenomenon of gene-dependent yields, positioning and optimization of qPCR reporter assays may also play an important role (Sieber *et al.*, 2010; Bustin *et al.*, 2015). For RT-qPCR, assays ought to be designed to target exons closer to the 3'end, making the transcript detectable even if RTase fails to reverse transcribe the whole transcript (Nolan, Hands and Bustin, 2006). Reported absolute RT yields vary substantially: 39-65 % (Miranda and Steward, 2017), 0-102 % (Levesque-Sergerie *et al.*, 2007), 2-83 % (Ståhlberg, 2004). The lower end is often occupied by the previously mentioned AMV and its derivatives or early generations of MMLV-derivatives, such as SuperScript II (Thermo Fisher Scientific). Studies investigating the state of RT then placed its successor, SuperScript III, as one of the top performers with yields closing on 100 % mark (Ståhlberg, 2004; Okello *et al.*, 2010; Schwaber, Andersen and Nielsen, 2019). The latest generation from Thermo Fisher Scientific RTases (SuperScript IV, Maxima H-) has pushed the limits further and found applicability in a multitude of scRNA-Seq protocols (Macosko *et al.*, 2015; Gierahn *et al.*, 2017; Bagnoli *et al.*, 2018; Zhu *et al.*, 2019).

Two equally important contributors affect the reproducibility of single-cell RT – sampling ambiguity and the reagents (Ståhlberg and Kubista, 2014). Sampling ambiguity touches on the randomness of reporting targets counting low copy numbers. This variability, inherent to the biological systems, is discussed in more detail in the *2.5 QPCR* section. Concerning the reagents, quantification of transcripts counted in hundreds were regarded reproducible (coefficient of variation (CV) < 15 %) (Schwaber, Andersen and Nielsen, 2019). However, when only tens of transcripts are to be targeted, reproducibility substantially decreases (CV > 40+ %) but the choice of high-end RTase helps to partially mitigate this effect (Lindén, Ranta and Pohjanvirta, 2012). Lack of reproducibility is therefore inherent to single-cell measurements and cannot be completely eliminated.

2.3.3 *Additives*

Some reagents were previously shown to have positive impact on the reaction performance, however, the advancements in the reaction chemistry (RTase, buffers) do not guarantee functional transfer of knowledge from past onto the latest protocols. As an example, earlier suggested RNA-based carrier molecules, tRNA (Ståhlberg *et al.*, 2004) or total extracted RNA (Levesque-Sergerie *et al.*, 2007; Miranda and Steward, 2017), were later regarded as not universally functional (Schwaber, Andersen and Nielsen, 2019). Similarly when we look into scRNA-Seq protocols, previously highlighted $MgCl_2$, betaine or trehalose (Picelli *et al.*, 2014) were regarded as inefficient in the later protocol of SCRB-Seq, despite the library construction is methodically similar, only the RTase and buffer mix changed (Bagnoli *et al.*, 2018). On the other hand, Bagnoli *et al.* (2018) showed that polyethylene glycol (PEG 8000) can increase the cDNA yield in RNA-concentration-dependent manner, making him a functional alternative for some scRNA-Seq protocols (Aicher *et al.*, 2019). The functional mechanism of PEG 8000 is thought to constrict the reagents within a smaller, thus more effective reaction volume. The benefits of minimizing the reaction volume were also previously noted elsewhere (Sieber *et al.*, 2010; Hashimshony *et al.*, 2016; Svensson *et al.*, 2017).

2.3.4 *Temperature profile and fidelity*

Shared property of the latest RTases is enhanced thermostability, as the elevated temperatures effectively melt RNA secondary structures, making primer annealing and thus cDNA synthesis more efficient (Nolan, Hands and Bustin, 2006; Álvarez and Menéndez-Arias, 2014). Higher temperatures also destabilize primer-dimer complexes, in turn increasing cDNA purity and preventing reagent exhaustion. Concurrently, elevated temperatures melt the RNA-cDNA duplex, exposing the RNA template for another primer-RTase complex annealing.

Downside of retrovirus-engineered RTases is their inherently low fidelity – rate of correct nucleotide pairing. The well-recognized SuperScript III (Thermo Fisher Scientific), for example, has a reported error rate of 6.5×10^{-5}, scoring comparably or better than some of its competitors (HIV-1 RTs, MMLV- and AMV-derivatives) (Álvarez and Menéndez-Arias, 2014). On the other side, retroelements requiring synthesis of long continuous cDNAs are dependent on

the high fidelity. Mobile group II introns found in prokaryotes or fungi are therefore an interesting source (Mohr *et al.*, 2013). Their RTases were shown to be highly processive, thermostable (up to 81°C), have substantial fidelity (8.4×10^{-6}) and possess template-switching activity.

2.4 Preamplification

After RT, the readily synthetized cDNA can be immediately measured by qPCR. This scenario allows quantification of only a limited number of assays, as the amount of material is limited and its dilution to a larger volume would result in lower concentration of the all present molecules, putting the qPCR's sensitivity to the test (Ståhlberg and Kubista, 2014). To secure sufficient sample volume and its concentration, preamplification is performed to allow for detection of virtually unlimited amounts of molecules. Nonetheless, when only few assays are to be measured, such as in targeted diagnostics (circulating tumor cells) or in quality control of collected cells (see *5.3 Quality control of the collected single cells* section), the preamplification step can be evaded.

In its simplicity, preamplification (preAMP) is PCR performed for predefined number of cycles, depending on quantity of the starting material. The difference from the ordinary PCR stems in the selection of primers, resulting in two preAMP strategies: i) Global, where the reaction is primed with a single pair of primers (Picelli *et al.*, 2014; Kroneis *et al.*, 2017), or ii) Target-specific, being a multiplex PCR consisting of a pool of assay primer pairs selectively targeting amplicons of interest (Livak *et al.*, 2013; Andersson *et al.*, 2015). Comparing target-specific variant to its global counterpart highlights poorer yield, sensitivity and higher variability of the latter (Kroneis *et al.*, 2017). The advantage of global preAMP is the adaptability, as it allows for investigation of additional assays, which is not possible with target-specific preAMP if they were not included in the initial pool of assay primer pairs.

Well-performing preAMP is a result of interplay between optimized factors including highly efficient primer pair for each individual assay, number of these assays, primer pool concentration, reaction temperature, time of the primer annealing step and the number of cycles. The rationale behind preAMP is to deliver reproducible output with minimum variation

in the amplification efficiency of the individual assays (Ståhlberg and Kubista, 2018). The most time-consuming step is validation of the assay primer pairs. All the assays must show target-specificity, produce no primer-dimers, need to be insensitive to genomic DNA contamination and deliver reproducible efficiencies ≥ 90 % (see *2.5 QPCR* section) (Ståhlberg and Bengtsson, 2010; Ståhlberg and Kubista, 2014; Korenková *et al.*, 2015). As quality control tool of the preAMP uniformity, difference between the cycle of quantification (Cq) for preamplified and non-preamplified cDNA samples is monitored. This Cq difference (ΔCq) is routinely measured on a selection of assays targeting transcripts expressed in high, medium and low levels. Two metrics are then considered, mainly that the intra-assay ΔCq variation must be minimal and then, the ΔCq ought to optimally remain consistent across the assays (see *5.5.1 PreAMP quality control* in the results section) (Korenková *et al.*, 2015). In general, preAMP introduces less variability as opposed to RT (Korenková *et al.*, 2015).

Primer concentrations 10 – 20 times lower (40 nM) than in a standard singleplex PCR, in combination with extended annealing time to 3 minutes, are regarded as an optimal balance between production of specific amplicons and minimized formation of the unspecific PCR products (Andersson *et al.*, 2015). Extended primer annealing time increases the likelihood of primer annealing to the complementary sequence, given its diluted state (Andersson *et al.*, 2015). Equally important is the annealing temperature, as it should be within ± 1°C interval for all assays of the primer pool, reducing the risk of unspecific product formation (Andersson *et al.*, 2015). Optimization of the assay pool size revealed that larger assay pools (> 50 assays) deliver higher yields, are less variable and produce fewer unspecific PCR products (Andersson *et al.*, 2015). The proposed mechanism of function is that downstream singleplex qPCR is less likely to amplify the unspecifity that could possibly arise from the myriad of possible primer combinations.

Driving the preAMP past the exponential PCR phase will cause it to the reach plateau phase due to exhaustion of dNTPs or primers for more abundant targets. This can be prevented by keeping the number of cycles in a sensible range: 15 – 18 cycles for bulk samples (> 1.25 ng of total RNA) (Korenková *et al.*, 2015); for single-cells or scarce transcripts 20 – 22 cycles are recommended (Ståhlberg and Kubista, 2018). Similarly to RT, when dealing with low amount of

the input material containing transcripts in low copy numbers, it is advised to prioritize fewer technical preAMP replicates compared to diluting the cDNA. This again minimizes the potential negative outreach of Poisson distribution on small copy numbers.

To retain the preAMP within its dynamic range, each targeted transcript ought to be counting fewer than 10^4 copies per reaction, otherwise the reaction will be inhibited due to exhaustion of dNTPs (Andersson *et al.*, 2015). However, if only few high abundant targets are included (e.g. ribosomal RNA), less abundant transcripts remain unaffected as the primers for the ribosomal RNA are exhausted sooner than other key reagents (Andersson *et al.*, 2015; Ståhlberg and Kubista, 2018).

preAMP is a step of scRT-qPCR workflow ensuring that sufficient amount of the material is available for the downstream analyses. Despite the potential caveats, preAMP is regarded as stable reaction introducing minimal bias, when the assays are carefully optimized and the number of cycles is not exceedingly exploited.

2.5 QPCR

qPCR is a well-established method, regarded as a golden standard in the field of genomics and transcriptomics due to its sensitivity and reproducibility. qPCR is distinct from the preAMP step in virtually only two factors: i) sample quantity is visualized after every cycle and ii) the material is amplified in a singleplex reaction. Nevertheless, assays remain the key reaction component shaping reaction's sensitivity, specificity or reproducibility (Nolan, Hands and Bustin, 2006; Ståhlberg and Bengtsson, 2010).

Design of well-performing assays minimizes the amplification of unspecific products – primer-dimers or genomic regions. As DNase is not employed in the scRT-qPCR (*2.2 RNA extraction* section), the specifity of primers to the mRNA must be embedded in the primer design. Individual primers from the pair are meant to bind separate exons, distanced by an intron of considerable length (Figure 1A). If not only the mRNA is amplified, the unspecific longer product of genomic origin is spotted in the melting curve analysis. In addition, this exon-exon junction design is good to be aimed onto exons closer to the 3'end, as this counters potential RT bias of oligo(dT) (3'end) priming (Nolan, Hands and Bustin, 2006).

A priori to having primers synthetized, it is advised to check them for primer-dimer formation *in silico*. Recommended online tools, free of charge, include NetPrimer (PREMIER Biosoft, USA) or OligoAnalyzer Tool (Integrated DNA Technologies, USA). Primer-dimer architecture that must be avoided is extendable in the 5' to 3' direction (Figure 1B), whereas the 5'end complementary primers are safe to use (Figure 1C). Nonetheless, assay performance must be tested experimentally in reactions without template (primer-dimer formation) or when sufficient genomic DNA is added (amplification of genomic regions) (see *5.6 quantitative PCR validation* section). For assays relevant in single-cell analysis, bottom boundary for reporting unspecific PCR products is settled for Cq = 35 (Ståhlberg and Kubista, 2018). Further, assays are required to have efficiency over 90 % (Ståhlberg, Rusnakova and Kubista, 2013; Ståhlberg and Kubista, 2018).

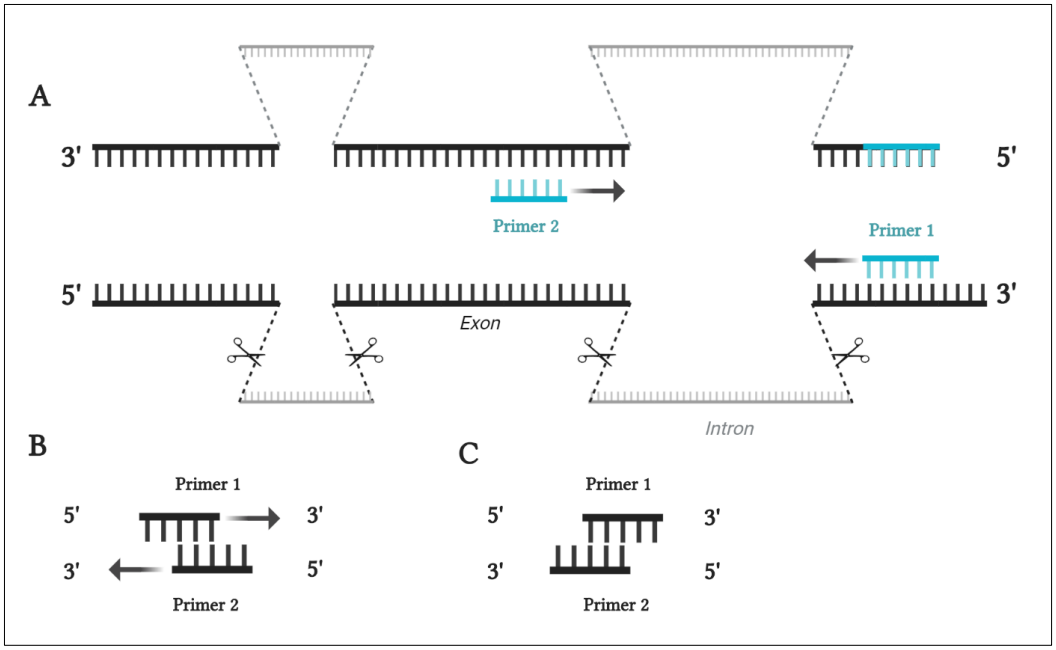

Figure 1 ***Preferred primer design positioning and its potential primer-dimers.*** *(**A**) PCR products amplified from a cDNA made of the processed mRNA (dark colored regions, intron removal illustrated by the scissor cut) are shorter than the PCR products derived from the genomic DNA containing intronic sequences (light grey regions). Exon-exon design ensures that amplification of genomic regions (especially of those surrounding a long intron of >1000 bases long) is less efficient and can be comfortably spotted by the melting curve analysis. (**B**) Design of an unfavorable primer-dimer that will be amplified during PCR. (**C**) Primer-dimer that is accepted in primer design and will not be amplified.*

Due to minute amounts of the material, single-cell measurements are limited by method's sensitivity. qPCR sensitivity is regarded superior to other methods quantifying nucleic acids (Ståhlberg and Kubista, 2014; Kroneis *et al.*, 2017), nonetheless two metrics are requested

for the publication of qPCR data – Limit of Detection (LoD) and Limit of Quantification (LoQ) (Bustin *et al.*, 2009). LoD is the measured concentration that produces at least 95 % positive replicates (Forootan *et al.*, 2017). From the statistical perspective, LoD is settled down to three molecules per reaction chamber (Ståhlberg and Kubista, 2014), but in practice this number is higher – reaction chamber should contain a minimum of 10 targeted molecules (Ståhlberg *et al.*, 2013). Sampling ambiguity comparably compromises accuracy of the measurement – quantification of molecules counting less than 35 copies produces $SD_{qPCR} > 0.25$ cycle. LoQ defines the lowest concentration of analyte that can be reproducibly quantified. The definition what is "reproducible" may vary. In practice, it can be defined as replicates that show a $SD < 0.5$ or $CV \leq 35$ % (Forootan *et al.*, 2017). By the logic of definition, LoQ can never be lower than LoD.

Undoubtedly, optimization of individual qPCR assays is important, but broader view on the RT-qPCR workflow should be kept in scope. qPCR was repeatedly highlighted as the least variable step of the RT-qPCR workflow (Ståhlberg *et al.*, 2004; Tichopad *et al.*, 2009; Lindén, Ranta and Pohjanvirta, 2012). Compared to the RT, RT-related variance is two times larger than that originating from qPCR (Tichopad *et al.*, 2009). This needs to be reflected in the experimental design. Power of the study increases mainly with the introduction of biological and RT replicates (Tichopad *et al.*, 2009; Ståhlberg and Kubista, 2014, 2018). Introducing preAMP or qPCR replicates in single-cell experiments can prove detrimental, separating rare transcripts into multiple chambers and empowering the uncertainty that comes with Poisson distribution of small copy numbers (Figure 2).

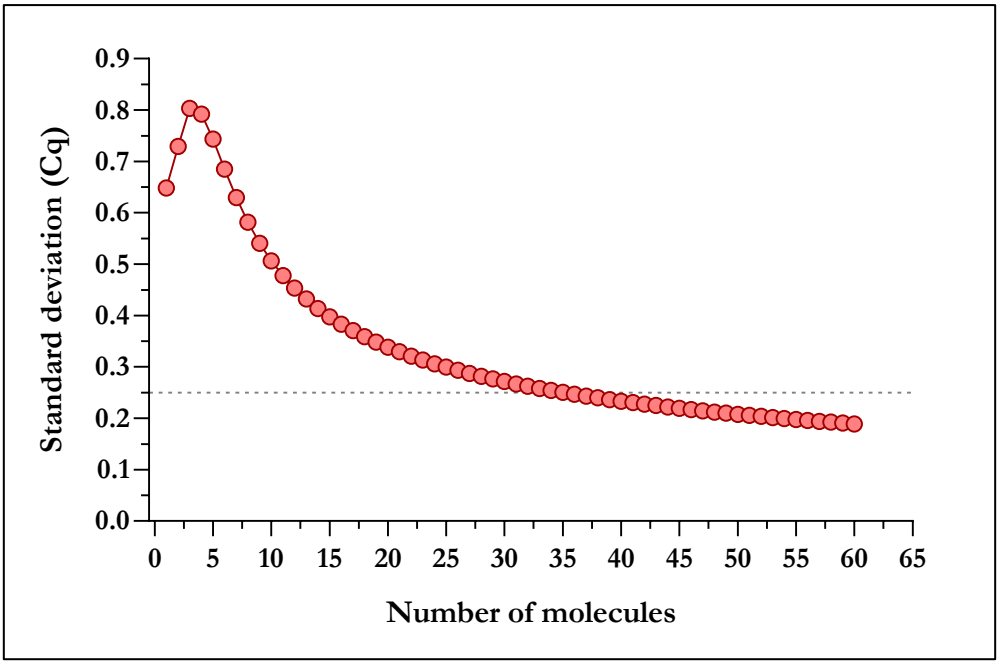

Figure 2 ***Sampling ambiguity due to Poisson distribution.*** *The XY plot depicts the expected SD of Cq values among replicates accounting for the average number of molecules per reaction. The indicated SD = 0.25 outlines the reproducibility of a typical qPCR reaction within its dynamic range. (adapted from* Ståhlberg and Kubista 2014*).*

qPCR is a robust and efficient reaction, delivering the least amount of the uncertainty into the scRT-qPCR workflow. This only comes at the cost of relatively low throughput, as the assessment of hundreds of assays may prove complicated.

2.6 Data processing

Single-cell data analysis in many ways resembles that of bulk samples, although the heterogeneity and variability arising from the nature of single-cell experiments adds a layer of complexity that requires to be addressed in the data processing steps (Figure 3). Firstly, gene-expression profiles of single cells distinct themselves by the frequency of missing data. Biological explanation to this observation are temporal changes in the RNA levels occurring due to transcriptional bursting (Chubb *et al.*, 2006; Raj *et al.*, 2006; Ståhlberg and Kubista, 2018). As a consequence, many cells will contain no target molecules at given times (Dzamba *et al.*, 2016). However, the missing data may also be of technical origin, as the number of targeted copies is below assay's LoD (Ståhlberg, Rusnakova and Kubista, 2013). Secondly, the studied effect can be covered up by the confounding variation inherent to single-cell experiments. Two main variation

components are: i) Inter-subject variation, a natural biological heterogeneity among the studied subjects, magnified by the single-cell heterogeneity (Bengtsson *et al.*, 2008) and ii) Technical variation, introduced by the imprecision of sample processing (Ståhlberg *et al.*, 2013). Validated protocols, control samples (no-template, genomic DNA) and reference samples help to minimize the impact of confounding variation on the studied effect.

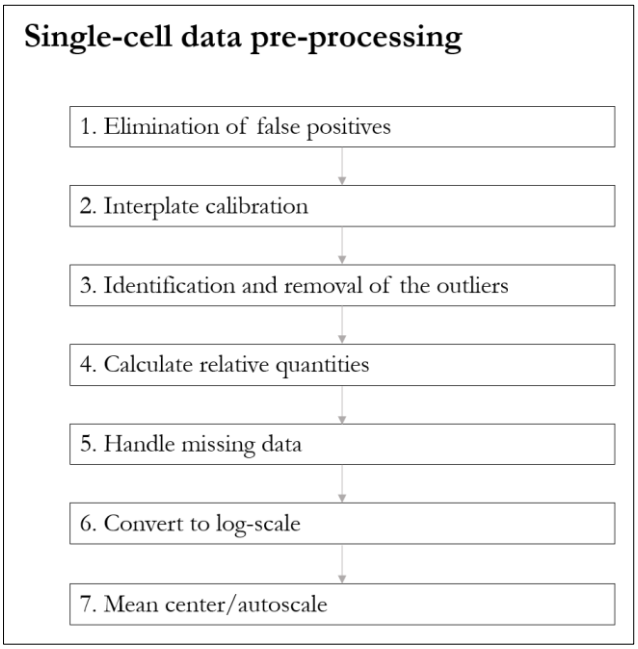

Figure 3 ***The workflow of scRT-qPCR data processing.***

Initial step of the data analysis is the elimination of false positive reactions. With the use of unspecific reporter dyes, e.g. SYBR Green, existing unspecific PCR products are reported but their identity can be recognized by the later melting curve analysis. Well-optimized assays should provide a singular peak (see *5.6 Quantitative PCR assays validation* results section, Figure 19). Aberrant products are recognized by a misshaped peak or by their multiplicity.

Disadvantage of running scRT-qPCR experiments is their relatively low throughput. The highest throughput approach is offered by a 96.96 microfluidic platform BioMark (Fluidigm), where 96 samples are measured on 96 assays simultaneously. Since the power of conclusions in single-cell experiments derives from the number of measured cells, multiple qPCR runs are executed. Individual qPCR runs have assigned individual baseline subtraction and Cq readout threshold level, invalidating their mutual direct comparisons. This is overcome by an interplate calibrator (IPC) – aliquoted sample assayed on all plates (Bengtsson *et al.*, 2008; Ståhlberg *et al.*,

2013). The calibration is done by averaging the Cq of IPC across the runs for every gene separately and then the corresponding difference in the Cq (= IPC – 'IPC average') is added or subtracted from Cq values at every individual plate.

Randomness of amplifying minute copy numbers will result in a failure of reporting the true abundancy of the reaction well. These failed reactions are either: i) Off-scale data - Cq too high to be trusted, or ii) Missing data - with no Cq reported. There are two ways a missing data value is looked upon: a) the reaction contained the molecule, but the PCR was not sensitive enough (under the LoD), or b) the molecule was not present. Off-scale data are not reliable as they correspond to very few molecules and might be a result of unspecific amplification (preAMP, PCR), inhibition or result of sampling ambiguity. In practice, all Cqs above a certain level (Cq_{Cutoff}) are discarded. This value corresponds to the limit of one targeted molecule per chamber – Cq of 35-37 for classical approach (i.e. RT-qPCR without preAMP), Cq of ~ 27 for high-throughput machinery (Bergkvist *et al.*, 2010; Ståhlberg *et al.*, 2013).

Better interpretation of gene expression results is done by converting Cqs into relative quantities (RQs):

$$RQ = 2^{Cq_{MAX} - Cq} \qquad (\textit{Equation 1})$$

where Cq_{MAX} is the highest trusted measured Cq per assay. The RQ of the cell with the highest Cq is equal to 1. Remaining missing data are assigned values of RQ = 0.5 (Cq off-scale = Cq_{MAX} + 1) or less. The more extreme offset is imputed, the more weight is assigned to the missing data point. Thus, when similar cells are analyzed, the offset should be lower (e.g. Cq_{MAX} +1), as the missing data point is most likely just a result of sampling ambiguity (Ståhlberg and Kubista, 2014). For samples heterogeneous in origin or function, the offset is set higher (e.g. Cq_{MAX} +4) and the distinct cell-type specific profiles are better distinguished. RQs are best presented in $\log_2$-scale, as the transcript distribution among the cells is lognormal (Bergkvist *et al.*, 2010; Ståhlberg and Bengtsson, 2010; Dzamba *et al.*, 2016). Thus, the last step is $\log_2$-transformation.

Before continuing with statistical tests, it is advisable to check for the general metrics of the genes and cells studied. Of interest is to record what percentage of cells is positive for a particular gene. Genes with fewer positive cells should be considered within the biological

context of the study and thus decided whether they ought to remain included. It is also advised to check for the correlation between the number of cells containing specific gene transcript and the mean gene expression. Gene's mean expression is calculated as arithmetic average of the $\log_2$-scaled RQs (Ståhlberg *et al.*, 2013). To reflect on the variability of measured Cqs, SD is calculated. This metric mainly presents the heterogeneity of the cells and usually scales with the gene's average expression (Ståhlberg *et al.*, 2013). For the genes of major importance, it is beneficial to visualize their distribution among studied cell types/treatments in the form of histograms (no. of cells ~ expression). Unusual distributions (highly skewed, bimodal) may indicate the presence of several cell types or a different response to stimuli (Ståhlberg, Rusnakova and Kubista, 2013).

Descriptive statistics provide check on the data composition and its quality; next step in the analysis is the differential statistical testing between the samples. The change in the expression of individual genes can be tested by univariate statistics (*t*-test, Anova, regression) being that single-cell expression data are lognormally distributed (Ståhlberg *et al.*, 2013). However, repeated testing for many genes of the same dataset is limited by the nature of statistics – chance of observing false positive results increases just by performing multiple comparisons, i.e. multiple genes are being repeatedly tested. Because of this, some genes would be misclassified as differentially expressed. Several methods were developed aiming to adjust the *p*-value's significance level (Bonferroni's correction, Benjamini and Hochberg False Discovery Rate). The involvement of a particular gene in a specific response to the treatment can be statistically tested by Fisher's exact test (or χ-square test) by listing the number of positive/negative cells versus the treatment groups.

More integrated look at the differences among cells offer multivariate statistical methods, including principal component analysis (PCA), hierarchal clustering, or t-distributed Stochastic Neighbor Embedding. These methods identify differences among cells based on their entire expression profiles, shedding more light on the heterogeneity and the dynamics of cellular change. To prevent some genes from dominating the analysis, all included genes are given equal significance by the data scaling. The most common approach is autoscaling – calculating z-score for each gene separately (Bergkvist *et al.*, 2010). This approach is however vulnerable when the

majority of genes are not responsive to the studied effect and they contribute mainly with noise. When one is uncertain which genes to consider noisy, mean-centering (subtracting gene mean expression from the actual value) is a viable option. Mean-centering equalizes every gene's average expression to zero but retains its variability. In practice, one can start with mean-centered data, look for responsive genes and then continue the analysis on the selected subset (Ståhlberg *et al.*, 2013). An interesting insight can be also brought when the autoscaling (or mean-centering) is applied per cell. This helps in characterization of new cell types by identifying cell-specific over- or under-expressed genes (Ståhlberg *et al.*, 2013).

The greatest power of multivariate statistics is derived from their power to decompose high-dimensional data into an easily interpretable output of two or three dimensions. PCA reduces the space (dataset of measured gene expression profiles) by searching for the main sources of information (variance) in the data and projecting them onto a space of fewer variables – principal components (PCs) (Figure 4A) (Ringnér, 2008; Bergkvist *et al.*, 2010; Riedmaier and Pfaffl, 2013). PCs are constructed in a successive order of importance. Meaning that the first few components are the most informative, their reciprocal plots thus visualize the most of systematic differences among the samples. Said simply, PCA is a low-dimensional plot of high-dimensional data displaying the individual samples in the newly constructed space as points. Samples with similar expression profiles appear closer in the space, forming clusters.

Hierarchal clustering is capable of dividing the dataset into subsets based on the similarity of gene expression profiles between the respective samples. Samples with more similar expression profiles will end up closer within the subset (Bergkvist *et al.*, 2010). Visual outcome of hierarchal clustering is called dendrogram. The individual subsets are constructed based on the underlying gene expression structure, which is uncovered from diverging trends that are present within the dataset. Hierarchal cluster subseting is equally informative on both samples and genes. Fusion of these two computations into two-dimensional output creates a heatmap (Figure 4B). Heatmap conveniently displays the mutual relationship in the expression matrix, identifying the trends among subsets in a color-coded scale of fold-changes.

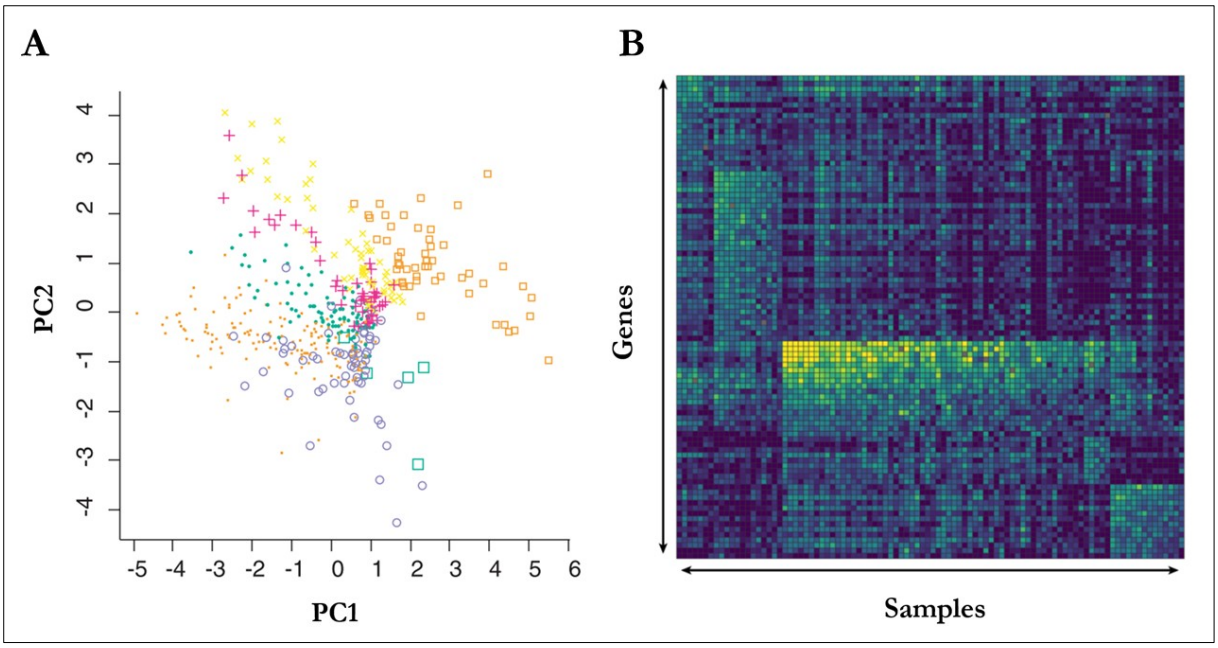

Figure 4 ***PCA and heatmap plots.*** *(**A**) PCA of representatory dataset of seven groups displayed by different symbols and colours on the two first PCs (adapted from Yeung, 2008). (**B**) Colorshaded heatmap depicting the continuity in change of gene expression while visualizing the underlying structure of the dataset (adapted from Androvic et al., 2019).*

2.7 Astrocytes and amyotrophic lateral sclerosis

Amyotrophic lateral sclerosis (ALS) is rapidly progressing neurodegenerative disease damaging motor neurons in the motor cortex, brain stem and spinal cord. Its manifestations are loss of function in the skeletal muscles and later spreading to other muscle groups, ultimately causing death due to respiratory problems within three years of the first symptoms (Kiernan *et al.*, 2011). Exact details on the causation and development of the disease are still unknown and provided treatment is largely symptomatic (Hardiman, Van Den Berg and Kiernan, 2011; Radford *et al.*, 2015).

The hallmarks of ALS are: i) mutations in *FUS*, *TARDBP, C9ORF72* and *SOD1* genes, ii) reactive gliosis, characterized by astrocytes of increased volume and proliferating microglia and iii) accumulation of cytoplasmic inclusions in neurons and some glia (Al-Chalabi *et al.*, 2012; Ng, Rademakers and Miller, 2015). Astrocytes with dysregulation of *C9ORF72* and *SOD1* exhibit substantial neurotoxicity, leading to neuroinflammation, causing degeneration of surrounding tissue and activation of phagocytic microglia. Mutation of *TARDBP* leads to astrogliosis through

the acting molecule of lipocalin-2, eventually leading to formation of glial scar that blocks axonal regeneration (Mayer, Huber and Peskind, 2013). Combination of these factors points to glia cells, namely astrocytes and microglia, to be important contributors in the disease progression.

In the healthy central nervous system (CNS), glial phagocytosis is a key modulator of the CNS plasticity; astrocytes phagocytose synapses and axonal mitochondria, and microglial phagocytosis has a role in the removal of toxic debris and reorganization of CNS connections (Radford *et al.*, 2015). However, during the onset of ALS several mutations were identified in microglia (*TREM2*, *GRN* and *PFN1*) that reduce their phagocytotic capacity (Kleinberger *et al.*, 2014; Radford *et al.*, 2015). Additional role of astrocytic resides in the debris removal and distribution of nutrients via the circulation of cerebrospinal fluid of the glymphatic system (Iliff *et al.*, 2014). This flow is supplemented by astrocyte-specific water transporter AQP4 with polarized positioning on the cell surface (Papadopoulos and Verkman, 2013). *SOD1* mutation was linked with the loss of AQP4 polarization, possibly leading to turbulent flow and reduced effectiveness in the debris clearance or nutrient distribution (Papadopoulos and Verkman, 2013; Iliff *et al.*, 2014; Kitchen *et al.*, 2020).

In summary, both astrocytes and microglia were shown to be substantially involved in the neurodegenerative ALS disorder with yet further work needed to be done elucidating the molecular background of the disease.

3 Aims of the thesis

Aims of the thesis include:

- Establish protocol for quality control of FACS-sorted astrocytes
- Examine factors influencing quality of single-cell experiments during and after FACS collection
- Define limits of direct lysis protocol for analysis of small bulk samples
- Compare performance of RTases for single-cell analysis
    - Define the differences between the latest commercially available RTases
    - Describe the influence of priming strategy
    - Validate the data in a model single-cell experiment
- Validate preAMP protocol for analysis of control and ALS astrocytes and investigate the role of reaction volume on the sensitivity of measurement
- Design and characterize a set of highly effective qPCR assays
- Apply the optimized protocol and procedures for the analysis of ALS astrocytes

4 Material and methods

4.1 Material

All procedures involving the use of laboratory animals were performed in accordance with the European Community Council Directive of 24 November 1986 (86/609/EEC) and animal care guidelines approved by the Institute of Experimental Medicine, Academy of Sciences of the Czech Republic (Animal Care Committee decision on 17 April 2009; approval number 85/2009). Double transgenic mice (*Mus musculus*) bearing SOD1(G93A) and GFAP/EGFP alterations were used as model organism. Mice with transgenic expression of mutant human superoxide dismutase SOD1(G93A) exhibit phenotype similar to ALS in humans, whereas GFAP/EGFP allows for visualization of astrocytes due to expression of EGFP protein under human glial fibrillary acidic protein (GFAP) promoter. Two types of samples were collected: 1) single cells and 2) tissue samples. Details on the material origin, collection and preparation are described in detail in the corresponding chapters. The material was stored at -80°C.

4.2 Detailed single-cell RT-qPCR protocol

This protocol encompasses the current complete set of recommendations for performing a single-cell experiment. This includes reaction volumes (RT, preAMP, qPCR), reagents (RTase), reagent concentrations (RTase, ribonuclease (RNase) inhibitors, primers), specifications on priming methods (RT, preAMP), thermal protocols (RT, preAMP, qPCR), dilutions, laboratory practice and data pre-processing (melt peaks specificity, Cq value cutoff). This protocol serves as the main methodical guideline and was used as a framework to all scRT-qPCR experiments in this thesis. The experiment-specific modifications are described in the corresponding chapters.

4.2.1 Preparation and collection of the single-cell suspension

GFAP/EGFP 3-months old transgenic mice were deeply anesthetized with pentobarbital (100 mg/kg) and transcardially perfused. The cerebellum was carefully dissected and placed into an isolation solution supplemented with papain (5 ml, 20 U/ml) and 0.2 ml DNase (both Worthington). The treatment was undertaken under countinous shaking at 37°C for 90 minutes.

After the treatment, the tissue was dissociated by trituration using a 1 ml pipette. Dissociated cells were further placed on Ovomucoid inhibitor solution and centrifuged (140×*g* for six minutes). Cell aggregates were filtered out with a 30 µM cell stainers (Becton Dickinson) and the cells were kept on ice until sorting.

Single cells were sorted using flow cytometry (FACS GRISORBEON system 1, 0.9.21 BDInflux) into 96-well plate. The flow cytometer was calibrated to deposit the cell in the centre of each collection tube. Hoechst 33258 (Thermo Fisher Scientific) was added to the cell suspension as their viability check. To begin with, the machinery was adjusted for fluorescence threshold by collecting non-fluorescent cells in order to precisely collect only $EGFP^+$ cells and avoid autoflorescent cells. Cells crossing the fluorescent threshold were collected into 5 µl lysis buffer (NFW + 1 mg/ml BSA (Fermentas)) into pre-cooled plates. Viable and $EGFP^+$ collected cells were immediately placed at -80°C. Full details regarding the sample preparation and collection are listed in Pivonkova *et al.* (2018).

The samples were prepared and collected in cooperation by the Department of Cellular Neurophysiology (Institute of Experimental Medicine, Academy of Sciences of the Czech Republic).

4.2.2 Reverse transcription

An exemplary single-cell RT reaction followed two-step Maxima H- RTase protocol (**Supplementary protocols**, *Attachment 1*) and consisted of: 5 µl of sample and 5 µl RT mastermix. Two-step RT protocol included: 1) RT1 mastermix contained: 0.5 µl 200,000× External RNA Controls Consortium (ERCC) Spike-in, 0.5 µl 10mM dNTPs, 0.5 µl RT primers (50 µM mixture of random hexamers and oligo$(dT)_{15}$ (further referred as RT primers mixture) or 10 µM oligo$(dT)_{15}$) and 0.5 µl nuclease-free water (NFW) (all Thermo Fisher Scientific). All reagents were previously briefly vortexed and centrifuged on the bench centrifuge. RT1 mastermix was prepared as pool for all samples, briefly vortexed, centrifuged and added to the samples (2 µl per well). Well contents were again briefly vortexed and centrifuged. Thermal protocol of step one: 65°C ($t = 5\ min$) and immediate cooling on ice. 2) RT2 mastermix contained: 2 µl 5× RT buffer, 0.5 µl RNaseOUT (40 U/µl) and 0.5 µl Maxima H- RTase (all Thermo Fisher Scientific).

Only 5× RT buffer was vortexed, all reagents were briefly centrifuged. Before addition to the RT2 mastermix, RNaseOUT and RTase were mixed by a gentle up-and-down pipetting inside the tip. RT2 mastermix was prepared as pool, shortly vortexed (3 brief contacts with the vortex), centrifuged and distributed (3 µl per sample). Prepared RT reactions were then again briefly vortexed and centrifuged. Thermal protocol of step two: 25°C (*t = 10 min*), 50°C (*t = 30 min*), 85°C (*t = 5 min*) and immediate storage on ice. RT was performed in Bio-Rad C1000 Thermal Cycler (Bio-Rad).

4.2.3 Preamplification

cDNA was preamplified in 40 µl total reaction volume comprising of 4 µl undiluted cDNA and 36 µl preAMP mastermix. PreAMP mastermix consisted of 12 µl NFW, 20 µl IQ Supermix buffer (Bio-Rad) and 4 µl 250 nM equimolar mixture of 96 primer pairs (Thermo Fisher Scientific). Selection of primer pairs reflects the experimental goals; the complete list is in **Primer sequences** tab (*Attachments 1*). All reagents were previously briefly vortexed and centrifuged. PreAMP mastermix was prepared in pool, briefly vortexed, centrifuged and distributed (36 µl preAMP mastermix per sample). Total reaction volume were again briefly vortexed and centrifuged. Thermal protocol comprised of heating to 95°C (*t = 3 min*), followed by 18 cycles of template denaturation at 95°C (*t = 20 s*), primer annealing at 57°C (*t = 4 min*) and primer elongation at 72°C (*t = 20 s*), then immediate cooling on ice. PreAMP cDNA was 4× diluted with NFW and stored at -80°C until use. Preamplification was done on Bio-Rad C1000 Thermal Cycler.

4.2.4 Quantitative PCR

For low-throughput measurements (up to 384 reactions), qPCR was done in thermal cycler Bio-Rad CFX 384 (Bio-Rad). A total reaction volume of 10 µl contained: 2 µl 4× diluted preAMP cDNA and 8 µl qPCR mastermix, which consisted of 2.6 µl NFW, 5 µl TATAA SYBR Green mix (TATAA Biocenter) and 0.4 µl of 10 µM assay primers (Thermo Fisher Scientific). Before use, all reagents were briefly vortexed and centrifuged. qPCR mastermix was prepared in pool and distributed. Complete well contents were again briefly vortexed and centrifuged. Cycling protocol consisted of initial enzyme activation at 95°C (*t = 3 min*), followed by 45 cycles of denaturation at 95°C (*t*

= *15 s*), annealing at 60°C (*t = 20 s*) and elongation at 72°C (*t = 20 s*). Melting curve analysis was performed for the temperature interval of 65°C to 95°C under increment of 0.5 °C.

For high-throughput measurements (up to 9216 consecutive reactions), qPCR was done using high-throughput 96.96 Fluidigm BioMark platform (Fluidigm). Firstly, primer assay plate was prepared by addition of 3.9 µl primer assay mastermix (consisting of 3.25 µl 2× Assay Loading Reagent (Fluidigm) and 0.65 µl NFW) into 2.6 µl 10 µM equimolar pair of forward and reverse qPCR assay primers; prepared in 96-well plate with each well dedicated to one qPCR assay pair; thus named as 'Primer assay plate'. Before use, all reagents were briefly vortexed and centrifuged. 'Sample plate' was readied by adding 5 µl sample assay mastermix (consisting of 0.42 µl 20× 20X DNA Binding Dye Sample Loading Reagent (Fluidigm), 4.17 µl 2× SSoFast EvaGreen Supermix (Bio-Rad), 0.017 µl ROX Reference Dye (Thermo Fisher Scientific) and 0.4 µl NFW) into 3.33 µl of 4× diluted preAMP cDNA. Before use, all reagents were briefly vortexed and centrifuged. The 96.96 Dynamic Array™ IFC chip was first primed with Control Line Fluid oil solution (Fluidigm) in the NanoFlex™ 4-IFC Controller (Fluidigm) to fill the chip's microfluidic system. The contents of primer assay plate (5.5 µl) and sample plate (6 µl) were then carefully transferred into reaction wells of the primed 96.96 Dynamic Array™ IFC chip. In continuation, the chip was placed for automatic loading and mixing into the NanoFlex™ 4-IFC Controller. After loading, the chip was placed into BioMark qPCR platform (Fluidigm). The cycling program consisted of activation at 95°C (*t = 3 min*), followed by 35 cycles of denaturation at 95°C (*t = 5 s*), annealing at 60°C (*t = 15 s*) and elongation at 72°C (*t = 20 s*). After qPCR, melting curve analysis was performed between 60°C and 95°C with 0.5°C increments.

4.2.5 Data analysis

Data analysis was done using R project software (R Foundation), Bio-Rad CFX Manager v3.1 (Bio-Rad) for low-throughput measurements and Real Time PCR analysis software (Fluidigm) for high-throughput. Initially, the data were investigated for the specificity of melting peaks. The reaction passed when only one specific peak was observed (see *5.6 Quantitative PCR validation* results). Next, Cqs > 28 (for high-throughput datasets) and Cqs > 40 (for low-throughput datasets) were cleared off, so only values within instrument's sensitive range were reported. For

graphing purposes GraphPad Prism 8 (GraphPad Software) was used. The further individual details on statistics are detailed in the dedicated chapters.

4.3 Experiment-specific protocols

Description of alterations made to the *4.2 Detailed single-cell RT-qPCR protocol*, in order to validate the individual steps of the scRT-qPCR workflow.

4.3.1 Factors influencing single-cell quality during and after FACS collection

$EGFP^+$ single cells from 3-months old mouse cerebellum were prepared and collected as described in *4.2.1 Preparation and collection of the single-cell suspension* section. The cells were reverse transcribed with SuperScript III (Thermo Fisher Scientific) RTase (**Supplementary protocols**, *Attachment 1*). RT was primed with 50 µM RT primers mixture and the resulting cDNA was 3× diluted in NFW. cDNA was not preamplified but directly quantified by low-throughput qPCR. The entire workflow closely followed *4.2 Detailed single-cell RT-qPCR protocol*. After checking for normality distribution, *one-way* ANOVA was applied.

4.3.2 Direct lysis of small bulk samples

$EGFP^+$ single cells (and the small bulks doubling in count up to 2048 cells per sample) were collected as described in *4.2.1 Preparation and collection of the single-cell suspension* section. The cells were reverse transcribed by SuperScript III (Thermo Fisher Scientific) (**Supplementary protocols**, *Attachment 1*). RT was primed with 50 µM RT primers mixture and the resulting cDNA was 6× diluted in NFW. cDNA was not preamplified but directly quantified by low-throughput qPCR. The entire workflow closely followed *4.2 Detailed single-cell RT-qPCR protocol*.

4.3.3 Quality control of the collected single cells

$EGFP^+$ single cells from 3-months old mouse cerebellum were prepared and collected as described in *4.2.1 Preparation and collection of the single-cell suspension* section. The samples were reverse transcribed by SuperScript II or Maxima H- (both Thermo Fisher Scientific) (**Supplementary protocols**, *Attachment 1*). RT was primed with either 50 µM RT primers mixture or 10 µM oligo$(dT)_{15}$. Undiluted cDNA was preamplified and resulting 4× diluted

preAMP cDNA was quantified by low-throughput qPCR. The entire workflow closely followed *4.2 Detailed single-cell RT-qPCR protocol.*

4.3.4 Comparison of reverse transcriptases for single-cell applications

RTases were compared in two subsequent experiments: 1) RTase benchmarking and 2) High-throughput RT validation. The goal of the RTase benchmarking was to compare the performance of 11 commercial enzymes for conditions mimicking single-cell and 100-cell bulk samples (Table 1). High-throughput RT validation built up on the obtained results and aimed to emphasize the RTase' impact in a routine single-cell experiment using real single cells. Both experiments were carried out using two RT priming strategies: 1) equimolar mixture of 50 µM RT primers mixture (standard RT-qPCR recommended concentration (**Supplementary protocols**, *Attachment 1*)) and 2) 10 µM oligo(dT)$_{15}$ (recommended for single-cell RNA-Seq protocols (Bagnoli *et al.*, 2018)).

4.3.4.1 RTase benchmarking

RNA contained within the samples originated from two sources: i) extracted RNA from mouse cerebellum tissue, and ii) ERCC Spike-in (set 1) (Thermo Fisher Scientific). The extracted RNA from mouse cerebellum mimicked the RNA abundancy of an average single cell (30 pg) or 100-cell bulk (3 ng). Secondly, ERCC Spike-in served as RNA standard, allowing for absolute quantification. Use of aliquoted material minimized the possible confounding biological variation (Marinov *et al.*, 2014). Mouse tissue samples from cerebellum (3-month old animals) were dissected, placed into TRI Reagent (Sigma-Aldrich) and immediately frozen on dry ice; later stored at -80°C. Before use, samples were thawed and total RNA was extracted following TRI Reagent (Guanidine Thiocyanate & Phenol) protocol (Sigma-Aldrich) according to the manufacturer. Samples did not undergo DNAse treatment. RNA quantity and purity were assessed using the NanoDrop 2000 spectrophotometer (Thermo Fisher Scientific) and RNA integrity was assessed using the Fragment Analyzer - DNF 489 Standard Sensitivity RNA Analysis Kit (Advanced Analytical Technologies), following manufacturers' protocols. The results are listed in **RNA material** (*Attachment 1*). To prepare aliquots, extracted RNA was diluted in NFW to 1.5 ng/µl and stored at -80°C. ERCC Spike-in (set 1) (Thermo Fisher Scientific) was used as the primary template for RTase benchmarking (External RNA Controls Consortium, 2005). ERCC Spike-in set consists of unlabeled polyadenylated transcripts of various lengths (250 to

2000 nucleotides) mimicking eukaryotic mRNAs. Copy numbers of individual ERCC Spike-in transcripts are declared by the manufacturer. Stock ERCC Spike-in was 200,000× diluted in TE-buffer supplemented with linear polyacrylamide (TE-LPA) for single-cell conditions or 2,000× for bulk conditions and stored in aliquots. For each experiment, fresh aliquot was mixed with either 30 pg or 3 ng mouse cerebral RNA. In total, the ERCC Spike-in accounted for about 13 % of the mRNA and about 0.5 % of the total RNA, as calculated under the assumption that mRNA within the cell typically constitutes approximately 3.5 % of the total RNA.

Sample processing followed the protocol described in *4.2 Detailed single-cell RT-qPCR protocol*, with every RTase closely used in compliance with the manufacturer's protocol (**Supplementary protocols**, *Attachment 1*). All reagents (NFW, RT primers, dNTPs, DTT, RNaseOUT) were supplied from a single aliquoted stock. Each experimental condition (combination of RT priming and material abundancy) was run in 10 replicates. 5 µl reactions contained 2 µl RNA and 0.25 µl ERCC Spike-in. Prepared cDNA was 5× diluted in NFW. Preamplification step was avoided to minimize the introduction of technical artefacts. Without freezing the 5× diluted cDNA, low-throughput qPCR measurents took place.

Table 1 ***List of the benchmarked RTases.***

Reverse Transcriptase	Manufacturer	Origin	RNase H activity	Reaction temperature (°C)	Cost per 20 µl reaction ($)
SuperScript II	Thermo Fisher Scientific (USA)	MMLV	reduced	42	7.5
SuperScript III	Thermo Fisher Scientific (USA)	MMLV	reduced	50	8.2
SuperScript IV	Thermo Fisher Scientific (USA)	MMLV	reduced	50	8.2
Sensiscript	Qiagen (Germany)	unspecified	present	37	6.0
PrimeScript	Takara Bio Inc. (Japan)	MMLV	none	42	6.5
Maxima H-	Thermo Fisher Scientific (USA)	MMLV	none	50	4.0
AccuScript Hi-Fi	Agilent (USA)	MMLV	none	42	12.0
iScript	Bio-Rad Laboratories (USA)	MMLV	present	42	6.5
MMLV	Promega (USA)	MMLV	present	42	2.0
eAMV	Merck (Germany)	AMV	unspecified	42	8.0
qScript	Quanta Biosciences (USA)	MMLV	present	42	5.2

The comparison of 11 RTases was performed using five thoroughly validated qPCR assays (Table 2). The assays were selected to target *ERCC Spike-in* molecules present at different

abundancies (22-2822 copies per RT reaction in single-cell set-up) mimicking the range of cell's genes expression.

RTases were characterized in terms of sensitivity, precision, yield, and reproducibility. RT sensitivity was reported as the percentage of positive reactions for transcripts counting 22 or 88 copies per RT reaction (*ERCC 84* and *ERCC 95*, respectively), approximating RTase efficiency for limiting concentrations.

RT precision informed on the quality of linear RT performance in the range from 22 to 282 200 RNA copies per RT. This was investigated by describing the relation between the amount of the input RNA and measured RNA concentration. In the linear regression model, the independent variable was represented by the number of RNA copies per RT reaction in $\log_{10}$ scale (Table 2) (*x* axis in Figure 12). The dependent variable was represented by the $\log_{10}$-scaled number of RNA copies that were inferred from the measured Cq using the DNA Standard curve (*y* axis in Figure 12) (for DNA standard curve construction see *4.3.6 QPCR validation* section). Coefficient of determination (R^2) of the linear regression model described quality of the linear fit.

Table 2 ***Assay specifications necessary for Precision and Absolute yield calculations****. $Cq_{RT=100\%}$ for single-cell or bulks describes the theoretical Cq that corresponds to the RNA copy numbers assuming 100 % RT efficiency.*

Name	GenBank accession	Single-cells: transcript count per RT	Single-cells: cDNA count per qPCR	DNA Standard curve [Cq = a × $\log_{10}$(copies per qPCR well) + b]	$Cq_{RT=100\%}$ for single cells	$Cq_{RT=100\%}$ for bulks
ERCC-00084-01	DQ883682	22.0	1.8	Cq= -3,448 × log(qPCR input) + 36,469	35.62	28.72
ERCC-00095-01	DQ516759	88.2	7.1	Cq= -3,702 × log(qPCR input) + 39,118	35.98	28.57
ERCC-00092-01	DQ459425	176.4	14.1	Cq= -3,39 × log(qPCR input) + 36,046	32.15	25.37
ERCC-00108-01	DQ668365	705.5	56.4	Cq= -3,407 × log(qPCR input) + 36,158	30.19	23.38
ERCC-00171-01	DQ854994	2821.9	225.8	Cq= -3,376 × log(qPCR input) + 36,579	28.63	21.88

Absolute yield was calculated from the relation between the RNA input and its cDNA output. The RNA input copy numbers were transformed into a theoretical Cq ($Cq_{RT=100\%}$) corresponding to successful conversion of all the RNA copies into cDNA. For the $Cq_{RT=100\%}$ and 'cDNA count per qPCR' see Table 2. The real cDNA output of RT reaction was represented by its measured Cq. The RT yield was thus calculated as:

$$E = 10^{\frac{-1}{a}} \qquad (Equation\ 2)$$

$$Yield = E^{-(Cq-1-Cq_{RT=100\%})} \qquad (Equation\ 3)$$

where "*a*" refers to slope of the individual ERCC Spike-in DNA standard curve and $Cq_{RT=100\%}$ is the expected Cq for 100 % RT efficiency. Adjusting the Cq by -1 accounted for the difference between the single-stranded cDNA and the double-stranded DNA standard used in the standard curve construction. Next, average yield was calculated across the five *ERCC Spike-in* assays for each RT reaction separately. This produced 10 RT yields per particular combination of RTase, template abundancy and priming strategy. Preceding any statistical testing, the four normality assumptions were inspected visually on the diagnostic plots: 1) linearity (Residuals vs fitted plot), 2) residual normality (Q-Q plot), 3) variance homogeneity (Scale-Location plot) and 4) Cook's distance (Residual vs leverage plot). The yield data passed the normality criteria upon $\log_{10}$-normalization. Firstly, statistical testing was done by *two-way ANOVA* (factors of priming and RTase) separately for single-cell and bulk dataset. The differences between RTases were tested by *one-way ANOVA* (factor of RTase) separately for each combination of template abundancy and priming strategy (Figure 14).

Performance reproducibility was commented on Z-scored Cq values, as detailed in the result's *Performance reproducibility* section. To test the variability of the performance reproducibility, Levene's test was applied concurrently on all 11 RTases. Levene's test informs on the significance of differences in the (Z-score) variance around the (RTase-specific Z-score) mean. Next, Levene's test was applied separately for each RTase' Z-scores separately, comparing the difference in performance reproducibility in the bulk and single-cell conditions. In the latter, the *p*-value was adjusted for Bonferroni's correction.

4.3.4.2 High-throughput RT validation

$EGFP^+$ single-cell samples from dissected mouse brain tissue (3-months old mice) were prepared and collected as described in *4.2.1 Preparation and collection of the single-cell suspension* section. Samples were reverse transcribed by Maxima H- or SuperScript II (Thermo Fisher Scientific) (**Supplementary protocols**, *Attachment 1*), in reactions primed with either 50 µM RT primers mixture or 10 µM oligo$(dT)_{15}$. Undiluted cDNA was preamplified (complete assay list is to be

found in **Primer sequences**, *Attachment 1*) and quantified using high-throughput qPCR. Entire sample processing closely followed the protocol described in *4.2 Detailed single-cell RT-qPCR protocol.*

Reactions producing nonspecific signal (melting curve analysis) or reported Cq > 28 were discarded. Also, only cells expressing all three astrocytic markers *Gja1*, *Slc1a3* and *Aqp4* were used. Data were divided based on RT priming strategy and henceforth processed separately. Assays that did not report any positive signal were discarded. Missing values were replaced by the assay's maximum Cq +2 (Ståhlberg *et al.*, 2013) and the relative quantities (RQs) were calculated relative to the least expressed sample within the assay according to the Equation 1. Finally, Cqs were $\log_2$ scaled.

The difference in the signal strength was tested using Wilcoxon signed rank test on the assay mean RQ. The use of nonparametric test was justified as no data transformation ensured the assay mean RQs to fulfill normality criteria.

PCA was applied to the autoscaled $\log_2$-scaled RQ values. Cluster centroid corresponded to the average point of the cluster defined by the combination of RTase and cell treatment. This value was calculated in the new reduced spaced defined by PCs. The distances between cluster centroids were calculated as Euclidean distances. Redundancy analysis (RDA) was also applied to the $\log_2$-scaled RQs. Starting with the full model ($RQ_{\text{gene expression dataset}}$ ~ RTase * Cell Treatment), Akaïke information criterion (AIC) was used to select the optimal minimal model. For both priming strategies, the AIC defined the optimal models without the interaction component ($RQ_{\text{gene expression dataset}}$ ~ RTase + Cell Treatment).

4.3.5 Preamplification validation

4.3.5.1 PreAMP quality control

In three replicates, 250 ng of extracted cerebral RNA and 0.25 µl of 1000× diluted ERCC Spike-in were used for targets for reverse transcription by SuperScript II RTase (**Supplementary protocols**, *Attachment 1*). RT- reaction was also included. Prepared cDNA was immediately 4× diluted in NFW and preamplified in duplicates (primer list enclosed in **Primer sequences**, *Attachment 1*). Preamplified cDNA was immediately 50× diluted in NFW and stored at -80°C.

Next, selection of high, medium and low abundant targets was measured in low-throughput qPCR. Both 50× diluted preAMP and non-preAMP cDNA was used as template. The data analysis is described in the *5.5.1 PreAMP quality control* results section. Otherwise, the workflow closely followed *4.2 Detailed single-cell RT-qPCR protocol*.

4.3.5.2 PreAMP volume

Single cell and 100-cell bulk aliquots of extracted mouse cerebellum tissues, identical to those in the *RTase Benchmarking* section, were used for RT using SuperScript III enzyme (Thermo Fisher Scientific) (**Supplementary protocols**, *Attachment 1*) in 10 µl reactions. RT was primed with 50 µM RT primers mixture. Resulting undiluted cDNA was pooled to mitigate the RT-related discrepancies and immediately preamplified (**Primer sequences**, *Attachment 1*). Three volume conditions were prepared: i) 10 µl, ii) 20 µl and iii) 40 µl; where cDNA always comprised $1/10^{th}$ of the total reaction volume. After preAMP, reaction contents were 4× diluted in NFW. Preamplified material was quantified by high-throughput qPCR. The entire workflow closely followed *4.2 Detailed single-cell RT-qPCR protocol*.

Data pre-processing reflected *4.2 Detailed single-cell RT-qPCR protocol*. The dataset was then processed for single cells and bulk samples separately. Assays counting less than 20 % of positive reactions were removed from further analysis. To compare the signal strength, missing values were substituted by Cq_{MAX} + 1 per assay and then, RQs were calculated relative to the least expressed sample (Equation 1). The mean assay RQs were checked for normality distribution by diagnostic plots and Shapiro-Wilk normality test. Since no group was found to be normally distributed (single cells or bulks), Friedman rank sum test was applied. The pairwise comparison of Friedman rank sums then identified the significance between groups.

4.3.6 QPCR validation

Note: Chronologically, this step was conducted first from the entire scRT-qPCR workflow validation.

Aliquoted RNA of extracted mouse cerebellum tissues, identical to that of *RTase Benchmarking* section, was used in 10 µl reactions using SuperScript IV RTase, according to manufacturer's protocol (**Supplementary protocols**, *Attachment 1*). Each assay was validated on samples: 1)

four replicates containing 4 µl of cerebral RNA (1.5 ng/µl) spiked-in with 1 µl 100× diluted ERCC Spike-in, 2) one replicate of 2 µl mouse gDNA (0.5 ng/µl) and 3) three replicates of 2 µl NFW. Priming strategy of choice was 50 µM RT primers mixture and resulting cDNA was 10× diluted. Samples were quantified without preamplification on low-throughput qPCR. The entire workflow closely followed *4.2 Detailed single-cell RT-qPCR protocol*.

After the qPCR, three PCR-amplified cDNA samples per assay were pooled, purified by DNA Clean & Concentrator-5 (Zymogen) and their size and purity was verified by capillary electrophoresis (Fragment Analyzer – dsDNA 905 Reagent Kit, 1 bp – 500 bp, Agilent), working strictly according to the manufacturers' protocols. The electrophoresis results are listed in the **ERCC Spike-in assay validation** (*Attachment 1*).

Purified PCR products (DNA standards) from the first round of primer testing (pool of three PCR amplified cDNA samples) were consequently used as a template for standard curves. DNA standard copy numbers were derived from the concentrations measured on Qubit 2.0 (Thermo Fisher Scientific). Qubit's 500 ng/ml standard was diluted into dilution series of 500 – 250 – 125 – 62.5 – 31.25 – 0 ng/ml. Linear regression model (template abundancy ~ raw fluorescence signal) regressed out the concentration of the cDNA samples. Due to known concentration and the theoretical weight of one double stranded ERCC Spike-in PCR product molecule, the number of molecules per 1 µl of sample was calculated:

$$number\ of\ copies = \frac{concentration * 6.022 \times 10^{23}}{weight * 10^{9}} \qquad (Equation\ 4)$$

where "*concentration*" is the one of PCR molecules and *"weight"* is the theoretical weight of the particular double stranded PCR amplicon of defined length. PCR products were thus diluted accordingly, in the TE-LPA buffer, to cover a range from 2×10^{5} to 2×10^{-1} copy numbers per qPCR reaction (n = 4 replicates) and measured by low-throughput qPCR. Parameters of the standard curves are listed in the Table 2 and the plots are in **ERCC Spike-in assay validation** (*Attachment 1*).

LoD and LoQ were obtained using the same purified aliquoted PCR products, as those from standard curves construction. For each assay, separate dilution series was readied: 100 – 40 – 16 – 6.4 – 2.6 – 1 – 0.4 – 0.16 copies per qPCR reaction. Low-throughput qPCR was done in

the n = 6 qPCR replicates per dilution point. LoD is defined as template concentration with 95% confidence to be detected in all undergoing qPCR reactions. LoQ was defined as template concentration with SD_{Cq} < 0.5 for replicates. LoD and LoQ results are listed in Figure 20 or in Table 3.

Table 3 ***Specifications of the benchmarking assays.*** *Limit of detection is the lowest concentration that gives rise to positive signal in 95 % of the cases. Limit of quantification is defined as the lowest concentration producing SD < 0.5 among replicates. Amount of nucleic acid in bulk samples was 100 times higher.*

Name	GenBank accession	Length [bases]	Single-cells: transcript count per RT	Single-cells: cDNA count per qPCR	Limit of detection [molecules per qPCR]	Limit of Quantification [molecules per qPCR]	Efficiency
ERCC-00084-01	DQ883682	970	22.0	1.8	5.7	6.4	0.950
ERCC-00095-01	DQ516759	495	88.2	7.1	5.7	100.0	0.863
ERCC-00092-01	DQ459425	1110	176.4	14.1	5.7	40.0	0.973
ERCC-00108-01	DQ668365	997	705.5	56.4	5.7	16.0	0.966
ERCC-00171-01	DQ854994	481	2821.9	225.8	5.4	6.4	0.978

4.3.7 ALS-induced change in astrocytic gene expression

$EGFP^+$ single-cell samples from dissected mouse brain tissue (3-months old mice) were prepared and collected as described in *4.2.1 Preparation and collection of the single-cell suspension* section. Samples were reverse transcribed using Maxima H- (Thermo Fisher Scientific) in 10 µl reactions. Undiluted cDNA was immediately preamplified, 4× diluted and quantified by high-throughput qPCR. The entire workflow and data pre-processing closely followed *4.2 Detailed single-cell RT-qPCR protocol*.

Only assays counting at least 5 % positivity were kept. Only cells negative for *Cspg4* were used. RQs were calculated relative to the least expressed sample per assay (Equation 1) and the missing values were imputed by RQ = 0.25 (equivalent of Cq_{MAX} +2). Lastly, the values were $\log_2$-scaled. Unpaired two-tailed t-test was then applied for each assay individually to search for differentially expressed genes between control and ALS single-cells. Dunn-Bonferroni correction was applied due to repeated testing and adjusted the p-value significance to 0.00081. The list of differentially expressed genes is in **ALS astrocytes** (*Attachment 1*). Heatmap was constructed

(Ward's algorithm for clustering, Euclidean measures of distances) for the differentially expressed genes. Finally, data for all assays were autoscaled and PCA was applied.

5 Results

5.1 Factors influencing single-cell quality during and after FACS collection

Sample preparation and handling are repeatedly mentioned as one of the major contributors on the quality of single-cell experiments (Bengtsson *et al.*, 2008; Hodne and Weltzien, 2015; Ståhlberg and Kubista, 2018). This does not come as surprise, as the variability in the preparation protocols is substantial (Lippi et al. 2011; Spidia) and the exact sample handling of the single-cell material is not clearly discussed in the methodical sections of the published literature. Thus, we set out to validate a set of practical events, often unavoidable in the practical setup, that could potentially bring bias into scRT-qPCR workflow analysis. In this case, 13 single astrocytes per group were exposed to different experimental conditions (described below) and expression of three endogenous transcripts was assessed – *Slc1a3, Aqp4* and *Actb*. Obtained Cqs were transformed to RQ (Equation 1) for each assay separately and then, average RQ per cell was calculated to represent cell's gene expression state. Only cells expressing all three genes were considered for further analysis.

FACS was developed to enable rapid selection of single cells. However, no collection method is fast enough to ensure processing of all samples in a short time span that would prevent changes in gene expression. When the cells of interest are abundant in the sample, the run time for collection of 96 single cells into 96-well plate, including setting of all collection parameters, may be approximated to 10 minutes. For rare cell types or sample of lower quality, the collection time may be even longer. To estimate the effect of the period when cells wait to be sorted, we left cell suspension in cooling vessel of FACS instrument and in defined periods collected 13 single cells (t = 0, 20, 30, 45, 60 min) that were immediately frozen and stored at -80°C until analyzed. The effect of waiting time on the cell quality was assessed by the RQ described above. The results did not reveal any significant changes in gene expression between selected time-points (*one-way* ANOV*A*, p-value = 0.20) (Figure 5). The highest signal was obtained with cells that were processed immediately (mean RQ = 4.27). For the remaining groups the mean RQ was observed between 3.04 and 3.56. Variation within the group data points was considerable, as individual groups recorded CVs of 29.7 %, 58.8 %, 44.7 %, 44.5 % and 28.6 %, respectively.

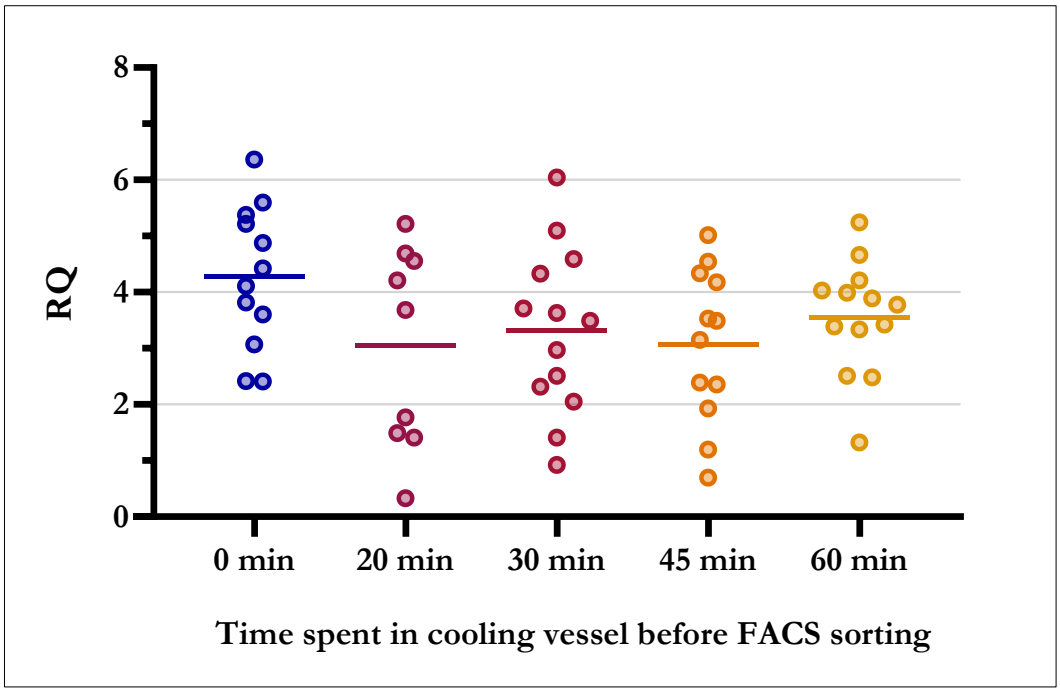

Figure 5 ***Resting in cooling vessel preceding FACS sorting does not compromise sample quality.*** *The plot reports on the effect of waiting time for FACS sorting on the quality of cell's gene expression profile. Individual dots represent individual single cells (collected n = 13 per group); color-adjusted line reports mean RQ per group.*

The design of previous experiment allowed to freeze single cells immediately after the collection which took just few seconds. However, in real settings, when low-abundant cells are sorted, the time period between the first and last cell is collected may take several minutes or longer. During this period, RNA released from lysed cell is unprotected and vulnerable to degradation. To assess the level of potential RNA degradation, we sorted 13 astrocytes which we kept for different time on ice before storing them at -80°C. Statistical testing did not reveal significant effect of waiting on ice after FACS sorting (*one-way* ANOVA, *p*-value = 0.597), hinting no major force being at play. Group mean RQs occupied range from 2.16 to 3.10. More noticeable was the substantial variation of every group, with reported CVs starting at 31.1 % (120 min) and ending at 56.9 % (15 min).

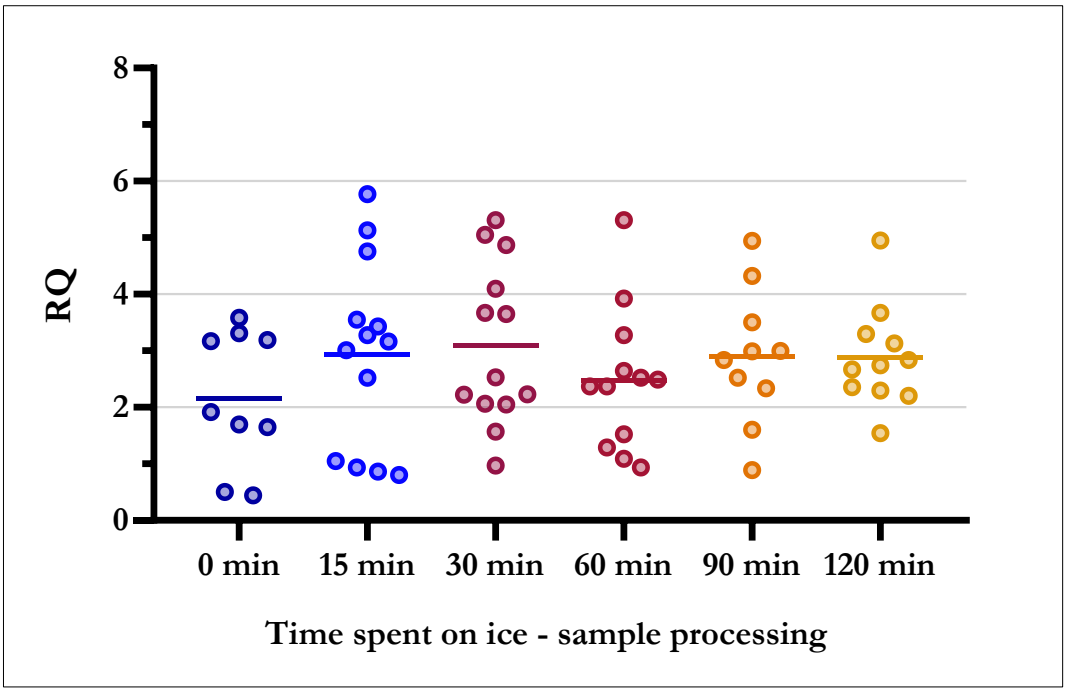

Figure 6 ***Storage of collected single cells on ice sufficiently protects RNA from degradation.*** *The plot displays the effect of keeping single cells on ice after FACS collection. Individual dots represent individual single cells (collected n = 13 per group); color-adjusted line reports mean RQ per group.*

Not all cells collected and stored in a single plate are always processed concurrently. This means that some cells are repeatedly thawed and frozen, which may leave a mark on cell's quality. Thus, we investigated the role of repeated freezing and thawing on the gene expression profile, where samples were kept at dry ice for one minute and then thawed at room temperature for one minute. The results did not reveal substantial effect of the repeated freeze and thawing of the sample (*one-way* ANOVA, *p*-value = 0.164). Despite the statistical insignifance, it is worth of highlighting the lowest RQ of 2.24 combined with enormous CV = 76 % for 12 repeated freeze-thawing cycles. RQ values were highest for 4 and 8 cycles with 3.64 and 3.41, while concurrently with the lowest variation of 31.8 % and 26.8 %, respectively.

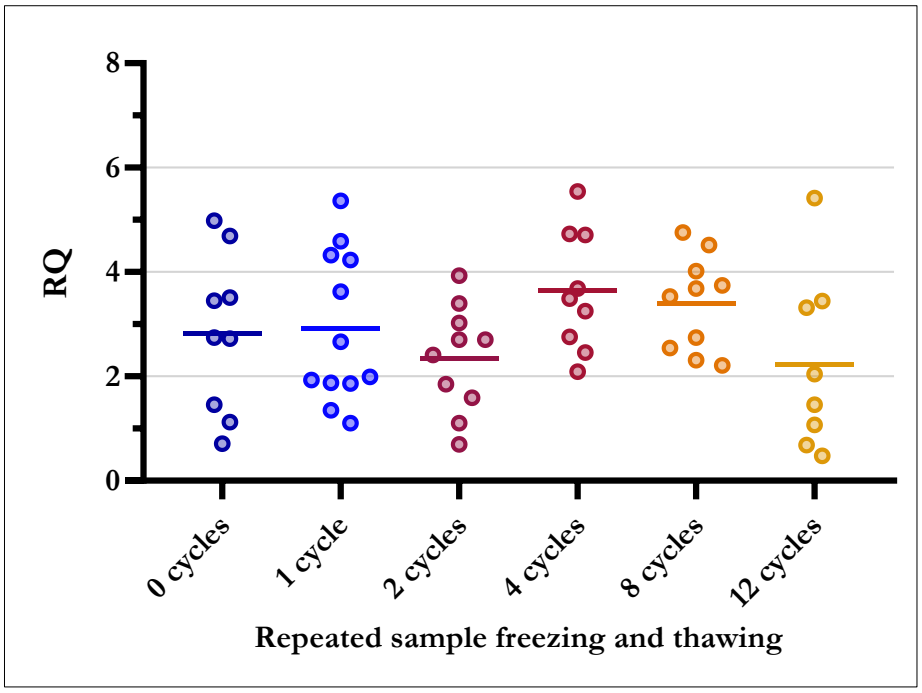

Figure 7 ***Repeated freezing and thawing of collected single cells do not have substantial impact on the quality of cell's material.*** *The plot depicts the influence of repeated sample freeze-thawing on the sample quality. Individual dots represent individual single cells (collected n = 13 per group); color-adjusted line reports mean RQ per group.*

5.2 *Direct lysis of small bulk samples*

Direct cell lysis is an efficient approach in the single-cell experiments, as the RNA extraction was shown to suffer of low efficiency causing substantial loss in sensitivity (Svec *et al.*, 2013). This stands true also for analysis with limited number of cells. In such situation, direct lysis may represent an interesting alternative to traditional extraction protocols. However, compared to analysis of a single cell, there is a risk of increasing concentration of RNases and inhibitors being released from the lysed cells that may affect the quality of the data. To investigate the capacity of the direct lysis method, we sorted increasing number of cells into 5 ul of lysis buffer (NFW + 1 mg/ml BSA) and measured the signal of three endogenous transcripts (*Slc1a3*, *Aqp4*, *Actb*) directly in the lysed material. We started from a single cell, then increasing by two-fold up to 2048 cells per reaction well (n = 6 for one to 8 cells, n = 3 for 16 to 2048 cells). Cqs were averaged per replicates, and then RQ was calculated (Equation 1).

Considering the ambiguity and the rate of positive reactions on the bottom end of the dynamic range, it can be commented that the reactions perform substantially well. After averaging assay RQ per sample, in the range from 1 to 256 cells the least well-performing were

templates of 8 and 16 cells being down by 32 % and 48 % from the expected value (dashed line in the Figure 8). Considering the variance between replicates, 256 cells were the most robust reaction being just 2 % below the expected value. Inhibition due to high cellular content became noticeable for reactions counting 512 and more cells. The most concentrated sample with 2048 cells reported only 4 % of the expected signal.

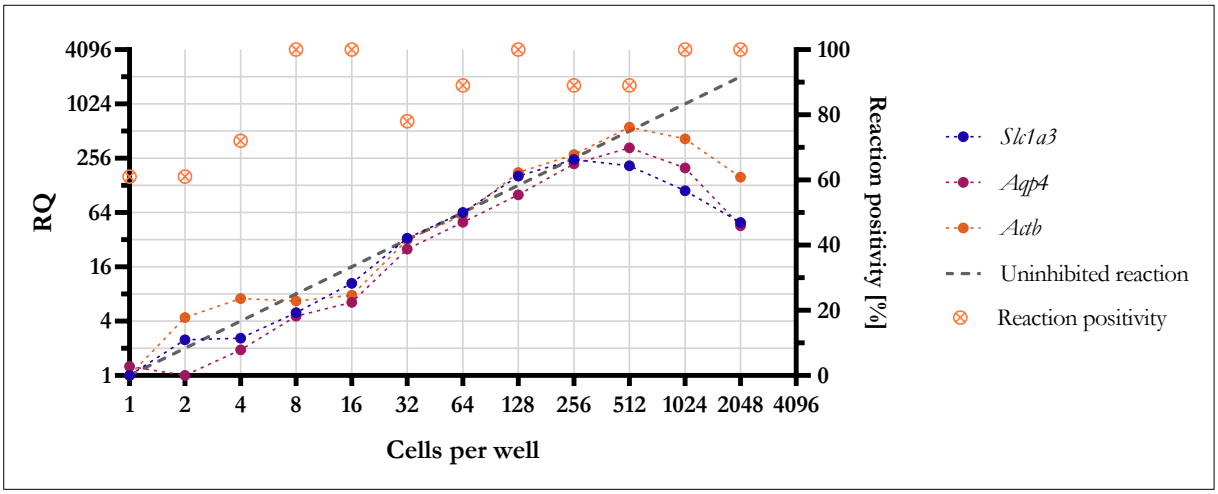

Figure 8 ***Up to 256 cells can be directly processed without the RNA extraction.*** *The plot shows the relation between the quantified signal and number of cells that were processed by the direct lysis (n = 6 for 1 to 8 cells, n = 3 for 16 to 2048 cells). Reactions starting at 512 cells began to be inhibited by cell's contents. The right Y axis reports on the reaction positivity. Dashed line presents the expected RQ for uninhibited reactions. The data for all samples were processed collectively, meaning the signal should double (or quadruple etc.) as the number of cells doubles (quadruples) since they were calculated relative to the least expressed sample (single cell per well). The x and left y axis were converted to* $\log_2$ *scale.*

5.3 Quality control of the collected single cells

Despite the unquestionable power of FACS, presence of an individual cell within the reaction well can not be blindly relied on. It is important to check for the material's quality, as the cell could have been e.g. sorted onto the side of reaction well and dried out or wrong cell type may be collected. Preceding the final qPCR itself, the expression of typical marker genes for given cell types may be controlled as well as the expression of genes that should be detected in the majority of cells and reflect overall cell quality. This simple selection procedure helps to reduce total experimental costs and provides higher data quality (only high-quality cells of interest are selected and analyzed). Typically, the expression is measured immediately after RT, but for the increase in sensitivity and reduction of false negativity preamplified cDNA may be used as well.

In the core of our biological interest were exclusively astrocytes that were sorted using GFAP/EGFP transgenic mice allowing for visualization of astrocytes due to expression of EGFP protein under GFAP promoter. Although *Gfap* gene is a canonical marker of astrocytes, also other cell types, particular NG2 cells, may be collected using this mouse model (Rusnakova *et al.*, 2013). To avoid the analysis of this cell type, we routinely measured expression of four markers in each cell before subsequent analysis – *Gja1* (astrocyte marker), *Cspg4* (NG2 cells), *Vim* and *Slc1a3* (commonly expressed in astrocytes, but also in other cell types). An exemplary quality control result of the experiment described in detail in *High-throughput RT validation* section material is displayed in Figure 9. Reactions positive for *Cspg4* were assigned value + 0.5 (red) and *Gja1* positive were assigned +1 (orange). Two remaining assays served as quality controls for selection of the most viable cells. Noticeable difference in the rate of cells of interest between the Figure 9A and B illustrates the importance of this quality control that minimized the unwanted analysis of samples of low quality or cells that are not the object of the study and thus improve the overall effectiveness of the experiment.

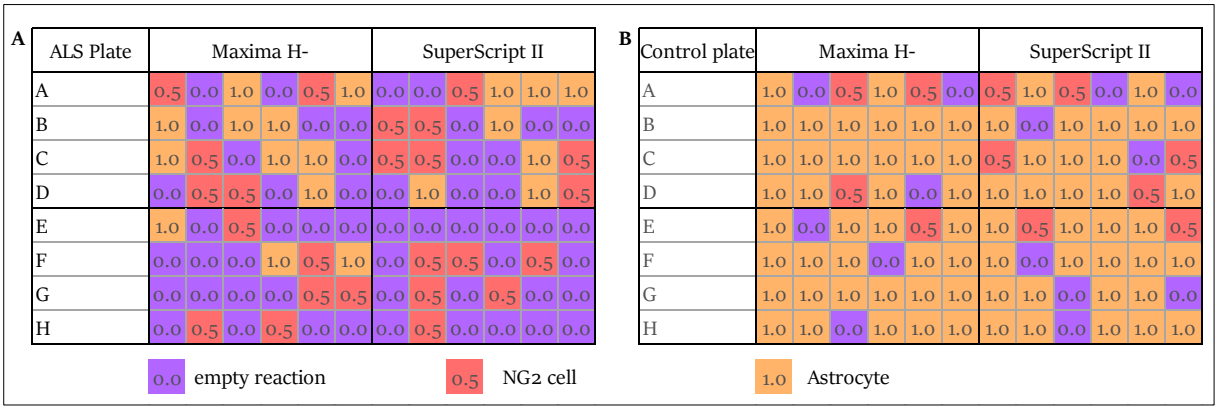

Figure 9 ***Quality control screening for the cells of interest.*** *96-well plates of FACS-sorted astrocytes were reverse transcribed using two different RTases, preamplified and screened for the astrocytes (Gja1), NG2 cells (Cspg4) and cells/samples of low quality. (**A**) Single cells sampled from a mouse with induced ALS. (**B**) Single cells sampled from a healthy control mouse.*

5.4 Comparison of reverse transcriptases for single-cell application

RT represents a critical step in the scRT-qPCR workflow (Ståhlberg, 2004; Ståhlberg *et al.*, 2004; Tichopad *et al.*, 2009; Bustin *et al.*, 2015). As discussed above, any RNA molecules that fail to be initially captured will be missing in the final data. Therefore, the selection of the RTase with high performance is undoubtly an important step in every study. However, thorough comparison of

RTases in low-RNA content applications was missing. In this thesis, we decided to fill the gap and benchmark a broad spectrum of currently available RTases for single-cell experiments. Comprehensive insight on the RTase was obtained by their benchmark on template concentrations regularly employed in scRNA-Seq experiments (*RTase benchmarking* section) (Figure 10A). To further validate the findings and their robustness, the performance of two selected RTases was examined in a conventional single-cell model experiment (*High-throughput RT validation* section) (Figure 10B).

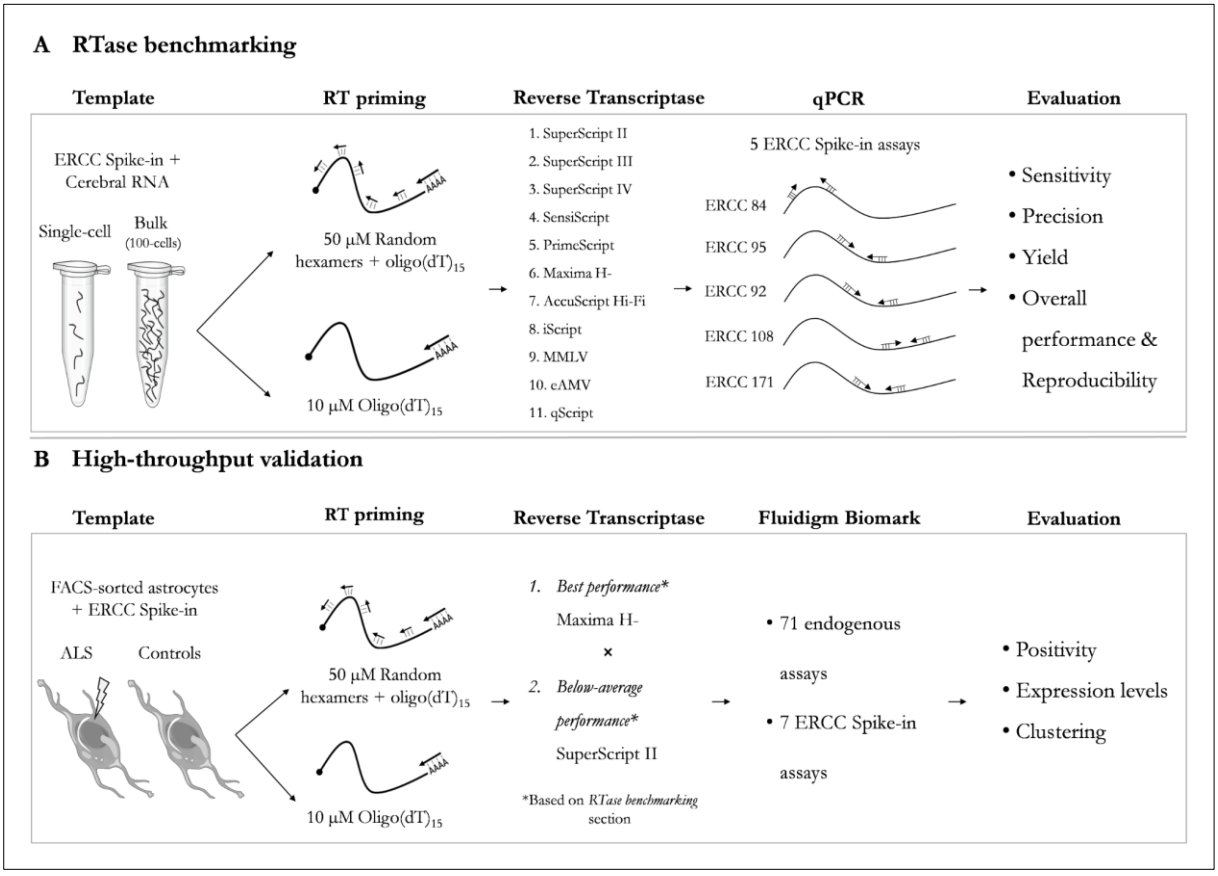

Figure 10 ***Experimental design of the RTase performance comparison in the single-cell reaction setup.***

5.4.1 RTase benchmarking

11 RTases were run in parallel on two priming strategies: i) RT primers mixture (common for RT-qPCR) or ii) oligo(dT)s (common for RNA-Seq). Their performance was assessed on five well optimized assays (*5.6 Quantitative PCR validation* section) targeting spike-in transcripts mimicking the spectrum from rare to highly abundant transcripts on samples corresponding to single cells and 100-cell bulks (Table 3). We characterized the RTases in terms of sensitivity, precision, yield, and reproducibility.

Sensitivity

RTases' ability to capture and successfully reverse transcribe template molecules were classified by counting the rate of positive reactions for assays of low (*ERCC 84*) and medium (*ERCC 95*) abundancy. Reactions were regarded positive upon quantification of specific qPCR signal. Reactions were deemed negative if i) no signal was acquired, ii) the signal was unspecific (melting curve analysis), or iii) measured Cq > 40 (Cq cutoff). RT priming strategy and RTase itself were the main influencers of reaction sensitivity.

Medium abundant template *ERCC* 95 present at 88 molecules per RT recorded modest differences between priming strategies (Figure 11A). 80 % reaction positivity rate was reported for 9 out of 11 RTases with both priming strategies. Out of the two remaining RTases – SuperScript II and eAMV, only the latter reported less than 50 % positive reactions.

Four times less abundant template of *ERCC 84* counting 22 molecules per RT proved to be a tougher nut to crack (Figure 11B). Median positivity rate across all RTases was 30 %. The best results were acquired with SuperScript IV and Maxima H- when primed with RT primers mixture scoring positivity rates of 90 %. With oligo(dT) priming their sensitivity decreased to ~45 %. Similar sensitivity halving due to the priming strategy was observed for SuperScript III. Notably, SuperScript II recommended in some RNA-Seq protocols (Picelli *et al.*, 2014; Hashimshony *et al.*, 2016) reliably reported only ~20 % of the reactions at the limiting concentration. The only AMV-derived RTase in the comparison, eAMV, failed to deliver any positive reactions.

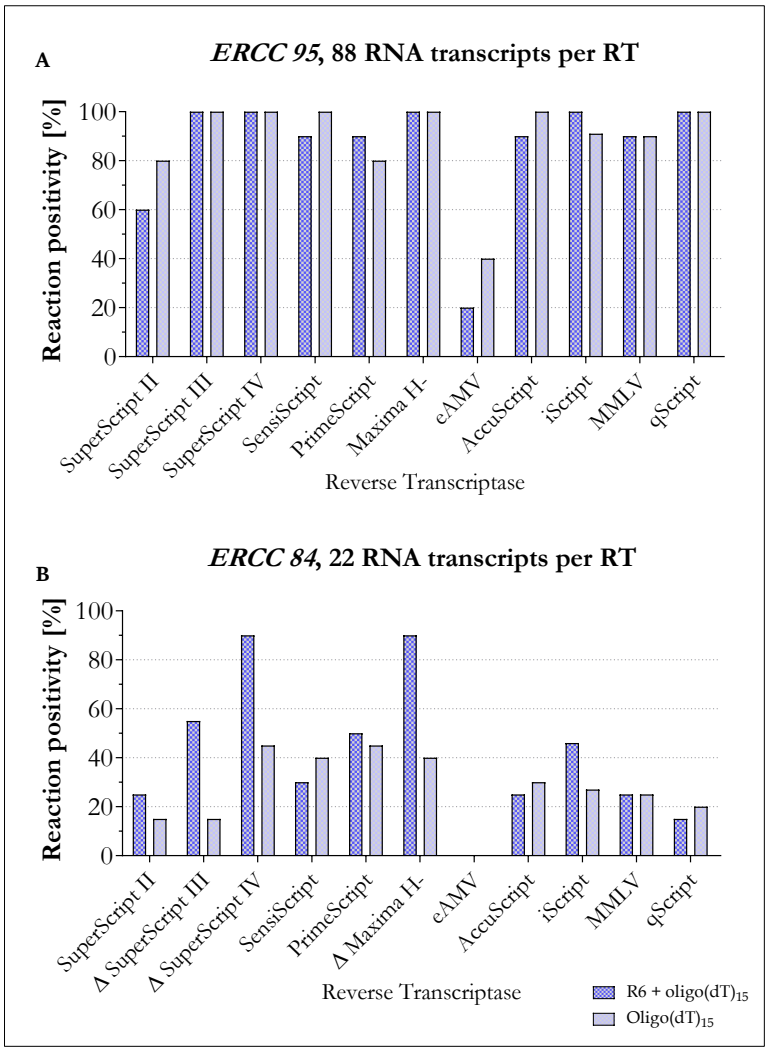

Figure 11 ***Sensitivity of the reaction is profoundly influenced by the choice of RTase and priming strategy.*** *RTases denoted with "Δ" doubled their rate of positive reactions with RT primers mixture. (**A**) Reaction positivity for medium abundant template (n = 10 reactions per RTase). (**B**) Reaction positivity for low abundant template (n = 20 reactions per RTase).*

Precision

Reliable and unbiased RT outcome is critically important in every study. Inconsistent RT efficiency at any template concentration could lead to false conclusions. The precision of RTase functioning was investigated over a wide concentration range; coupling of single-cell and 100-cell measurements enabled to plot RNA-molecule concentration (22 to 282,000 specific ERCC Spike-in copies per RT chamber) versus qPCR-estimated cDNA concentrations. Absolute cDNA concentrations were calculated using Equations 2 and 3, accounting for assay-specific efficiencies. The R^2 evaluated dispersion of the data points along the linear fit.

All studied RTases reported substantially precise performance with both priming strategies (two representative RTases shown in Figure 12; results for remaining RTases are listed in **Precision-linearity**, *Attachment 1*). R^2 for the RT primers mixture ranged from 0.9463 to 0.9896, whereas with oligo(dT)$_{15}$ priming the values ranged from 0.9445 to 0.9825. Reproducibility among RT replicates substantially varied between single-cell and bulk templates (Figure 13). Despite it, the performance remained linear for the given RNA input range. Among the RTases, cDNA copies per single-cell reaction varied in median by 40.06 % (CV_{RT}), whereas for bulk samples the median variation settled at lower CV_{RT} = 10.27 %. In single-cell conditions, Maxima H- and SuperScript IV were the most reproducible enzymes with median CV_{RT} = 29.15 % and 30.25 %, respectively (Figure 13A). The least reproducible RT was recorded for SuperScript II (CV_{RT} = 53.65 %). In conclusion, although RT reproducibility decreases with template concentration, RT retains overall precision even at single-cell level.

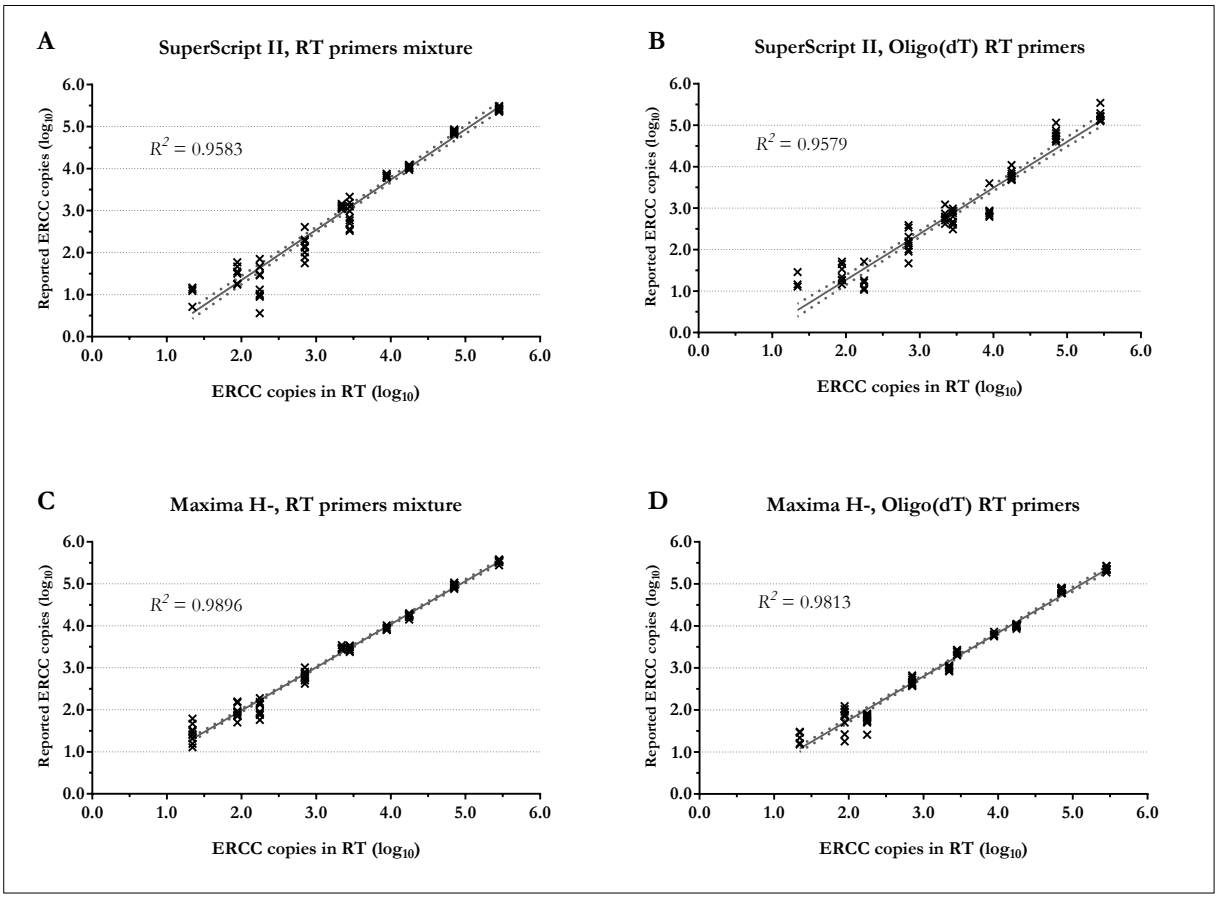

Figure 12 ***RT works with substantial precision even at single-cell conditions.*** *Linear regression plots reporting log_{10}(reported ERCC copies) versus log_{10}(input ERCC copies) for SuperScript II and Maxima H- using RT primers*

mixture and oligo(dT) primers. Graphs display the best linear fit and its 95 % CI. R^2 reflects the quality of fitted regression line. Reproducibility decreases for lower template concentrations.

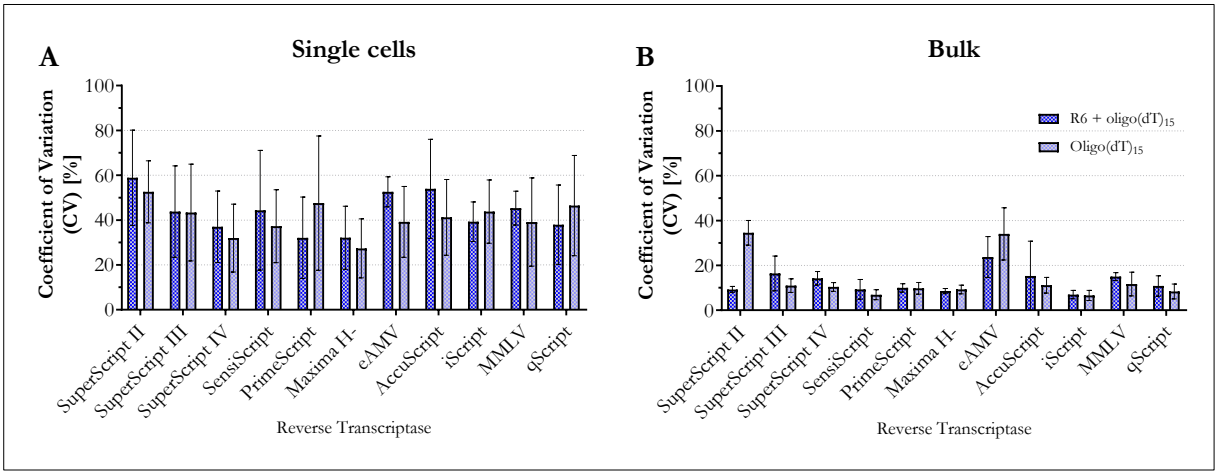

Figure 13 ***Estimates for assessing cDNA copy numbers are substantially more precise for bulk samples.*** *Bar plots show the average CV_{RT} among the five ERCC Spike-in assays for the exact cDNA copy number estimate. The error bars display SD of the mean.*

Yield

In ideal scenario the reaction would come close to 100 % yield value; however, previous studies have shown that the actual rate varies substantially (Ståhlberg, 2004; Levesque-Sergerie *et al.*, 2007; Miranda and Steward, 2017). Absolute yield values were quantified due to use of ERCC Spike-ins and DNA standards, building on top of the known target copy numbers per reaction (Equation 2 and 3).

Significant yield differences were observed between RTases and priming strategies (*two-way* ANOVA, $p_{RTase} < 0.001$, $p_{priming} = 0.005$ and $p_{interaction} < 0.001$ for single-cell template; $p_{RTase} < 0.001$, $p_{priming} < 0.001$ and $p_{interaction} < 0.001$ for bulk template). To explore the studied effect of RTase respectively, dataset was halved by priming strategies and *one-way* ANOVA was applied. Individual differences between RTases were identified by Tukey post-hoc multiple comparison test (Tukey HSD). Letter coding partitions the RTases into subsets based on the magnitude of their performance differences (Figure 14).

For the single-cell template, the effect of RTase was more dominant for reactions primed with RT primers mixture (*one-way* ANOVA, $p < 0.001$, explained variation – $R^2 = 0.8212$) as

compared to polyA-targeted priming (*one-way* ANOVA, $p < 0.001$, $R^2 = 0.6657$). The most efficient RTases with RT primers mixture (Figure 14A) were SuperScript IV, Maxima H- and SuperScript III with the average yields of 125 %, 102 % and 88 %, respectively. Yields over 100 % are feasible for RTases with the strand displacement activity, producing multiple cDNA copies from a single RNA transcript. The lowest yields with RT primers mixture were recorded for SuperScript II and eAMV – 24 % and 7 %, respectively. With polyA priming, no RTase clearly surpassed the others (Figure 14B); SuperScript IV and Maxima H- recorded the highest (71 % and 66 %, respectively) and eAMV the lowest yield (14 %).

With bulk samples, SuperScript IV and Maxima H- repeatedly reported the highest yields of 138 % and 118 % with RT primers mixture, respectively (Figure 14C). The lowest yields with RT primers mixture were conceded to MMLV and SensiScript enzymes (44 % and 43 %), respectively. For oligo(dT) primed reactions the differences were more modest; Maxima H-, SuperScript IV, SuperScript III and qScript ended up as top scorers yielding 71 %, 67 %, 67 % and 66 %, respectively (Figure 14D). The least yielding result was reported by SensiScript (40 %). Akin to the single-cell data, differences between RTases were more prominent with RT primers mixture (*one-way* ANOVA, $p < 0.001$, $R^2 = 0.9319$) than with oligo(dT)s (*one-way* ANOVA, $p < 0.001$, $R^2 = 0.674$).

For the most conditions, RTases with the highest cDNA yields were SuperScript IV and Maxima H-. On the contrary, eAMV was found to retrieve the least cDNA per reaction. Use of RT primers mixture in some cases resulted in absolute yields over 100 %, while with oligo(dT)s the yield was capped around 75 %.

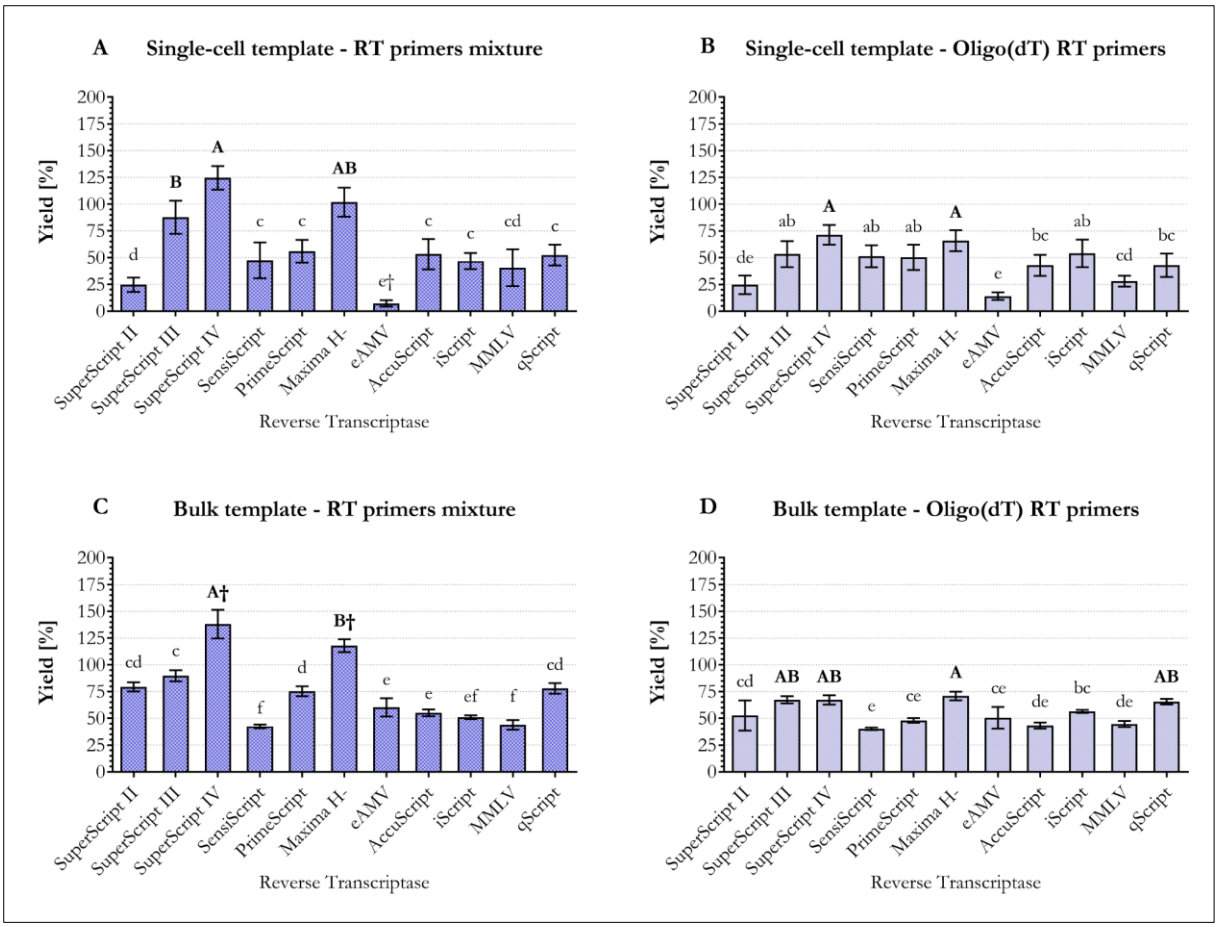

Figure 14 ***Reaction yield is dependent on the choice of RTase and priming strategy.*** *Bar plots show average yield per 10 RT replicates (1 RT replicate = average yield across five assays) with 95 % CI. Letters indicate the differences between RTases, with the highest value in bold. Subsets of RTases that were insignificantly different are labelled with the identical letter (one-way ANOVA, $p < 0.05$, Tukey HSD). "†" marks subsets that consisted of single RTase only.*

Performance reproducibility

Generalized comparison of RTase performances, relative between each other and independent from transcript abundancy, was effectively carried out by the data Z-score scaling:

$$Z = -\frac{Cq - Cq_{AV}}{SD_{AV}} \qquad (Equation\ 5)$$

where Cq was the actual Cq; Cq_{AV} was the average Cq across 11 RTases and 10 RT replicates specified by combination of an assay, template concentration and priming strategy; SD_{AV} was calculated from the identical set of Cqs as Cq_{AV}. Z-score boxplots (Figure 15) display general RTase performance (higher Z-score indicates better performance), as well as the reproducibility of such result (spread of values). RTase' Z-score = 1 indicates that its Cq was repeatedly lower

by the size of one standard deviation from dataset average. For graphing purposes, the results were combined by priming strategies.

Mutual comparison between RTases unveils the dominance of SuperScript IV and Maxima H- (Figure 15). With single-cell template, a median Z-score of 0.99 (interquartile range: 0.78 – 1.25) and 0.84 (0.59 – 1.09) was documented for SuperScript IV and Maxima H-, respectively. For bulk measurements the SuperScript IV and Maxima H- produced a median Z-scores of 1.27 (0.94 – 1.62) and 1.18 (0.95 – 1.43), respectively. The generally lower performance of eAMV and SuperScript II at single-cell level is reported by median Z-scores of -1.58 (-2.21 – -1.02) and -0.74 (-1.59 – -0.23), respectively.

Performance reproducibility varied significantly between tested RTases (*classical Levene's test,* $p < 0.001$ for both templates). The most reproducible results with single cells, measured as Z-score interquartile range, were recorded for SuperScript IV, Maxima H- and PrimeScript (Figure 15A). With bulk samples, SensiScript, Maxima H- and AccuScript were the most robust performers (Figure 15B). Five RTases were found to report less reproducible performance in single-cell conditions (indicated with "*" in Figure 15; classical Levene's test, $p < 0.05$, adjusted with Bonferroni's correction).

In summary, the RTases substantially varied in their performance and reproducibility. Among the benchmarked RTases, Maxima H- and SuperScript IV were repeatedly superior to their counterparts. In the light of these results, they are the most suitable candidates for low RNA input applications for a wide range of reaction conditions.

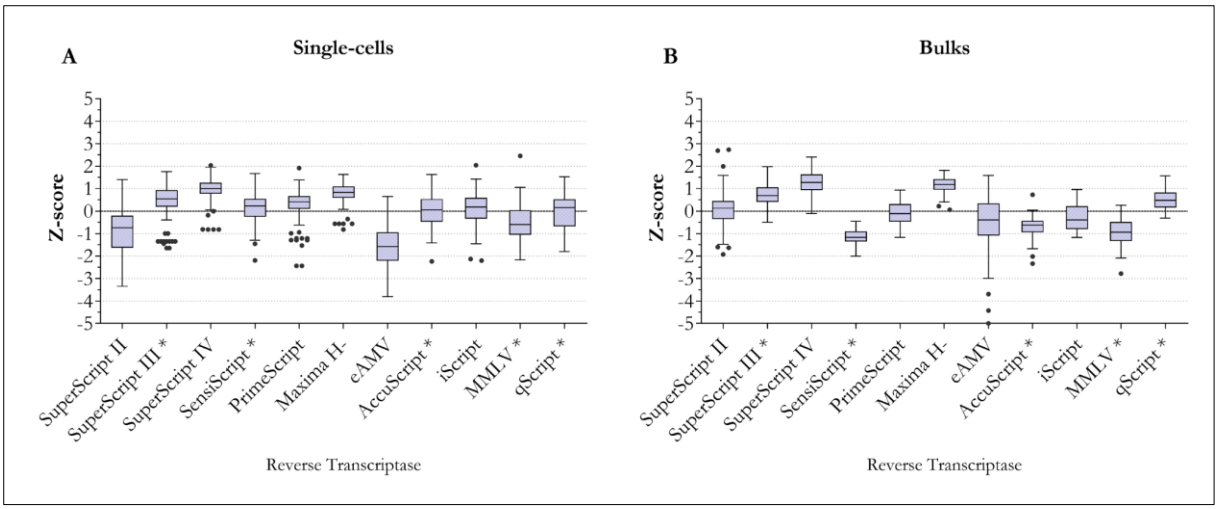

Figure 15 ***Best performing RTases retain high-level performance even in single-cell conditions.*** *Z-scores inform on the reproducibility and overall relative performance of RTases in single-cell* ***(A)*** *and 100-cell reactions* ***(B)****. Enzymes denoted with "*" were significantly less reproducible with single-cell samples than with bulks (Levene's test). Performance of the highest-scoring RTases was consistent.*

5.4.2 High-throughput RT validation

The benchmarking classified 11 RTases based on their performance. Main factors holding back applicability of the benchmarking results are quantification of a synthetic template (ERCC Spike-in) and limited number of assays. In continuation, two RTases were further evaluated, Maxima H- and SuperScript II, in a routine high-throughput scRT-qPCR profiling experiment based on 78 assays (Figure 10B). These candidates were selected due their performance (best- vs. below-average performer) and their enrollment in scRNA-Seq protocols (Picelli *et al.*, 2014; Macosko *et al.*, 2015; Hashimshony *et al.*, 2016; Ziegenhain *et al.*, 2017; Bagnoli *et al.*, 2018). In consistency with the previous section, two priming strategies (RT primers mixture and oligo$(dT)_{15}$) were used. FACS-sorted astrocytes from healthy and ALS mouse brains were used as single-cell samples. 15 control and 5 ALS cells were then analyzed with each combination of RTase and priming strategy (Figure 10B). Three metrics were assessed – reaction positivity, expression levels and cluster separation.

Reaction positivity and expression levels

Positive reactions were identified identically as in *Sensitivity* section – only specific qPCR reactions were counted. Maxima H- totaled 42.9 % positive reactions when counting across all assays and both priming strategies; on the contrary, SuperScript II reported 36.1 % reactions as

positive (**Reaction positivity and RQs (High-throughput RT validation)**, *Attachment 1*). More informative insight is delivered when comparing RTase' performance separately for every assay. With RT primers mixture, Maxima H- had higher reaction positivity than SuperScript II for 55 % of the assays (on average, there were 12 % more positive reactions per assay); same positivity rate was found for 25 % of the assays and SuperScript II prevailed for 20 % of the assays (average increase by 10 % per assay) (Figure 16A). The difference in reaction positivity between the enzymes widened when oligo(dT) primers were used. Maxima H- provided more positive reactions for 74 % of the assays (on average 14 % more positive reactions per assay), while SuperScript II recorded more positive reactions just for 9 % of the assays (average increase by 13 % per assay) (Figure 16D). The remaining 17 % assays had equal positivity rates with both RTases.

Aside reaction positivity, the measured quantity (reflected by the Cqs) is similarly affected by the RTase and priming strategy. An RTase eventually delivering stronger signal is more favourable in both qualitative and quantitative applications. The expression data were examined as RQs. For both priming strategies Maxima H- obtained significantly higher expression levels (Wilcoxon signed rank test, $p < 0.001$) (Figure 16B, E). Mean RQ for reactions primed with RT primers mixture reached 1.81 for Maxima H- and 1.50 for SuperScript II, whereas when primed with oligo(dT)s the mean RQs were 1.86 and 1.31 for Maxima H- and SuperScript II, respectively. The difference in the number of assays included in the test confirmed the observation of *5.4.1 RTase benchmarking – Sensitivity*, as oligo(dT) reported fewer positive reactions, potentially missing out on the most rarely expressed genes.

Clustering

High-throughput gene expression experiments are typically analyzed using multivariate statistics (Ringnér, 2008; Bergkvist *et al.*, 2010; Riedmaier and Pfaffl, 2013; Ståhlberg *et al.*, 2013). RTase' influence on the separation of different cell treatments was investigated by PCA onto autoscaled $\log_2$-scaled RQs (Figure 16C, F). The RTase effect can be readily quantified by the Euclidean distances between the two cluster's centroids. Maxima H- separated clusters further apart that SuperScript II with both priming instances. With RT primers mixture, the cluster distance was ~20 % greater (6.79 to 5.68 scores), and with oligo(dT)s the clusters were

separated ~60 % further (7.52 to 4.64 scores). Next, RDA quantified the significance RTase had in the cell separation/cluster formation. Low values of explained variability (R^2) described the RTase effect as minor contributor to the cell separation, the choice of RTase was regarded significant for both priming strategies (*RDA – covariate: enzyme;* $p = 0.036$, $R^2 = 0.0386$ for RT primers mixture and $p < 0.001$, $R^2 = 0.0825$ for oligo(dT)s). As expected, the main observed contributor to cell separation was the cell condition (control vs ALS) – with RT primers mixture the reported variability was of $R^2 = 0.241$ and with oligo(dT)s an $R^2 = 0.28$ (*RDA – covariate: cell treatment*).

In summary, the high-throughput experiment demonstrated the importance of employing better performing RTase in a routine single-cell study as well as validated the previous findings obtained on the synthetic RNA template. The better-performing RTase obtained higher positivity rates and robust signals, as well as substantially contributed to better separation of two distinct cellular populations.

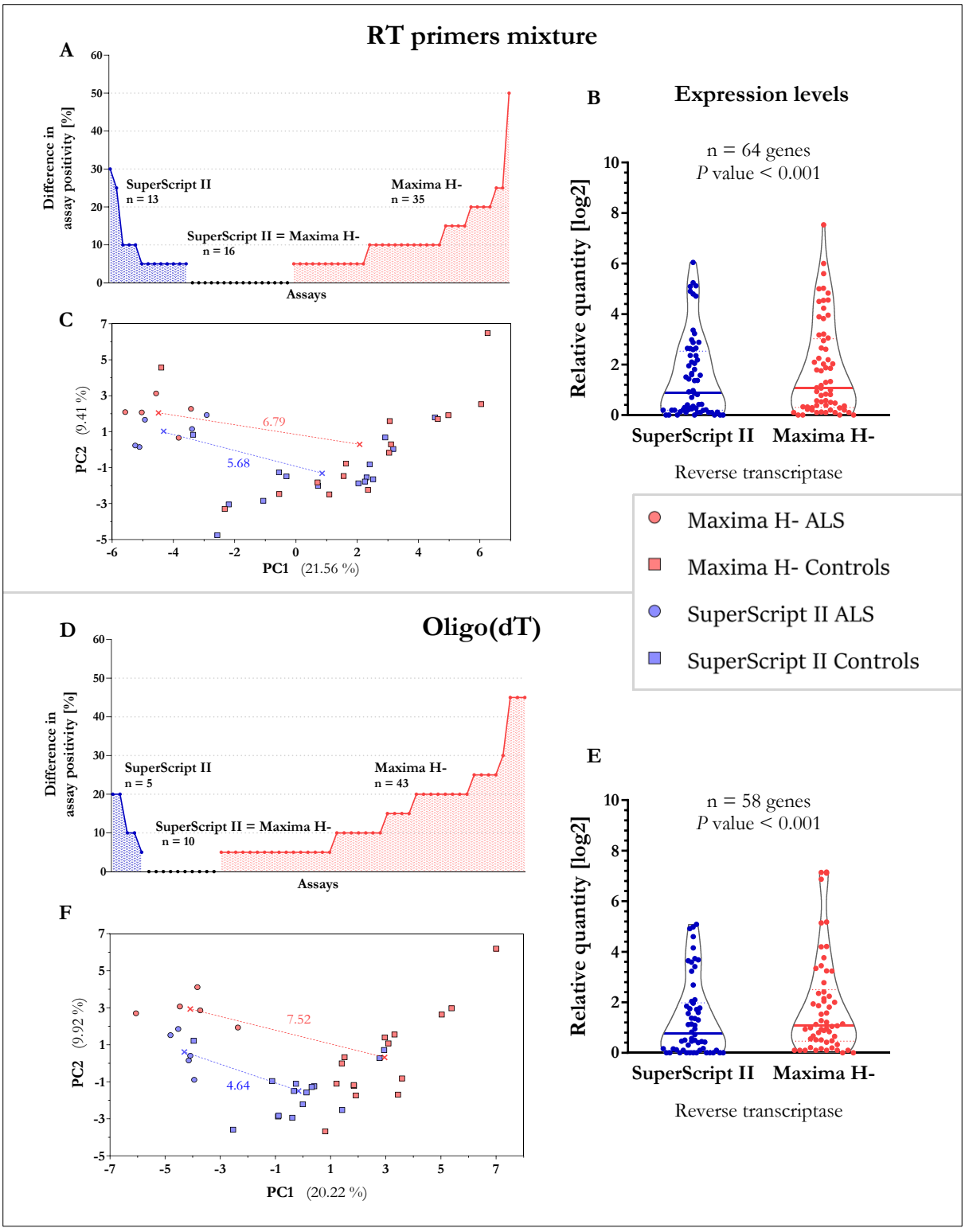

Figure 16 ***Maxima H- significantly improves experiment resolution.*** *The RTase influence is observable for a diverse list of metrics.* ***A,D*** *- increased RT-qPCR reaction positive call rate;* ***B,E*** *– Higher expression levels; Violin scatterplots, thick middle line depicts median;* ***C,F*** *– Maxima H- separates clusters of control (n =15 per group) and diseased cells (n = 5 per group) better than SuperScript II. Brackets inform on PC accounted variance. Cluster centroid is shown in the color-adjusted cross.*

5.5 Preamplification validation

The role of preamplification step in scRT-qPCR workflow is somewhat overlooked, as its parameters were investigated in a judicious detail on bulk samples (Andersson *et al.*, 2015; Korenková *et al.*, 2015; Kroneis *et al.*, 2017). Despite its status of well-established reaction, control of preamplification reproducibility needs to precede any qPCR measurements performed on real samples, especially when a new preamplification primer pool is prepared *(5.5.1 PreAMP quality control* section). Although various parameters of preamplification were thoroughly examined, a single aspect missed unnoticed - reaction volume. However, this parameter may have several consequences, primarily on the cost of the experiment (smaller volumes are more cost-efficient) and sensitivity to amplify and consequently detect less abundant targets (larger volumes allow preamplification of higher cDNA proportions and are less prone to the reaction exhaustion). The finding of the optimal ratio was the goal of the *5.5.2 PreAMP volume* section.

5.5.1 PreAMP quality control

For the high-throughput validation of RTases performed above (*5.4.2 High-throughput RT validation* section) and analysis of ALS astrocytes decribed below (*5.7 ALS-induced change in astrocytic gene expression* section), new experiment-specific pools of 96 primers were prepared (**Primer sequences**, *Attachment 1*). Here, only the validation data for the first pool are reported for illustrative purposes.

The quality control consisted of calculating ΔCq, a difference in the Cq signal between nonpreamplified and preamplified cDNA. Three samples of extracted RNA were reverse transcribed and then preamplified in two parallel reactions. ΔCq was acquired by subtracting the average Cq of the two preAMP reactions from the Cq of nonpreamplified sample. The quality control was measured on assays of either biological relevance or due to their abundancy – high (*Actb*, *Ywhaz*), medium (*Glul*, *Aqp4*, *Kcnk1*, *Vim*) and low expressed (*ERCC 25*) genes were measured. The mean ΔCq and standard deviation of ΔCq ($SD_{\Delta Cq}$) of the three samples is plotted in the Figure 17. Although some differences are observable in absolute ΔCq, the $SD_{\Delta Cq}$ are low – 0.16 (*Glul*), 0.03 (*Aqp4*), 0.10 (*Kcnk1*), 0.09 (*Vim*), 0.32 (*Actb*), 0.15 (*Ywhaz*) and 0.32 (*ERCC 25*), indicating high reproducibility of the preamplication.

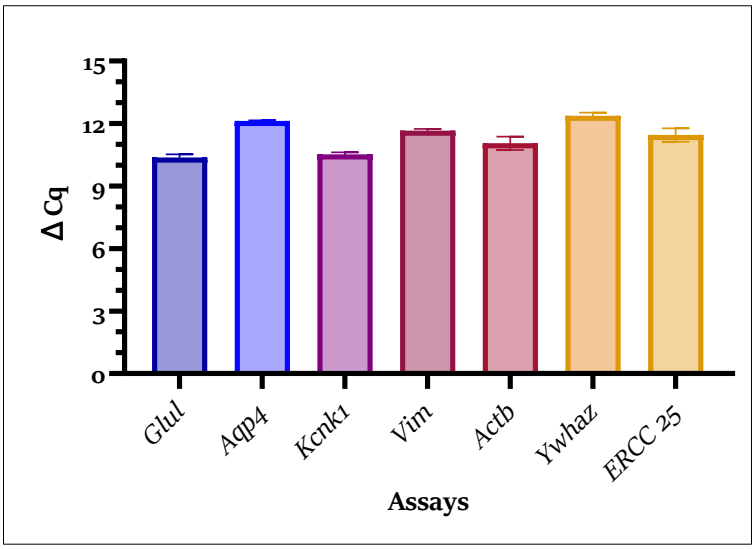

Figure 17 ***Selected assays representing high, medium and low expressed genes highlight highly reproducible preAMP conditions.*** *Barplot depicts average ΔCq, calculated as difference between nonpreamplified and preamplified sample (n = 3), with SD for error bars. Keeping the preAMP reproducibile (low SD) is more important than obtaining comparable ΔCqs, since the absolute difference in ΔCq is later deleted by transformation of the Cqs into RQs.*

5.5.2 PreAMP volume

The effect of varying preAMP reaction volume (10,20 and 40 µl, respectively) was investigated on single cells (n = 6) and 100-cell bulks (n = 4) by reporting the percentage of positive reactions per assay (sensitivity) and the signal strength (RQ). Only assays with more than 20 % positive reactions per sample concentration (67 – single cells, 92 – bulk samples) were included in the analysis of signal strength. This cutoff value should negate the technical noise due to relatively small sample size. Noteworthy, even though different preamplification volumes were used, the concentration of the cDNA (mimicking single cells or 100-cell bulk) and subsequent dilution factors were identical for all samples allowing the direct comparison of obtained data.

For single-cells, median reaction positivity per assay was 50 % (10 µl preAMP), 66.7 % (20 µl) and 83.3 % (40 µl) (Figure 18A). As expected, analyzing smaller portion of the cell's content lead to a substantial decrease in the analytical sensitivity. To study the signal strength differences, mean RQs per assay were assessed (Figure 18C). In comparison, median of the mean assay RQs were 1.64 for 10 µl preAMP reaction, 1.82 for 20 µl and 1.84 for 40 µl. Statistical analysis confirmed that the signal strength substantially rose for reactions with higher cell contents (*Friedman rank sum test*, p = 0.027). Further pairwise comparison of Friedman rank

sums confirmed significant difference between 10 µl and 40 µl groups (*Pairwise comparison of Friedman rank sums*, $p = 0.0082$).

For bulk template the differences in the reaction positivity of individual assays were not that pronounced (Figure 18B). Median positivity for all three preAMP volume variables was 100 % (arithmetic means were 91.6 %, 95.4 % and 98.4 % for 10, 20 and 40 µl, respectively). Analytical sensitivity is therefore regarded sufficient even for smaller sample volumes. Median value of the mean assay RQs were 1.56 for 10 µl, 1.5 for 20 µl and 1.36 for 40 µl preAMP reaction (Figure 18D). Friedman rank sum test reported significant differences between the groups (Friedman rank sum test, $p < 0.001$). Pairwise comparison of Friedman rank sums reported significant differences between groups of 10 µl - 40 µl ($p < 0.001$) and 20 µl - 40 µl ($p < 0.001$).

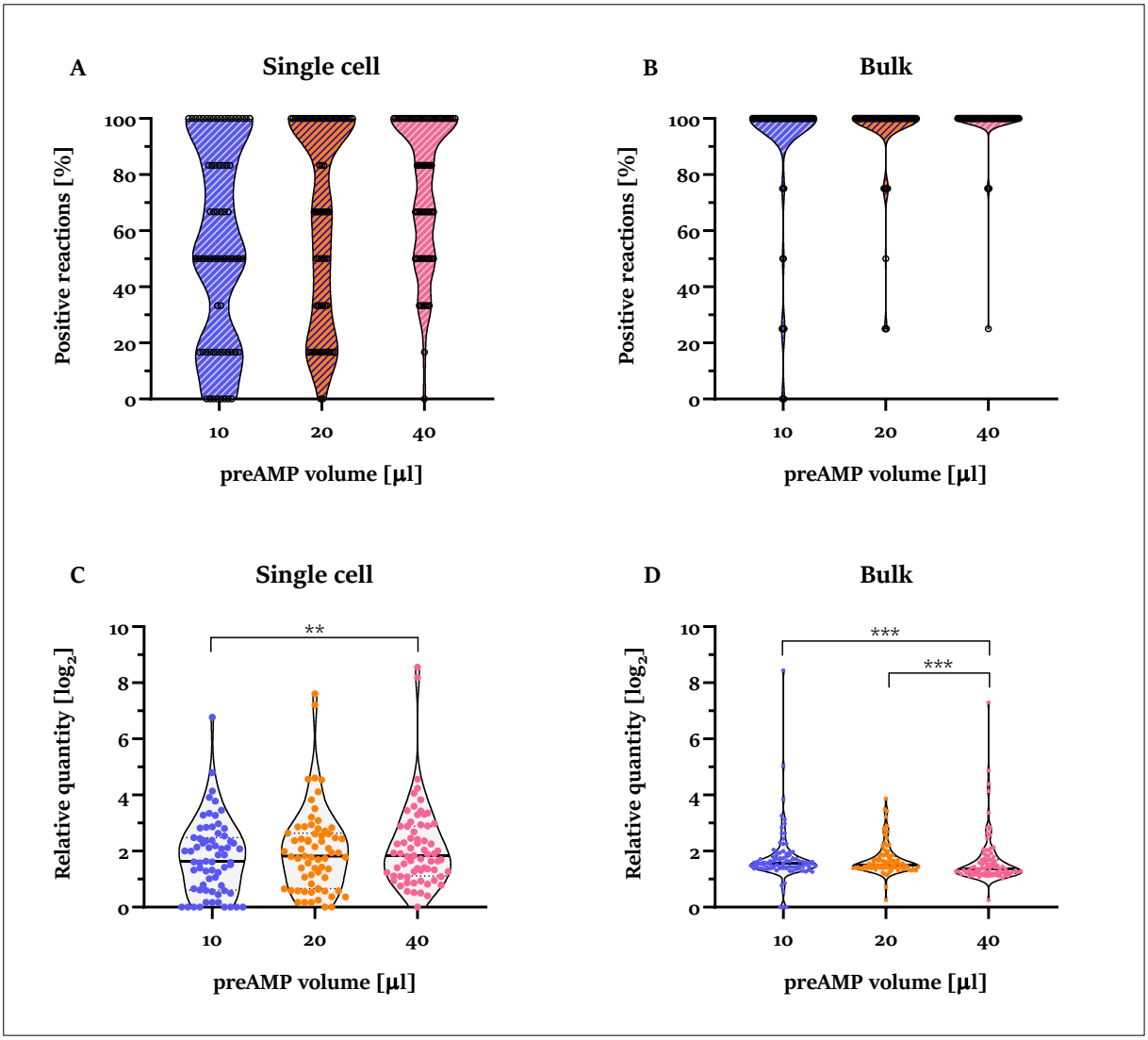

Figure 18 ***Larger preAMP reaction volumes empower the analysis of single-cell samples.*** *(**A**) and (**B**) Violin scatterplots report the percentage of positive reactions per assay (single cells = 67 assays, bulk = 92 assays; individual assays are indicated as clear circles). (**C**) and (**D**) Violin scatterplots report mean RQ per assay. Significantly different groups are indicated by "*" (Pairwise comparison of Friedman rank sums, p < 0.01 "**", p < 0.001 "***"). Individual assays are indicated as full dots, median RQ is indicated by thick middle line and quartiles by thin dotted line.*

5.6 Quantitative PCR assays validation

The data quality can be enhanced also on qPCR level by utilization of thoroughly optimized qPCR assays what further mitigates the introduced technical variability (Tichopad *et al.*, 2009; Lindén, Ranta and Pohjanvirta, 2012). Features of a well-optimized assay are: i) high sensitivity, ii) absolute target specificity and iii) high efficiency. The process of assay optimization typically involved *in-silico* design and wet-lab validation (both decribed in *2.5 QPCR* section). As an

example, the results of wet-lab validation of *ERCC Spike-in* assays used in *5.4.1 RTase benchmarking* section are presented.

The performance metrics of several *ERCC Spike-in* assays were measured on cDNA prepared from ERCC Spike-in supplemented by healthy mouse cerebellum mimicking the complex RNA background; genomic DNA was supplied in amounts resembling expected gDNA-mRNA cell ratio; and three non-template replicates controlled for primer-dimer formation. When reactions mirrored contents of 150-200 cells per RT/qPCR, all five assays obtained Cqs < 30 (Figure 19A-E), being in line with recommendations by Ståhlberg and Kubista (2018). Next, the assays reported absolute specificity to its cDNA target, reflected by single uniform peaks of melting curve analysis (Figure 19F-J). Genomic DNA was not amplified, or the signal was weaker by several orders of magnitude (Figure 19E). Non-template reactions did not form any unspecific products.

The efficiency of individual assays was obtained by performing dilution standard series individually for each assay (see *4.3.6 QPCR validation* section in methods). Individual assay efficiencies were 95 % (*ERCC 84*), 86.3 % (*ERCC 95*), 97.3 % (*ERCC 92*), 96.6 % (*ERCC 108*) and 97.8 % (*ERCC 171*) (Figure 20). When the LoD and LoQ was investigated, the inter-assay differences were better observable. LoD and LoQ for the selected assays go as follows: 5.7 and 6.4 (*ERCC 84*), 5.7 and 100 (*ERCC 95*), 5.7 and 40 (*ERCC 92*), 5.7 and 16 (*ERCC 108*), 5.4 and 6.4 (*ERCC 171*). Interestingly, although all assays achieved similar LoD values, their LoQ differed more profoundly indicating positive influence of higher assay afficiency on the ability of assays to reliably quantified even very low target concentration.

In summary, the assays selected for validation in *5.4 Reverse transcription* section generally showcase excellent performance, as indicated by lack of unspecific products, high PCR efficiency and low LoD and LoQ values. The main drawback among the assays is the considerably high LoQ of *ERCC 95*, which also affected assay's efficiency metric.

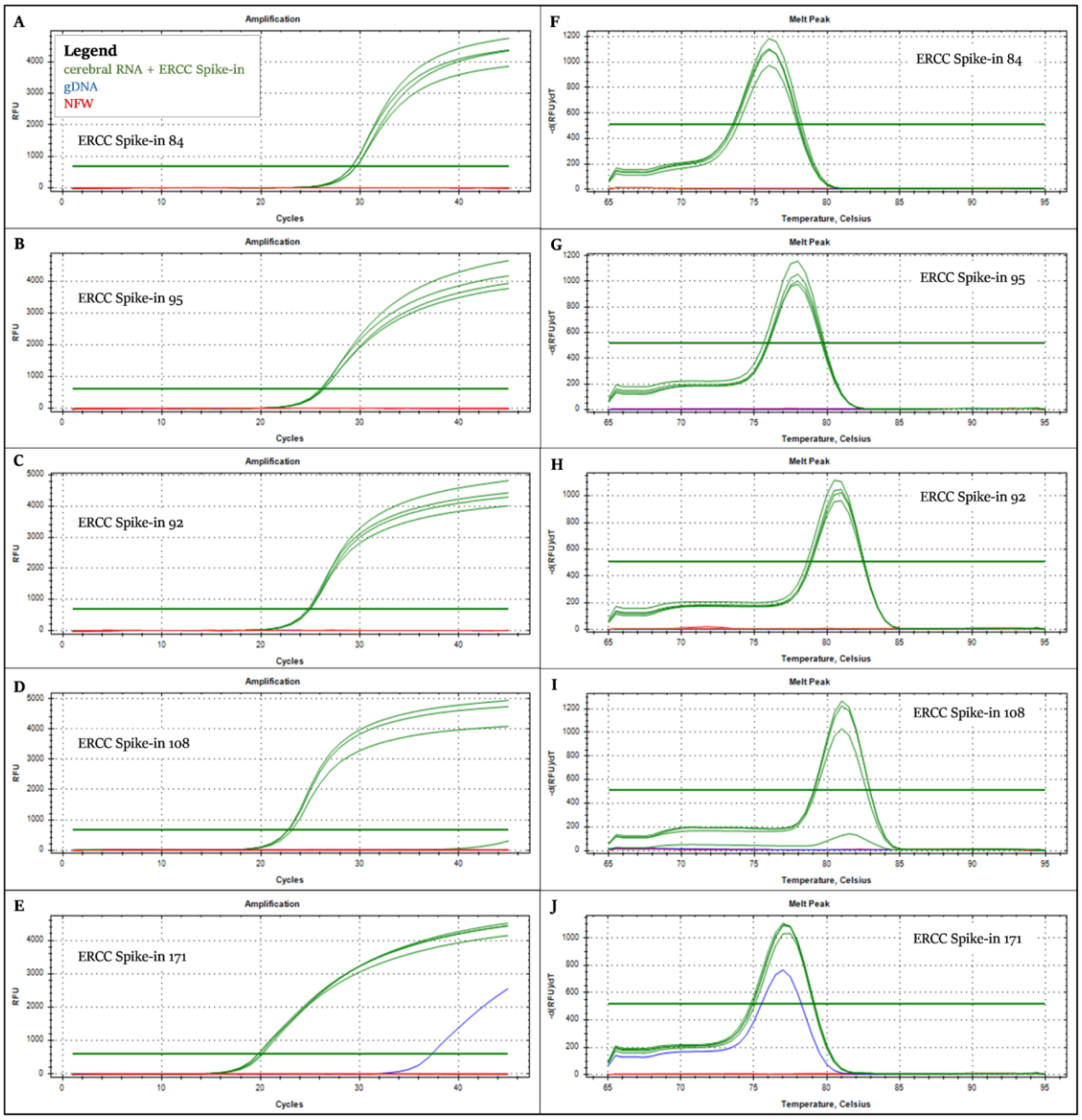

Figure 19 ***Assays employed in the RTase benchmarking measurements perform with substantial sensitivity and specificity.*** *(**A – E**) Green qPCR amplification curves depict signal obtained on a template of extracted and reverse transcribed cerebral RNA combined with ERCC Spike-in (n = 4). Blue curves report signal obtained from genomic DNA for a template of identical quantity as green curves (n = 1). Red curves depict non-template control reactions screening for primer-dimer formation (n = 3). (**F - J**) Melting curve analysis screening for specific product amplification.*

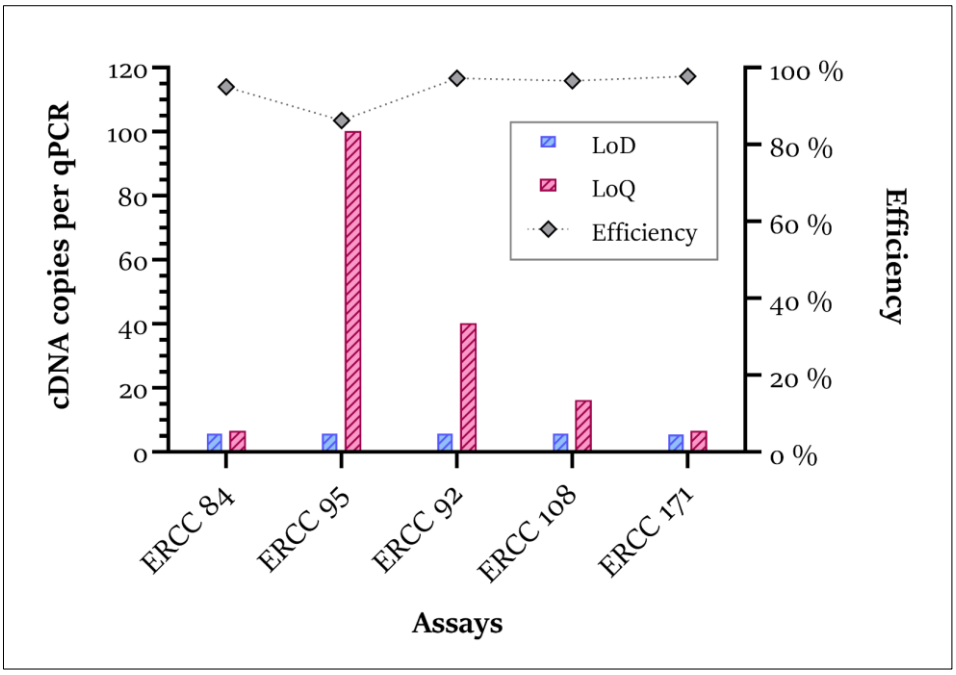

Figure 20 ***Performance metrics of the selected ERCC Spike-in assays.*** *LoD and LoQ metrics are plotted on the left Y axis, assay efficiency is on the right Y axis.*

5.7 ALS-induced change in astrocytic gene expression

Putting all the acquired knowledge together, we set out to explore the degree of change in gene expression profiles of astrocytes with ALS. In total, gene expression profiles of 22 ALS and 34 control single-cell astrocytes were assessed on assays including markers for various glial cell types, astrocyte subtypes, glutamate receptors, channels of potassium, sodium or chloride, GABA receptors and few more others (**ALS astrocytes**, *Attachment 1*). Astrocytes were shown to play an important role in the development and progression of the ALS disease, with multiplicity of the these pathways involved in the altered state (Radford *et al.*, 2015).

PCA revealed that the induced change is large enough to clearly separate the cells into two clusters, with an exception of two control single cells that are more similar to their ALS counterparts (Figure 21A). Cluster separation is identifiable on the both most explanatory PCs. Unparied two-tailed t-tests with Dunn-Bonferroni correction identified genes responsible for the separation (Figure 21B). For the case of ALS, gene expression of several transmembrane transporting proteins were downregulated, including subunit sodium/potassium-transporting ATPase (*Atp1a2* – 200-fold decrease), aquaporin (*Aqp4* – 28-fold decrease), potassium channels (*Kcnk1* – 22-fold decrease, *Kcnj10* – almost 4-fold decrease). Additionally to transporters, also

metabolism of amino acids (glutamine synthetase *Glul* – 42-fold decrease, serine peptidase inhibitor *Serpina3n* – 8-fold decrease), GABA receptors (*Gabbr1* – almost 5-fold decrease) and structural membrane proteins (connexin 43 *Gja1* – almost 6-fold decrease) were negatively affected. On the other hand, transcripts for cellular skeleton (intermediate filaments *Vim* and actin *Actb* – 167-fold and 3-fold increase, respectively), regulators of protein phosphorylation (*s100a10* and *Ywhaz* – almost 6-fold and 8.5-fold increase, respectively) or chloride transporter (*Clcn4* – 5.5-fold increase) were found in abundance. For some genes (*Glul, Serpina3n, S100a10* among others), the ratio of positive reactions could be even more informative than fold-changes, as it indicated complete lack or oppositely the presence of gene transcription (Figure 21C). The similarity between significantly differentiated genes was visualized by heatmap (Figure 21D), as some genes showed highly similar matching patterns of response to the disease. On the other hand, the partial heterogeneity of response among the single cells is also visible, e.g. the variable expression of *H2-D1* among control single cells.

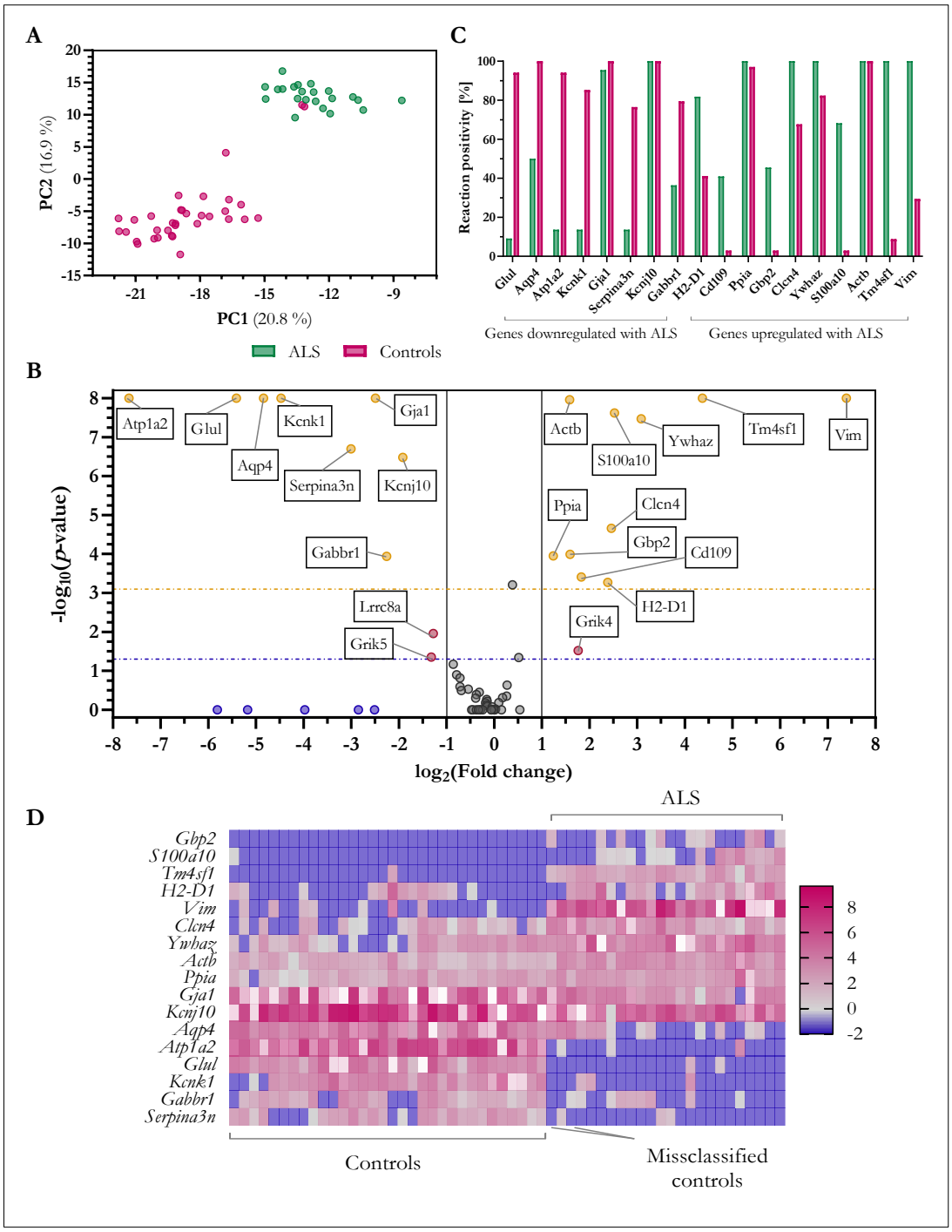

Figure 21 ***Transcriptome of astrocytes with ALS disease is substantially altered.*** *(**A**) Two astrocyte groups are clearly separated on the two most informative PCs. Brackets inform on the explained variance by the PC. (**B**) Volcano plot shows the significance of differential gene expression in relation to its (log_2-scaled) fold change. Genes labelled in yellow were tested significantly different with repeated-testing correction (<0.00081), red-labeled genes are significant for the uncorrected p-value (<0.05), blue genes were not significant but their fold-change was apparent and lastly, grey genes did not show notable change. Lines show color-adjusted testing significance thresholds. (**C**) Reaction positivity is shown for the significantly differentiated genes (yellow from figure B), with label describing the fold-change status. (**D**) Heatmap of significantly differentiated genes (yellow from figure B) demonstrating the absolute markers of the condition (strict presence/absence; listed on the y axis ends) and genes undergoing some level of change (middle of y axis). Legend codes the degree of change from blue (no expression) to pink (maximum).*

6 Discussion

In this thesis, we set out to systematically fill out missing understanding that surrounds scRT-qPCR, starting with technical details on material handling and single-cell collection, continued with search for best-performing commercial RTase and validation of its results in an exemplary single-cell experiment, followed by exploring the utility of smaller reaction volumes for preAMP and lastly, proposing a set of practical hints for design and quality testing of highly-efficient qPCR assays. On top of all this, quality control checks for the selection of most viable single cells and testing for preAMP reproducibility were employed to reduce experimental costs and increase the experiment's reliability. Key findings include: (*a*) single-cell samples are resilient and can withstand prolonged waiting times without reduction in quality (when handled appropriately), (*b*) repeated freeze-thawing does not hamper the quality of scRT-qPCR data, (*c*) up to 256 cells can be processed in a single reaction without RNA extraction without adverse effect on the expression profiles, (*d*) employment of better-performing RTase substantially increases the sensitivity, reproducibility and yield of the reaction, resulting in the improved gene detection rate and separation of different cell populations, (*e*) decrease of preAMP volume lowers the quality of single-cell expression profiles, increases the number of false negative reactions and causes a decrease in the quantified signal, (*f*) ALS in astrocytes is accompanied by a decrease of expression of sodium/potassium transmembrane ion channels/transporters and also affects metabolism of amino acids. On the other side, genes for cellular skeleton are upregulated along with regulators of protein phosphorylation and chloride transporter.

Compromised RNA quality has detrimental effects on the aftermath analysis, as half degraded, sheared or broken-down transcripts influence the effectivity of quantification and currently it remains unclear how evenly this damage is spread throughout the transcriptome. Quick processing and cold environment are therefore the most suitable, especially for material such as single cells, which have low RNA content and are stored in minute volumes which unfreeze rapidly. In our hands, we saw little-to-no effect on the analyte abundance, whether waiting in the cooling vessel before the FACS sorting (Figure 5) or waiting on ice after sorted into the lysis buffer (Figure 6). Noticeable differences were observed in the variation of the individual single cells within the group in both experimental setups (CV of 28.6 – 58.8 % and

31.1 – 56.9 %, respectively). The variation may stem from the natural heterogeneity of single cells as well as from the RTase precision. A part of the variability may be also ascribed to the qPCR step, although its contribution is considered to be marginal (Tichopad *et al.*, 2009). How precisely the cDNA is quantified was investigated in the section *5.4.1 RTase benchmarking – Precision* section using five optimized *ERCC Spike-in* assays, where RT reactions with SuperScript III RTase primed by RT primers mixture recorded CV of 43.8 % (Figure 13A). The data are well in line with a recent study based on digital PCR that determined the variability of single-cell RT to be in the range of 12 to 36 % CV (Schwaber, Andersen and Nielsen, 2019). Taken together, the variability observed in the data is predominantly of RT origin and is not influenced by heterogeneity of single cells or experimental conditions.

Time between the collection of specimen and consecutive processing was already of a concern before, although with focus on tissue samples. Our results are in agreement with testing by Micke *et al.* (2006) who showed that keeping fresh tonsil and colon tissue samples on ice for up to 16 hours followed by RNA extraction, left the RNA profiles unaltered. The authors hypothesize the RNA remains stable due to maintenance of cellular integrity. As RNA remains inside the cells, it is protected from the hydrolytic degradation. Since FACS-collected cells do not preserve their cellular architecture, RNA hydrolysis becomes a notable threat, which can be mitigated by proper buffer use (Svec *et al.*, 2013). Our cells were sorted into the buffer deemed the most appropriate by Svec *et al.* (NFW + 1 mg/µl BSA), and our results are in line with their findings that RNA does not undergo noticeable damage for two hours of waiting, especially when kept cooled. Placing collected cells on ice thus can be viewed as precaution to preserve rarer marker RNAs (Marinov *et al.*, 2014), which would be the most affected by the miniscule changes. Despite no significant effect of waiting in the cooled state was observed, it is still recommended to keep running times at minimum and place the cells into low-temperature freezers for long-term storage (Micke *et al.*, 2006).

Single cells are routinely collected to completely fill 96-well plates but in practice, not all cells are required for analysis at one time. Due to this, a part of cells undergoes repeated thawing and freezing, possibly causing analyte loss/degradation. Since the risk factor of improper sample handling might affect technical outcome of the experiment, e.g. making them harder to compare

(Svensson *et al.*, 2017), we set out to what degree is RNA quantity affected by up to 12 repeated freeze-thawing cycles. Despite our results do not report significant changes in RNA quantity even after 12 cycles (Figure 7), we note that for 12 cycles we were able to obtain signal only from 8 out of 13 collected cells with one cell reporting surprisingly high signal (RQ = 5.42), what is documented by the increased variance (CV = 76 %) being out of range for SuperScript III reports (as discussed in the paragraph above). Unchanged single-cell RNA levels due to freeze-thawing were also previously documented up to 6 cycles by Svec *et al.* (2013). Quite interestingly, repeated freeze-thaw handling of whole tissue specimen was observed to substantially hamper RNA quality and quantity with every cycle (Wang *et al.*, 2015). This phenomenon was later observed to be partially linked with tissue's metabolic activity, as RNA from liver and muscle cells was more prone to degradation than those from brain or testis (Ji *et al.*, 2017). The authors further showed that thawing the samples on ice slowed down the degradation rate, most likely due to reduced RNase activity. The difference in the degradation rate between single-cell and tissue samples might reflect presence of RNases. Preparation of cell suspension for FACS causes the extracellular RNases to be washed away that would otherwise be present in the storage vessel and become active when unfrozen (Svec *et al.*, 2013). Remaining intracellular RNases are still present but they get diluted as the cell is lysed upon collection. RNA in the repeatedly frozen and thawn tissue sample faces different situation since overall tissue structure is maintained and contents of the ruptured cells are not that well diluted. We believe this fact with the added presence of extracellular RNases is behind the difference freeze-thawing has on the sample types.

The findings of Svensson *et al.* (2017) are however in part in disagreement with our findings, reporting that the rate of RNA degradation is ~20 % per freeze-thaw cycle. Main methodical differences to our experiments were that reaction vessels contained different lysis buffers (we – BSA, Svensson *et al.* – Triton X-100), RNA quantity was measured on ERCC Spike-ins (with single cells as RNA background) (we – endogenous transcripts *Actb, Slc1a3* and *Aqp4*) and their method of quantification was not scRT-qPCR but scRNA-Seq. All these factors could have played a role. BSA might function as carrier and protect the RNA (Svec *et al.*, 2013). ERCC Spike-ins are dissimilar to endogenous mRNAs in many ways, they are not 5' end capped, have

shorter polyA-tails, do not have complex secondary structures and most importantly, they are not bound by natural RNA-binding proteins (Svensson *et al.*, 2017). Lack of these properties make ERCC Spike-in RNA more prone to RNase digestion or self-hydrolysis. Lastly, partial degradation is not as problematic for RT-qPCR primed by random primers and quantified by short PCR assays (our case) than for oligo(dT)-primed RT-qPCR or scRNA-Seq (Svensson *et al.*), because the two latter approaches rely on the intactness of RNA molecule. In the light of this, we call for caution and suspect that repeated freeze-thawing magnifies the differences between expression profiles of the individual cells and 3' end-oriented quantification methods relying on full length cDNAs are hampered more severely than random-oriented approaches.

Transition between the measurements of single cells and tissue samples is represented by the analysis of bulk samples, where a variable number of cells (tens to hundreds) is collected into a single reaction chamber. Bulk samples embody a trade-off where the loss of detail on the cell heterogeneity is exchanged for higher copy numbers of rare transcripts. Choosing the optimal RNA extraction procedure can be difficult as the bulk samples similarly to single cell samples contain only low RNA amounts (few ng), causing substantial losses in the traditional RNA isolation methods of Trisol-chloroform extraction (TRI Reagent (Guanidine Thiocyanate & Phenol) protocol) or column-based (e.g. RNeasy Mini Kit, QIAGEN). Since direct lysis is regarded as the optimal procedure for single cells due to no RNA losses during the processing (Svec *et al.*, 2013), we tested its capacity by processing up to 2048 cells per 5 ul of lysis buffer. Our results confirmed the results of Svec *et al.* (2013) that up to 256 cells per reaction can be efficiently lysed and processed, whereas for higher cell counts the efficiency drops significantly (Figure 8). The most likely explanation to this phenomenon is that cells contain agents that inhibit RT or qPCR, which is plausible since single-cell workflow prefers to maintain "volumes low and concentrations high" (Dzamba *et al.*, 2016). Varying sample-originating compounds were previously identified to inhibit RT or PCR reactions, including heme, heparin, IgG, bile salts or urea (Bustin and Nolan, 2004; Nolan, Hands and Bustin, 2006; Huggett *et al.*, 2008). This offers a lead that cells themselves might contain agents that are not blocked by the protective BSA properties (Hodne 2015). Therefore in practice we find the analysis of up to 256 cells per bulk

sample sufficient as balance between the detection of rare transcripts and ease-of-use, given the sensitivity and cost-/time-efficiency of the proposed protocol (*4.2 Detailed single-cell protocol*).

RT is the first enzymatic reaction within the scRT-qPCR workflow that has been repeatedly examined with respect to the choice of RTase (Ståhlberg, 2004; Levesque-Sergerie *et al.*, 2007; Okello *et al.*, 2010; Sieber *et al.*, 2010; Lindén, Ranta and Pohjanvirta, 2012; Bustin *et al.*, 2015; Schwaber, Andersen and Nielsen, 2019), priming strategy (Ståhlberg *et al.*, 2004; Ståhlberg and Bengtsson, 2010; Miranda and Steward, 2017; Schwaber, Andersen and Nielsen, 2019) and potential additives (Bagnoli *et al.*, 2018; Schwaber, Andersen and Nielsen, 2019). Interplay of these factors dictates the variability, that RT is recognized for. With decreasing template concentrations the variability increases, as the absolute number copies are counted in tens (Marinov *et al.*, 2014) and the effect of Poisson distribution becomes more prominent (Figure 2) (Ståhlberg and Kubista, 2014). Since nearly all RT-qPCR publications investigating RT performance were conducted using RNA extracted from tissue samples and only rarely the inputs were close to single-cell concentrations (Schwaber, Andersen and Nielsen, 2019), we set out to validate palette of metrics eminent for precise scRT-qPCR.

Biologically relevant biomarkers that accompany changes in cell's fate are expressed in just few individual copies (Marinov *et al.*, 2014), making their quantification a challenging task. To look into the efficiency of reporting rare transcripts, we counted the number of positive reactions with specific signal for *ERCC Spike-ins* counting 88 or 22 copies per RT reaction, respectively (Figure 11). When looking at *ERCC 95* (88 RNAs per RT), we did not observe substantial difference in the reaction positivity rate between individual RTases, with the exception of eAMV (Figure 11A). The poor performance of eAMV was already highlighted before (Ståhlberg, 2004; Okello *et al.*, 2010; Sieber *et al.*, 2010; Lindén, Ranta and Pohjanvirta, 2012) and has been attributed to its dimeric structure (Konishi, Yasukawa and Inouye, 2012). For the four-times less abundant template *ERCC 84* (22 RNAs per RT), the gap between RTases substantially widened and underlined the difference high-sensitivity RTase makes (Figure 11B). Measurement of small copy numbers is problematic and RTases do not perform equally in these limiting conditions (Levesque-Sergerie *et al.*, 2007; Bengtsson *et al.*, 2008; Okello *et al.*, 2010). In the work of Okello *et al.* (2010), only 5 out 11 RTases were capable of quantifying whole range

from 10 to 1000 RNA copies per RT. Out of these five well-performing RTases, SuperScript III, AccuScript and MMLV RTases were also included in our study and they demonstrated an average performance (Figure 11B and Figure 15). The weakside of Okello *et al.*'s work is the use of two RT replicates only, posing strict criteria for selection of 'succesful' RTase when such minute transcripts counts are targeted. We tackled this problem by running the RT reactions in 10 replicates. In addition, *ERCC 84* assay was measured in qPCR duplicates aiming to prevent reporting falsely negative reactions, as eventually just ~ 2 copies are present per qPCR reaction (Table 3). In short, RTase has a considerable impact on the capture rate of rare transcripts and the choice for more sensitive option is highly recommended for single-cell application.

The assumption that RT performs with constant efficiency regardless of template concentration may sound naturally. However, there are contradictory results in the literature. Whereas some studies reported constant efficiency across wide input ranges (Bengtsson *et al.*, 2008; Okello *et al.*, 2010; Sieber *et al.*, 2010; Schwaber, Andersen and Nielsen, 2019), others showed the opposite (Ståhlberg, 2004; Ståhlberg *et al.*, 2004). In addition, the data in the low concentration range typical for single cells are missing completely. Therefore we set out to explore the efficiency of quantification across wide dynamic range from 22 to 282 200 ERCC Spike-in copies per RT reaction. In our hands, all enzymes retained constant linear efficiency (Figure 12 and **Precision – linearity**, *Attachment 1*) showcasing that low copy numbers do not distort RTase performance and the RNA contents are reliably reflected with particular RTase-specific effectivity (Figure 14). RTase-specific was also the variability of measurements that increased in single-cell reactions (Figure 13A and B). Conclusively, better-performing RTases do not only capture rare transcripts but also reflect their abundancy in corresponding cDNA numbers with less uncertainty (=variability). This effect of noise was modeled in detail by Bengtsson *et al.* (2008) who similarly stressed out the prominent role of optimized RT and qPCR assays for the noise reduction. Noteworthy, several studies suggested that differences in RT efficiency may also be gene-dependent (Bustin and Nolan, 2004; Ståhlberg, 2004; Ståhlberg *et al.*, 2004; Schwaber, Andersen and Nielsen, 2019). We were unable to observe this phenomenon in our data which is probably attributed to the use of synthetic ERCC Spike-in standard molecules that lack secondary structures, naturally bound RNA binding proteins and have

shorter polyA tails. Similar reasoning is proposed by Svensson *et al.* (2017) who observed that synthetic ERCC Spike-ins are being captured and transcribed with different efficiency than endogenous mRNAs. To sum, mRNA transcripts can be reported with varying efficiency but this is due to the biochemical properties of that particular molecule rather than a technical artefact of RT. RT efficiency is consistent for different input concentrations but measurements of rare transcripts are linked with inherent variability which can be partially minimized with more efficient RTase.

Another important metric of RT is reaction yield, describing the rate of conversion from RNA to cDNA. cDNA synthesis yields were typically reported to be in range of 50 % - 80 % (Ståhlberg, 2004; Okello *et al.*, 2010; Lindén, Ranta and Pohjanvirta, 2012; Bustin *et al.*, 2015; Svensson *et al.*, 2017; Schwaber, Andersen and Nielsen, 2019). Our experimental results showed that reaction yields are highly dependent on both the RTase and priming strategy (Figure 14). The differences between RTases are better spotted for reactions primed by RT primers mixture, where SuperScript IV and Maxima H- handily outperformed other candidates. Their superior yields above 100 % are most likely ascribed to use of multiple priming locations mediated by random hexamer priming. Multiplicity of priming locations combined with strand displacement activity, high substrate binding affinity, lack of RNase H function and high processivity can result in synthesis of more than just 1 cDNA copy per RNA transcript, therefore leading to yields > 100 % (Bustin and Nolan, 2004). Differences in the yield between single-cell and bulk templates were minor with the exception of SuperScript II and eAMV (Figure 14). This result has been however expected, as the single-cell template is below the recommended template input range declared by the manufacturer. The only previously published results contradictory to ours were reported by Levesque-Sergerie *et al.* (2007), what may be however attributed to imprecise qPCR standard curve construction, as spotted by Miranda and Steward (2017).

The broad spectrum of tested RTases allowed us to assess RT-related features that were not the main goal of our study, such as influence of RT protocol or RNase H activity, as well as practical aspects of the analysis as is the cost of the experiment. Elevated RT reaction temperatures are also regarded beneficial as they ought to destabilize secondary RNA structures, as susceptible GC repeats and adjacent paired regions are melted, allowing for more frequent

and evenly spaced priming (for RT primers mixture) and prevents RTase stalling (Ståhlberg, 2004; Nolan, Hands and Bustin, 2006; Svensson *et al.*, 2017). Our results undirectly confirm these hypotheses, since our top performing RTases (SuperScript IV, Maxima H-, SuperScript III) were those functioning at the highest temperatures of 50°C (Figure 15 and Table 1). For Maxima H- and SuperScript IV manufacturer's protocol allows even higher running temperatures. Majority of manufacturer-recommended protocols include preincubation step, increasing the primer binding efficiency. From the tested RTase panel, the exceptions were iScript and SensiScript, both manifesting relatively lower-end performance, demonstrating the benefits of heating the reaction contents, relaxation of the secondary structures which in turn opens up the RNA sequence for more evenly spaced hexamer annealing. Formerly, RTases with unfunctional RNase H domain were preferred, as this was believed to increase reaction yields by preventing cleavage of RNA transcripts in the RNA-DNA duplexes (Ståhlberg, 2004). Lack of RNase H activity was not observed to be of substantial importance in our data, in agreement with the current view (Sieber *et al.*, 2010; Lindén, Ranta and Pohjanvirta, 2012). The power of scRT-qPCR experiments lies in the exploration of biological heterogeneity, what calls for the analysis of larger number of cells. Analysis of greater numbers does not only help to better spot the true biological differences (Tichopad *et al.*, 2009), but unfortunately also increases experimental costs. Considering the price per RT reaction, Maxima H- is the most recommendable choice since it combines high performance with low price (second lowest in our comparison, Table 1). Notably, Maxima H- and SuperScript IV also possess the terminal transferase activity, necessary for template-switching reaction dynamics utilized in some RNA-Seq protocols (Svensson *et al.*, 2017; Ziegenhain *et al.*, 2017; Bagnoli *et al.*, 2018).

Although the primary goal was to compare commercially available RTases for scRT-qPCR, the results provided us with insight on the role of priming strategies. Different priming methods were noted to be variably efficient for different gene transcripts (Ståhlberg *et al.*, 2004) but the general consensus is that the mixture of random hexamers with oligo(dT) primers (in the thesis termed as RT primers mixture) is the most efficient choice for scRT-qPCR (Sieber *et al.*, 2010; Ståhlberg and Bengtsson, 2010). The random hexamers access multiple priming locations what has previously lead to over 100 % yields (Bustin and Nolan, 2004; Schwaber,

Andersen and Nielsen, 2019). On the other hand, oligo(dT)s prime only polyA-tailed mRNAs and do not waste reaction resources on the RT of rRNA. Our experiments were employed in a factorial design, having equal number of reactions with 50 μM RT primers mixture and also with 10 μM oligo$(dT)_{15}$s (mimicking their typical use in RT-qPCR or RNA-Seq experiments, respectively) putting no priming strategy into a disadvantage simply due to smaller number of replicates. The differences were the most apparent for positivity of an assay at limiting abundancy (Figure 11B) and for the yield metrics (Figure 14) with oligo(dT)s reporting fewer positive reactions and lower yields. Although one presented explanation is the role of multiple priming locations of random hexamers, we cannot exclude that the differences arose due to use of different primer concentrations. This factor was reported to have a dominant effect on the primer's performance and when optimized properly, two different priming methods can deliver comparable yields (Miranda and Steward, 2017). Therefore it is not advised to oversimplify the interpretation that the RT primers mixture always outperforms oligo(dT)s. Such claims for single-cell experiments would request their direct comparison at equal primer concentrations.

High-throughput RT validation in our setup aimed to validate and extend the findings of the low-throughput RTase benchmarking (measured on five ERCC Spike-in assays) by measuring 71 endogenous assays on real astrocytes (ALS vs controls). We hypothesized that the technical differences arising due to differential performance between the two tested RTases (Maxima H- and SuperScript II) (in such as reaction positivity, sensitivity or signal strength) would be reflected in the better separation of biologically distinct single-cell clusters in PCA. Indeed, as better-performing Maxima H- recorded more positive reactions per assay with stronger signal (Figure 16A, B, D, E), the clusters' separation was more apparent as reflected by increased cluster distances (Figure 16C, F). As the PCA reduces the dimensions of the computational space by searching for the greatest portions of variation within the dataset (Ringnér, 2008), the biological differences were better defined and they were assigned greater significance. To our knowledge, this is the first example demonstrating direct effect of RT on separation of two distinct groups of single cells in the multidimensional expression analysis.

Minimal dilution of newly synthetized cDNA in combination with small RT reaction volume restricts the number of assays that can be measured from a single cell. Quantification of

scarce transcripts additionally faces complications with qPCR's limits of detection (> 5 molecules are requested for reliable qPCR detection) (Ståhlberg *et al.*, 2013; Andersson *et al.*, 2015). Thus, reproducible material preamplification can solve these problems one at a time. PreAMP reaction had been thoroughly studied and the reaction is nowadays regarded as reproducible. When the reaction components are balanced out properly (Andersson *et al.*, 2015; Korenková *et al.*, 2015; Kroneis *et al.*, 2017), the reaction forms minimal unspecific PCR products and works within sensible dynamic range (see *2.4 Preamplifcation* section). Although many of the reaction parameters can be generalized (primer concentration, primer annealing time and temperature, number of assays), every individual mix for targeted preamplification needs to be *in house* tested. Since preamplification mixes are prepared from tens of primer pairs, unexpectable interference could occur among the myriad of possible primer combinations that would hamper the preamplification reproducibility. We recommend screening of every newly prepared mix of preAMP primer assays by examining the reproducibility of the Cq difference (ΔCq) between nonpreamplified and preamplified samples for a selection of high, medium and low abundant targets (*5.5.1 PreAMP quality control*). There are two points worth highlighting from our exemplary testing of the seven assays included in preAMP primer mixture. Firstly, the absolute ΔCq vary from assay to assay and secondly, all of them reported $SD_{\Delta Cq}$ below ~0.3 (Figure 17). The variation in the absolute ΔCq does not represent a drawback, since later data processing steps cancel it out by calculating RQs for each assay separately (*Equation 1*), unifying the signal to the common ground level. Keeping the preAMP reproducible is more critical as addition of unnecessary noise would limit the ability to assign biological differences (Ståhlberg and Kubista, 2014). Maintaining the preAMP $SD_{\Delta Cq}$ below 0.25 is considered optimal since it reflects the expectable qPCR variation within its dynamic range (Ståhlberg and Kubista, 2014).

Single-cell experiments are costly to conduct and the sample volumes are limiting. When peculiarities of specific pathways are the scope of research (Androvic *et al.*, 2019), one can quickly run out of the material as multitude of validation runs is done. Therefore here we set out to validate how much information is lost by decreasing the preAMP reaction volume while keeping the ratio sample-preAMP mix constant (ratio 1:9, which is mandatory to mitigate inhibitory effect of RT reagents in preAMP reaction). As expected, single-cell reactions were

substantially negatively influenced by analysing smaller portion of cell's contents (Figure 18A, C). In the preAMP reactions with greater volumes more sample is used (2- or 4-times more in 20 µl or 40 µl reaction when compared to 10 µl, respectively), thus increasing the chance of containing those rare 'on-the-edge of sensitivity' transcripts in quantities sufficient for their reliable capture and reporting by qPCR (Andersson *et al.*, 2015). The increase in reaction positivity was not observed for bulk samples (Figure 18B), where all targets were presented in sufficient copy numbers regardless of sample volume used. Surprisingly, we observed a decrease in the signal strength in the 40 µl preAMP reaction (Figure 18D). We suspect a technical error and new experiment with more replicates would be needed to validate observed changes. In practice, we advocate for use of increased preAMP volumes in the single-cell approaches enabling analysis of greater portion of cell's transcriptome. For the analysis of bulk samples, we recommend to use smaller reaction volume.

Specificity and sensitivity, the factors that qPCR is often highlighted for, are shaped by the quality of designed assays (Bustin *et al.*, 2009; Andersson *et al.*, 2015; Ståhlberg and Kubista, 2018). Their careful design (*2.5 QPCR* section) is evermore important when unspecific reporting chemistry is used, as in our case. High-performing assays for preAMP and qPCR are tasked to encompass exon-exon junction spans, neglect formation of primer-dimers and perform with absolute target specificity and high efficiency. All five assays used in *5.4.1 RTase benchmarking* section met these stringent requirements, producing single target-specific peak without amplification of any abberant products or amplification of genomic DNA (Figure 19). The only exception was *ERCC 171* assay reporting gDNA with the shift of 17 Cqs, nonetheless indicating that gDNA does not contribute substantially to the reported cDNA signal. As the absolute copy numbers of targeted cDNA molecules in the qPCR were extremely low (Table 2), LoD and LoQ metrics informed on the reliability of collected RT metrics, such as *Sensitivity*. The only questionable quality metric of the designed assays is the 86.3 % efficiency of the *ERCC 95*, in turn being directly translated to the assay's significantly elevated LoQ (Figure 20). Despite its high LoQ value, LoD remained below the theoretical qPCR copy count (5.7 and 7.1, respectively) making it suitable for collection of the *Sensitivity* metric. Well-optimized assays increase measurement fidelity and negate the necessity for running the qPCR in replicates, as the

uncertainty associated with this step is minimal among the scRT-qPCR workflow steps (Tichopad *et al.*, 2009; Lindén, Ranta and Pohjanvirta, 2012). Running the qPCR in replicates can actually cause problems, especially when preAMP is not performed, since transcripts counting just few copies may be split into separate reactions, ending up below the assay's LoD. We advocate for thorough assay optimization which truly empowers the experiment's potential to precisely identify novel discoveries of even minute perturbations in the cell's transciptome.

Single-cell experiments have the power to reveal the complex interweb associated with the onset and progression of neuronal diseases at unprecedented resolution. Although ALS results in irreversible motor neurons damage, different glial subtypes are involved in the process, with astrocytes and microglia in charge of the disease progression (Yamanaka *et al.*, 2008; Radford *et al.*, 2015). This makes the ALS a perfect candidate for transcriptomic exploration at single-cell resolution, as individual subtypes are investigated separately. Transcriptomic landscape of ALS-affected astrocytes is substantially different from wildtypes (Figure 21A). Neurotoxicity of ALS astrocytes involves distribution of glutamate (Howland *et al.*, 2002), which can be generated in overabundance by inhibition of glutamate-glutamine conversion that would be caused by significant downregulation of glutamate synthetase. We observed this phenomenon in our data, with only 10 % of ALS astrocytes reporting any signal of glutamate synthetase (*Glul*) transcripts (Figure 21 C). Cell size and turgor is regulated by the influx of ions, when brought to imbalance, cells swell and increase in volume. As we have observed, ALS astrocytes exhibit dysregulation of numerous across-membrane transport complexes, i.e. aquaporins (Aqp4), sodium/potassium ATPase (*Atp1a2*), potassium channels (*Kcnk1, Kcnj10*) (Figure 21B), indicating that changes in astrocyte volume take place and may impair their ability to effectively clear debris and distribute nutrients, eventually creating hostile environment to its surroundings (Papadopoulos and Verkman, 2013; Iliff *et al.*, 2014; Kitchen *et al.*, 2020). Astrocytes do not only increase in volume but also tend to proliferate forming a glial scar, in the wake of preventing spread of neuronal damage (Liddelow *et al.*, 2017). Glial scar is formed by astrocytic proliferation and heavy rebranching and growth of their cellular skeleton, forming a dense protective layer. We, observing the extreme upregulation of genes for intermediate filaments (*Vim*) or actin (*Actb*), agree that astrocytic skeletons undergo heavy

remodelling. The just described varying roles of astrocytes do not occur uniformly across the population. A recent model divided activated astrocytes into two groups of A1 and A2 astrocytes (Liddelow *et al.*, 2017). A2 astrocytes retain their normal protective character and inhibit neuroinflammation, whereas A1 astrocytes abandon their neuroprotective program and turn sinister, characterized by production of neurotoxin, loss of phagocytic activity and blockage of proper synapse formation and functioning. Type of disease determines which astrocyte subtype becomes activated what is reflected in the expression of specific marker set (i.e. A1 – *H2-D1*, *Gbp2*, A2 – *Tm4sf1, S100a10*). As A1/A2 markers were often expressed together within the same cell in our data, we hypothesize that these cells represent an intermediate state or possibly a distinctive subtype of astrocytes specific for ALS (Figure 21D). Further work will be needed to provide conclusive answers for these hypotheses.

In conclusion, this thesis evaluates individual steps of single-cell analysis using RT-qPCR method and its potential caveats that may arise with processing of such minute amounts of material. Sample handling in generally does not impact the RNA quality but may introduce additional unwanted variability. We confirmed the previous observation that up to 256 cells collected in bulk can be comfortably processed with direct cell lysis protocol. We showed substantial differences in the performance of RTases, highlighting the importance of their selection for single-cell studies. As of now, preAMP is a well-performing reaction that is recommended to be performed with maximal sample input for detection of the rarest transcripts. Following amplification, the utility of high-quality PCR assays in undoubtable and allows for reliable detection of scarce templates. Putting this knowledge together, we have identified important components of ALS-induced damage to astrocyte transcriptome, being in agreement with the published literature. We believe that this thesis provides complete set of recommnedations for performing single-cell RT-qPCR experiment, where researcher can make educated decisions based on the provided literature, our experimental results and practical notes securing savings on experimental costs and statistical power.

7 Conclusions

The aim of this thesis was to complete a guide for conducting single-cell experiment, informing the reader on both the strong and weak sides of the single-cell transcriptomic analysis. Experiments performed aimed to validate and extend the current knowledge on single-cell processing but also on practical checkpoints saving researcher's time and funding, as well as empowering his conclusions with reliability on the method's practice. Despite the fact that single-cell handling (waiting before or after FACS collection, repeated freezing and thawing) is susceptible to undesired changes as the cells are kept under suboptimal conditions, we have not observed substantial changes. Still, we caution against increased working times and vouche for quick processing as undesired variability can be introduced. Direct lysis of small bulk samples was deemed efficient for up to 256 cells per 5 ul of lysis buffer, being an accessible and cheap alternative for nucleic acid extraction with no analyte losses. Quality control of FACS-sorted astrocytes resides in measurement for marker of astrocytes and other related glial cell types, primarly selecting cells expressing cell-type specific genes and genes reflecting cell quality. Choice of better RTase makes significant differences in the ability to characterize cell populations as well as discover the role of new putative markers that previously went unnoticed or their quantification seemed troublesome. Priming strategy was found to be of secondary importance since its concentrations can be optimized to deliver requested yields. PreAMP's most important factors include reproducibility and sensitivity. Reproducibility must be checked for each set of preAMP primer mix, whereas the best sensitivity in the single-cell experiments is obtained by maximizing the sample input. The set of assays used for both preAMP and qPCR must be ultimately screened for amplification of unspecifities, which needs to be strictly avoided, as any confounding signal might be later translated into misleading conclusions. Applying optimized protocol to the ALS experiment helped to identify several genes affecting astrocytes in this neurodegenerative disease, being in line with published literature.

8 Publications

Throughout the work on this thesis, we published a part of the results in renown journal Clinical Chemistry (Zucha *et al.*, 2020) and selected methodological aspects were utilized in two other publications (Pivonkova *et al.*, 2018; Androvic *et al.*, 2019).

1. **Zucha, D.**, Androvic, P., Kubista, M. and Valihrach, L. (2020) 'Performance Comparison of Reverse Transcriptases for Single-Cell Studies', *Clinical Chemistry*, 66(1), pp. 217–228. doi: 10.1373/clinchem.2019.307835. *IF* = 6.891.
2. Androvic, P., Kirdajova, D. B., Tureckova, J., **Zucha, D.**, Rohlova, E., Abaffy, P., Kriska, J., Anderova, M., Kubista, M. and Valihrach, L. (2019) 'Decoding the transcriptional response to ischemic stroke in young and aged mouse brain', *bioRxiv*, p. 769331. Preprint available at: https://doi.org/10.1101/769331. Accepted in Cell Reports (29/4/2020). IF = 7.815.
3. Pivonkova, H., Hermanova, Z., Kirdajova, D., Awadova, T., Malinsky, J., Valihrach, L., **Zucha, D.**, Kubista, M., Galisova, A., Jirak, D., *et al.* (2018) 'The Contribution of TRPV4 Channels to Astrocyte Volume Regulation and Brain Edema Formation', *Neuroscience*, 394, pp. 127–143. doi: 10.1016/j.neuroscience.2018.10.028. *IF* = 3.244.

In the study Zucha et al. (2020) we benchmarked a broad spectrum of the currently available RTases under low-template applications. Our results provide a point of reference for the improvement of current single-cell quantification protocols. I contributed to the experimental design, performed all the measurements, analyzed and interpreted the data, wrote the manuscript and prepared all figures. In addition, I presented the preliminary data on two international conferences (Single cell Europe, 2018, Prague and 9th Gene Quantification Event – qPCR dPCR NGS, 2019, Freising). Based on the presentation, my poster was once awarded as the best conference poster and I was invited to present my results on EMBL Course of Functional Genomics.

Cerebral stroke is one of the leading causes of mortality affecting mainly aged population. In the study Androvic et al. (2019) we used RNA-Seq to analyze the impact of aging, stroke and their interaction on genome-wide expression in mice. We identified pathways associated with age-dependent vulnerability to stroke, including over-activation of type-I interferon signaling

and downregulation of synaptic maintenance program. My part on this project included design and validation of qPCR assays, validation of preAMP mix and complete high-througput RT-qPCR workflow for analysis of 100-bulk samples as well as single cells. In the workflow were utilized several aspects that were optimized in this thesis, including the use of top-performing RTase or analysis of 100-bulk samples.

Lastly, in the work of Pivonkova *et al.* (2018) we aimed to elucidate the role of TRPV4 channels in volume regulation in astrocytes *in situ* and whether lack of TRPV4 channels might lead to higher edema formation after cerebral stroke. Our data suggest that TRPV4 channels are not involved in astrocyte volume regulation *in situ*; however, they play a protective role during the ischemia-induced brain edema formation. My responsibilities on this project included design and validation of qPCR assays, followed by conducting low-throughput single-cell and bulk RT-qPCR measurements and necessary quality controls.

9 References

Aggerholm-Pedersen, N., Safwa, A., Bærentzen, S., Nordsmark, M., Nielsen, O. S., Alsner, J. and Sørensen, B. S. (2014) 'The importance of reference gene analysis of formalin-fixed, paraffin-embedded samples from sarcoma patients — An often underestimated problem', *Translational Oncology*, 7(6), pp. 687–693. doi: 10.1016/j.tranon.2014.09.012.

Aicher, T. P., Carroll, S., Raddi, G., Gierahn, T., Wadsworth, M. H., Hughes, T. K., Love, C. and Shalek, A. K. (2019) 'Seq-Well: A Sample-Efficient, Portable Picowell Platform for Massively Parallel Single-Cell RNA Sequencing', in, pp. 111–132. doi: 10.1007/978-1-4939-9240-9_8.

Al-Chalabi, A., Jones, A., Troakes, C., King, A., Al-Sarraj, S. and Van Den Berg, L. H. (2012) 'The genetics and neuropathology of amyotrophic lateral sclerosis', *Acta Neuropathologica*, pp. 339–352. doi: 10.1007/s00401-012-1022-4.

Álvarez, M. and Menéndez-Arias, L. (2014) 'Temperature effects on the fidelity of a thermostable HIV-1 reverse transcriptase', *FEBS Journal*, 281(1), pp. 342–351. doi: 10.1111/febs.12605.

Andersson, D., Akrap, N., Svec, D., Godfrey, T. E., Kubista, M., Landberg, G. and Ståhlberg, A. (2015) 'Properties of targeted preamplification in DNA and cDNA quantification', *Expert Review of Molecular Diagnostics*, 15(8), pp. 1085–1100. doi: 10.1586/14737159.2015.1057124.

Androvic, P., Kirdajova, D. B., Tureckova, J., Zucha, D., Rohlova, E., Abaffy, P., Kriska, J., Anderova, M., Kubista, M. and Valihrach, L. (2019) 'Decoding the transcriptional response to ischemic stroke in young and aged mouse brain', *bioRxiv*, p. 769331. doi: 10.1101/769331.

Bagnoli, J. W., Ziegenhain, C., Janjic, A., Wange, L. E., Vieth, B., Parekh, S., Geuder, J., Hellmann, I. and Enard, W. (2018) 'Sensitive and powerful single-cell RNA sequencing using mcSCRB-seq.', *Nature communications*, 9(1), p. 2937. doi: 10.1038/s41467-018-05347-6.

Baranauskas, A., Paliksa, S., Alzbutas, G., Vaitkevicius, M., Lubiene, J., Letukiene, V., Burinskas, S., Sasnauskas, G. and Skirgaila, R. (2012) 'Generation and characterization of new highly thermostable and processive M-MuLV reverse transcriptase variants', *Protein Engineering, Design and Selection*, 25(10), pp. 657–668. doi: 10.1093/protein/gzs034.

Batiuk, M. Y., Martirosyan, A., Wahis, J., de Vin, F., Marneffe, C., Kusserow, C., Koeppen, J., Viana, J. F., Oliveira, J. F., Voet, T., *et al.* (2020) 'Identification of region-specific astrocyte subtypes at single cell resolution', *Nature Communications*, 11(1), p. 1220. doi: 10.1038/s41467-019-14198-8.

Bengtsson, M., Hemberg, M., Rorsman, P. and Ståhlberg, A. (2008) 'Quantification of mRNA in single cells and modelling of RT-qPCR induced noise', *BMC Molecular Biology*, 9(1), p. 63. doi: 10.1186/1471-2199-9-63.

Bergkvist, A., Rusnakova, V., Sindelka, R., Garda, J. M. A., Sjögreen, B., Lindh, D., Forootan, A. and Kubista, M. (2010) 'Gene expression profiling - Clusters of possibilities', *Methods*, 50(4), pp. 323–335. doi: 10.1016/j.ymeth.2010.01.009.

Van Den Brink, S. C., Sage, F., Vértesy, Á., Spanjaard, B., Peterson-Maduro, J., Baron, C. S., Robin, C. and Van Oudenaarden, A. (2017) 'Single-cell sequencing reveals dissociation-induced gene expression in tissue subpopulations', *Nature Methods*, 14(10), pp. 935–936. doi: 10.1038/nmeth.4437.

Bustin, S. A., Benes, V., Garson, J. A., Hellemans, J., Huggett, J., Kubista, M., Mueller, R., Nolan, T., Pfaffl, M. W., Shipley, G. L., *et al.* (2009) 'The MIQE guidelines: Minimum information for publication

of quantitative real-time PCR experiments', *Clinical Chemistry*, 55(4), pp. 611–622. doi: 10.1373/clinchem.2008.112797.

Bustin, S. A. and Nolan, T. (2004) 'Pitfalls of quantitative real- time reverse-transcription polymerase chain reaction', *Journal of Biomolecular Techniques*, 15(3), pp. 155–166. doi: 15/3/155 [pii].

Bustin, S., Dhillon, H. S., Kirvell, S., Greenwood, C., Parker, M., Shipley, G. L. and Nolan, T. (2015) 'Variability of the reverse transcription step: Practical implications', *Clinical Chemistry*, 61(1), pp. 202–212. doi: 10.1373/clinchem.2014.230615.

Chen, S., Lake, B. B. and Zhang, K. (2019) 'High-throughput sequencing of the transcriptome and chromatin accessibility in the same cell', *Nature Biotechnology*, pp. 1452–1457. doi: 10.1038/s41587-019-0290-0.

Chubb, J. R., Trcek, T., Shenoy, S. M. and Singer, R. H. (2006) 'Transcriptional pulsing of a developmental gene.', *Current biology : CB*, 16(10), pp. 1018–25. doi: 10.1016/j.cub.2006.03.092.

Chung, W., Eum, H. H., Lee, H. O., Lee, K. M., Lee, H. B., Kim, K. T., Ryu, H. S., Kim, S., Lee, J. E., Park, Y. H., *et al.* (2017) 'Single-cell RNA-seq enables comprehensive tumour and immune cell profiling in primary breast cancer', *Nature Communications*, 8(1), pp. 1–12. doi: 10.1038/ncomms15081.

Darmanis, S., Gallant, C. J., Marinescu, V. D., Niklasson, M., Segerman, A., Flamourakis, G., Fredriksson, S., Assarsson, E., Lundberg, M., Nelander, S., *et al.* (2016) 'Simultaneous Multiplexed Measurement of RNA and Proteins in Single Cells', *Cell Reports*, 14(2), pp. 380–389. doi: 10.1016/j.celrep.2015.12.021.

Dzamba, D., Valihrach, L., Kubista, M. and Anderova, M. (2016) 'The correlation between expression profiles measured in single cells and in traditional bulk samples', *Scientific Reports*, 6(1), p. 37022. doi: 10.1038/srep37022.

External RNA Controls Consortium (2005) 'Proposed methods for testing and selecting the ERCC external RNA controls.', *BMC genomics*, 6(1), p. 150. doi: 10.1186/1471-2164-6-150.

Forootan, A., Sjöback, R., Björkman, J., Sjögreen, B., Linz, L. and Kubista, M. (2017) 'Methods to determine limit of detection and limit of quantification in quantitative real-time PCR (qPCR)', *Biomolecular Detection and Quantification*, 12, pp. 1–6. doi: 10.1016/J.BDQ.2017.04.001.

Gierahn, T. M., Wadsworth, M. H., Hughes, T. K., Bryson, B. D., Butler, A., Satija, R., Fortune, S., Christopher Love, J. and Shalek, A. K. (2017) 'Seq-Well: Portable, low-cost rna sequencing of single cells at high throughput', *Nature Methods*, 14(4), pp. 395–398. doi: 10.1038/nmeth.4179.

Hardiman, O., Van Den Berg, L. H. and Kiernan, M. C. (2011) 'Clinical diagnosis and management of amyotrophic lateral sclerosis', *Nature Reviews Neurology*, pp. 639–649. doi: 10.1038/nrneurol.2011.153.

Hashimshony, T., Senderovich, N., Avital, G., Klochendler, A., de Leeuw, Y., Anavy, L., Gennert, D., Li, S., Livak, K. J., Rozenblatt-Rosen, O., *et al.* (2016) 'CEL-Seq2: Sensitive highly-multiplexed single-cell RNA-Seq', *Genome Biology*, 17(1), pp. 1–7. doi: 10.1186/s13059-016-0938-8.

Higuchi, R., Fockler, C., Dollinger, G. and Watson, R. (1993) 'Kinetic PCR analysis: Real-time monitoring of DNA amplification reactions', *Bio/Technology*, 11(9), pp. 1026–1030. doi: 10.1038/nbt0993-1026.

Hodne, K. and Weltzien, F.-A. (2015) 'Single-Cell Isolation and Gene Analysis: Pitfalls and Possibilities', *International Journal of Molecular Sciences*, 16(11), pp. 26832–26849. doi: 10.3390/ijms161125996.

Howland, D. S., Liu, J., She, Y., Goad, B., Maragakis, N. J., Kim, B., Erickson, J., Kulik, J., DeVito, L., Psaltis, G., *et al.* (2002) 'Focal loss of the glutamate transporter EAAT2 in a transgenic rat model of SOD1 mutant-mediated amyotrophic lateral sclerosis (ALS)', *Proceedings of the National Academy of Sciences of the United States of America*, 99(3), pp. 1604–1609. doi: 10.1073/pnas.032539299.

Huggett, J. F., Novak, T., Garson, J. A., Green, C., Morris-Jones, S. D., Miller, R. F. and Zumla, A. (2008) 'Differential susceptibility of PCR reactions to inhibitors: An important and unrecognised phenomenon', *BMC Research Notes*, 1, pp. 1–9. doi: 10.1186/1756-0500-1-70.

Iliff, J. J., Chen, M. J., Plog, B. A., Zeppenfeld, D. M., Soltero, M., Yang, L., Singh, I., Deane, R. and Nedergaard, M. (2014) 'Impairment of glymphatic pathway function promotes tau pathology after traumatic brain injury', *Journal of Neuroscience*, 34(49), pp. 16180–16193. doi: 10.1523/JNEUROSCI.3020-14.2014.

Ji, X., Wang, M., Li, L., Chen, F., Zhang, Y., Li, Q. and Zhou, J. (2017) 'The Impact of Repeated Freeze-Thaw Cycles on the Quality of Biomolecules in Four Different Tissues', *Biopreservation and Biobanking*, 15(5), pp. 475–483. doi: 10.1089/bio.2017.0064.

Kelley, K. W., Nakao-Inoue, H., Molofsky, A. V. and Oldham, M. C. (2018) 'Variation among intact tissue samples reveals the core transcriptional features of human CNS cell classes', *Nature Neuroscience*, 21(9), pp. 1171–1184. doi: 10.1038/s41593-018-0216-z.

Kiernan, M. C., Vucic, S., Cheah, B. C., Turner, M. R., Eisen, A., Hardiman, O., Burrell, J. R. and Zoing, M. C. (2011) 'Amyotrophic lateral sclerosis', in *The Lancet*. Elsevier, pp. 942–955. doi: 10.1016/S0140-6736(10)61156-7.

Kitchen, P., Salman, M. M., Halsey, A. M., Clarke-Bland, C., MacDonald, J. A., Ishida, H., Vogel, H. J., Almutiri, S., Logan, A., Kreida, S., *et al.* (2020) 'Targeting Aquaporin-4 Subcellular Localization to Treat Central Nervous System Edema', *Cell*, 181(4), pp. 784-799.e19. doi: 10.1016/j.cell.2020.03.037.

Kleinberger, G., Yamanishi, Y., Suárez-Calvet, M., Czirr, E., Lohmann, E., Cuyvers, E., Struyfs, H., Pettkus, N., Wenninger-Weinzierl, A., Mazaheri, F., *et al.* (2014) 'TREM2 mutations implicated in neurodegeneration impair cell surface transport and phagocytosis', *Science Translational Medicine*, 6(243), pp. 243ra86-243ra86. doi: 10.1126/scitranslmed.3009093.

Kolodziejczyk, A. A., Kim, J. K., Svensson, V., Marioni, J. C. and Teichmann, S. A. (2015) 'The Technology and Biology of Single-Cell RNA Sequencing', *Molecular Cell*, 58(4), pp. 610–620. doi: 10.1016/j.molcel.2015.04.005.

Konishi, A., Yasukawa, K. and Inouye, K. (2012) 'Improving the thermal stability of avian myeloblastosis virus reverse transcriptase α-subunit by site-directed mutagenesis', *Biotechnology Letters*, 34(7), pp. 1209–1215. doi: 10.1007/s10529-012-0904-9.

Korenková, V., Scott, J., Novosadová, V., Jindřichová, M., Langerová, L., Švec, D., Šídová, M. and Sjöback, R. (2015) 'Pre-amplification in the context of high-throughput qPCR gene expression experiment', *BMC Molecular Biology*, 16(1), p. 5. doi: 10.1186/s12867-015-0033-9.

Kroneis, T., Jonasson, E., Andersson, D., Dolatabadi, S. and Ståhlberg, A. (2017) 'Global preamplification simplifies targeted mRNA quantification', *Scientific Reports*, 7(1), p. 45219. doi: 10.1038/srep45219.

Kubista, M., Dreyer-Lamm, J. and Ståhlberg, A. (2018) 'The secrets of the cell', *Molecular Aspects of Medicine*, pp. 1–4. doi: 10.1016/j.mam.2017.08.004.

Levesque-Sergerie, J.-P., Duquette, M., Thibault, C., Delbecchi, L. and Bissonnette, N. (2007) 'Detection

limits of several commercial reverse transcriptase enzymes: impact on the low- and high-abundance transcript levels assessed by quantitative RT-PCR.', *BMC molecular biology*, 8, p. 93. doi: 10.1186/1471-2199-8-93.

Li, H., Gyllensten, U. B., Cui, X., Saiki, R. K., Erlich, H. A. and Arnheim, N. (1988) 'Amplification and analysis of DNA sequences in single human sperm and diploid cells', *Nature*, 335(6189), pp. 414–417. doi: 10.1038/335414a0.

Liddelow, S. A., Guttenplan, K. A., Clarke, L. E., Bennett, F. C., Bohlen, C. J., Schirmer, L., Bennett, M. L., Münch, A. E., Chung, W. S., Peterson, T. C., *et al.* (2017) 'Neurotoxic reactive astrocytes are induced by activated microglia', *Nature*, 541(7638), pp. 481–487. doi: 10.1038/nature21029.

Lindén, J., Ranta, J. and Pohjanvirta, R. (2012) 'Bayesian modeling of reproducibility and robustness of RNA reverse transcription and quantitative real-time polymerase chain reaction', *Analytical Biochemistry*, 428(1), pp. 81–91. doi: 10.1016/j.ab.2012.06.010.

Lippi, G., Chance, J. J., Church, S., Dazzi, P., Fontana, R., Giavarina, D., Grankvist, K., Huisman, W., Kouri, T., Palicka, V., *et al.* (2011) 'Preanalytical quality improvement: From dream to reality', *Clinical Chemistry and Laboratory Medicine*, pp. 1113–1126. doi: 10.1515/CCLM.2011.600.

Livak, K. J., Wills, Q. F., Tipping, A. J., Datta, K., Mittal, R., Goldson, A. J., Sexton, D. W. and Holmes, C. C. (2013) 'Methods for qPCR gene expression profiling applied to 1440 lymphoblastoid single cells', *Methods*, 59(1), pp. 71–79. doi: 10.1016/J.YMETH.2012.10.004.

Macosko, E. Z., Basu, A., Satija, R., Nemesh, J., Shekhar, K., Goldman, M., Tirosh, I., Bialas, A. R., Kamitaki, N., Martersteck, E. M., *et al.* (2015) 'Highly Parallel Genome-wide Expression Profiling of Individual Cells Using Nanoliter Droplets.', *Cell*, 161(5), pp. 1202–1214. doi: 10.1016/j.cell.2015.05.002.

Marinov, G. K., Williams, B. A., McCue, K., Schroth, G. P., Gertz, J., Myers, R. M. and Wold, B. J. (2014) 'From single-cell to cell-pool transcriptomes: Stochasticity in gene expression and RNA splicing', *Genome Research*, 24(3), pp. 496–510. doi: 10.1101/gr.161034.113.

Mayer, C. L., Huber, B. R. and Peskind, E. (2013) 'Traumatic Brain Injury, Neuroinflammation, and Post-Traumatic Headaches', *Headache: The Journal of Head and Face Pain*, 53(9), p. n/a-n/a. doi: 10.1111/head.12173.

Micke, P., Ohshima, M., Tahmasebpoor, S., Ren, Z. P., Östman, A., Pontén, F. and Botling, J. (2006) 'Biobanking of fresh frozen tissue: RNA is stable in nonfixed surgical specimens', *Laboratory Investigation*, 86(2), pp. 202–211. doi: 10.1038/labinvest.3700372.

Millington, A. L., Houskeeper, J. A., Quackenbush, J. F., Trauba, J. M. and Wittwer, C. T. (2019) 'The kinetic requirements of extreme qPCR', *Biomolecular Detection and Quantification*, 17, p. 100081. doi: 10.1016/j.bdq.2019.100081.

Miranda, J. A. and Steward, G. F. (2017) 'Variables influencing the efficiency and interpretation of reverse transcription quantitative PCR (RT-qPCR): An empirical study using Bacteriophage MS2.', *Journal of virological methods*, 241, pp. 1–10. doi: 10.1016/j.jviromet.2016.12.002.

Mohr, S., Ghanem, E., Smith, W., Sheeter, D., Qin, Y., King, O., Polioudakis, D., Iyer, V. R., Hunicke-Smith, S., Swamy, S., *et al.* (2013) 'Thermostable group II intron reverse transcriptase fusion proteins and their use in cDNA synthesis and next-generation RNA sequencing', *Rna*, 19(7), pp. 958–970. doi: 10.1261/rna.039743.113.

Mullis, K., Faloona, F., Scharf, S., Saiki, R., Horn, G. and Erlich, H. (1986) 'Specific enzymatic

amplification of DNA in vitro: The polymerase chain reaction', *Cold Spring Harbor Symposia on Quantitative Biology*, 51(1), pp. 263–273. doi: 10.1101/sqb.1986.051.01.032.

Newman, A. M., Steen, C. B., Liu, C. L., Gentles, A. J., Chaudhuri, A. A., Scherer, F., Khodadoust, M. S., Esfahani, M. S., Luca, B. A., Steiner, D., *et al.* (2019) 'Determining cell type abundance and expression from bulk tissues with digital cytometry', *Nature Biotechnology*. doi: 10.1038/s41587-019-0114-2.

Ng, A. S. L., Rademakers, R. and Miller, B. L. (2015) 'Frontotemporal dementia: a bridge between dementia and neuromuscular disease', *Annals of the New York Academy of Sciences*, 1338(1), pp. 71–93. doi: 10.1111/nyas.12638.

Nolan, T., Hands, R. E. and Bustin, S. A. (2006) 'Quantification of mRNA using real-time RT-PCR', *Nature Protocols*, 1(3), pp. 1559–1582. doi: 10.1038/nprot.2006.236.

Okello, J. B. A., Rodriguez, L., Poinar, D., Bos, K., Okwi, A. L., Bimenya, G. S., Sewankambo, N. K., Henry, K. R., Kuch, M. and Poinar, H. N. (2010) 'Quantitative assessment of the sensitivity of various commercial reverse transcriptases based on armored HIV RNA.', *PloS one*, 5(11), p. e13931. doi: 10.1371/journal.pone.0013931.

Papadopoulos, M. C. and Verkman, A. S. (2013) 'Aquaporin water channels in the nervous system', *Nature Reviews Neuroscience*, pp. 265–277. doi: 10.1038/nrn3468.

Picelli, S., Faridani, O. R., Björklund, A. K., Winberg, G., Sagasser, S. and Sandberg, R. (2014) 'Full-length RNA-seq from single cells using Smart-seq2.', *Nature protocols*, 9(1), pp. 171–81. doi: 10.1038/nprot.2014.006.

Pivonkova, H., Hermanova, Z., Kirdajova, D., Awadova, T., Malinsky, J., Valihrach, L., Zucha, D., Kubista, M., Galisova, A., Jirak, D., *et al.* (2018) 'The Contribution of TRPV4 Channels to Astrocyte Volume Regulation and Brain Edema Formation', *Neuroscience*, 394, pp. 127–143. doi: 10.1016/j.neuroscience.2018.10.028.

Podgorny, O. V (2013) 'Live cell isolation by laser microdissection with gravity transfer.', *Journal of biomedical optics*, 18(5), p. 55002. doi: 10.1117/1.JBO.18.5.055002.

Radford, R. A., Morsch, M., Rayner, S. L., Cole, N. J., Pountney, D. L. and Chung, R. S. (2015) 'The established and emerging roles of astrocytes and microglia in amyotrophic lateral sclerosis and frontotemporal dementia', *Frontiers in Cellular Neuroscience*, p. 414. doi: 10.3389/fncel.2015.00414.

Raj, A., Peskin, C. S., Tranchina, D., Vargas, D. Y. and Tyagi, S. (2006) 'Stochastic mRNA Synthesis in Mammalian Cells', *PLoS Biology*. Edited by U. Schibler, 4(10), p. e309. doi: 10.1371/journal.pbio.0040309.

Riedmaier, I. and Pfaffl, M. W. (2013) 'Transcriptional biomarkers - High throughput screening, quantitative verification, and bioinformatical validation methods', *Methods*, 59(1), pp. 3–9. doi: 10.1016/j.ymeth.2012.08.012.

Ringnér, M. (2008) 'What is principal component analysis?', *Nature biotechnology*, 26(3), pp. 303–4. doi: 10.1038/nbt0308-303.

Rusnakova, V., Honsa, P., Dzamba, D., Ståhlberg, A., Kubista, M. and Anderova, M. (2013) 'Heterogeneity of astrocytes: from development to injury - single cell gene expression.', *PloS one*, 8(8), p. e69734. doi: 10.1371/journal.pone.0069734.

Saliba, A. E., Westermann, A. J., Gorski, S. A. and Vogel, J. (2014) 'Single-cell RNA-seq: Advances and

future challenges', *Nucleic Acids Research*, 42(14), pp. 8845–8860. doi: 10.1093/nar/gku555.

Schwaber, J., Andersen, S. and Nielsen, L. (2019) 'Shedding light: The importance of reverse transcription efficiency standards in data interpretation', *Biomolecular Detection and Quantification*, 17(December 2018), p. 100077. doi: 10.1016/j.bdq.2018.12.002.

Sieber, M. W., Recknagel, P., Glaser, F., Witte, O. W., Bauer, M., Claus, R. A. and Frahm, C. (2010) 'Substantial performance discrepancies among commercially available kits for reverse transcription quantitative polymerase chain reaction: A systematic comparative investigator-driven approach', *Analytical Biochemistry*, 401(2), pp. 303–311. doi: 10.1016/j.ab.2010.03.007.

Ståhlberg, A. (2004) 'Comparison of Reverse Transcriptases in Gene Expression Analysis', *Clinical Chemistry*, 50(9), pp. 1678–1680. doi: 10.1373/clinchem.2004.035469.

Ståhlberg, A. and Bengtsson, M. (2010) 'Single-cell gene expression profiling using reverse transcription quantitative real-time PCR', *Methods*, 50(4), pp. 282–288. doi: 10.1016/j.ymeth.2010.01.002.

Ståhlberg, A., Håkansson, J., Xian, X., Semb, H. and Kubista, M. (2004) 'Properties of the Reverse Transcription Reaction in mRNA Quantification', *Clinical Chemistry*, 50(3), pp. 509–515. doi: 10.1373/clinchem.2003.026161.

Ståhlberg, A. and Kubista, M. (2014) 'The workflow of single-cell expression profiling using quantitative real-time PCR', *Expert Review of Molecular Diagnostics*, 14(3), pp. 323–331. doi: 10.1586/14737159.2014.901154.

Ståhlberg, A. and Kubista, M. (2018) 'Technical aspects and recommendations for single-cell qPCR', *Molecular Aspects of Medicine*, 59, pp. 28–35. doi: 10.1016/j.mam.2017.07.004.

Ståhlberg, A., Rusnakova, V., Forootan, A., Anderova, M. and Kubista, M. (2013) 'RT-qPCR work-flow for single-cell data analysis', 59, pp. 80–88. doi: 10.1016/j.ymeth.2012.09.007.

Ståhlberg, A., Rusnakova, V. and Kubista, M. (2013) 'The added value of single-cell gene expression profiling', *Briefings in Functional Genomics*, 12(2), pp. 81–89. doi: 10.1093/bfgp/elt001.

Ståhlberg, A., Thomsen, C., Ruff, D. and Åman, P. (2012) 'Quantitative PCR Analysis of DNA, RNAs, and Proteins in the Same Single Cell', *Clinical Chemistry*, 58(12), pp. 1682–1691. doi: 10.1373/clinchem.2012.191445.

Svec, D., Andersson, D., Pekny, M., Sjöback, R., Kubista, M. and Ståhlberg, A. (2013) 'Direct Cell Lysis for Single-Cell Gene Expression Profiling', *Frontiers in Oncology*, 3(November), pp. 1–11. doi: 10.3389/fonc.2013.00274.

Svec, D., Tichopad, A., Novosadova, V., Pfaffl, M. W. and Kubista, M. (2015) 'How good is a PCR efficiency estimate: Recommendations for precise and robust qPCR efficiency assessments', *Biomolecular Detection and Quantification*, 3, pp. 9–16. doi: 10.1016/j.bdq.2015.01.005.

Svensson, V., Natarajan, K. N., Ly, L.-H., Miragaia, R. J., Labalette, C., Macaulay, I. C., Cvejic, A. and Teichmann, S. A. (2017) 'Power analysis of single-cell RNA-sequencing experiments.', *Nature methods*, 14(4), pp. 381–387. doi: 10.1038/nmeth.4220.

The Spidia Project (no date) *Spidia*. Available at: https://www.spidia.eu/.

Tichopad, A., Kitchen, R., Riedmaier, I., Becker, C., Ståhlberg, A. and Kubista, M. (2009) 'Design and optimization of reverse-transcription quantitative PCR experiments', *Clinical Chemistry*, 55(10), pp.

1816–1823. doi: 10.1373/clinchem.2009.126201.

Valihrach, L., Androvic, P. and Kubista, M. (2018) 'Platforms for Single-Cell Collection and Analysis', *International Journal of Molecular Sciences*, 19(3), p. 807. doi: 10.3390/ijms19030807.

Walch, A., Specht, K., Smida, J., Aubele, M., Zitzelsberger, H., Höfler, H. and Werner, M. (2001) 'Tissue microdissection techniques in quantitative genome and gene expression analyses', *Histochemistry and Cell Biology*, 115(4), pp. 269–276. doi: 10.1007/s004180100253.

Wang, Yaogeng, Zheng, H., Chen, J., Zhong, X., Wang, Yu, Wang, Z. and Wang, Yanping (2015) 'The Impact of Different Preservation Conditions and Freezing-Thawing Cycles on Quality of RNA, DNA, and Proteins in Cancer Tissue', *Biopreservation and Biobanking*, 13(5), pp. 335–347. doi: 10.1089/bio.2015.0029.

Worthington Tissue Dissociation Guide (no date). Available at: http://www.worthington-biochem.com/tissuedissociation/default.html (Accessed: 1 May 2020).

Yamanaka, K., Chun, S. J., Boillee, S., Fujimori-Tonou, N., Yamashita, H., Gutmann, D. H., Takahashi, R., Misawa, H. and Cleveland, D. W. (2008) 'Astrocytes as determinants of disease progression in inherited amyotrophic lateral sclerosis', *Nature Neuroscience*, 11(3), pp. 251–253. doi: 10.1038/nn2047.

Yeung, K. Y. (2008) 'Principal component analysis for clustering gene expression data', *Bioinformatics (Oxford, England)*, 21(13), pp. 3009–3016. doi: 10.1093/bioinformatics/bti465.Differential.

Zeng, J., Mohammadreza, A., Gao, W., Merza, S., Smith, D., Kelbauskas, L. and Meldrum, D. R. (2014) 'A minimally invasive method for retrieving single adherent cells of different types from cultures', *Scientific Reports*, 4(1), pp. 1–10. doi: 10.1038/srep05424.

Zheng, G. X. Y., Terry, J. M., Belgrader, P., Ryvkin, P., Bent, Z. W., Wilson, R., Ziraldo, S. B., Wheeler, T. D., McDermott, G. P., Zhu, J., *et al.* (2017) 'Massively parallel digital transcriptional profiling of single cells', *Nature Communications*, 8(1), pp. 1–12. doi: 10.1038/ncomms14049.

Zhu, C., Yu, M., Huang, H., Juric, I., Abnousi, A., Hu, R., Lucero, J., Behrens, M. M., Hu, M. and Ren, B. (2019) 'An ultra high-throughput method for single-cell joint analysis of open chromatin and transcriptome', *Nature Structural and Molecular Biology*, 26(11), pp. 1063–1070. doi: 10.1038/s41594-019-0323-x.

Zhu, S., Qing, T., Zheng, Y. and Shi, L. (2017) 'Advances in single-cell RNA sequencing and its applications in cancer research', *Oncotarget*, 8(32), pp. 53763–53779. doi: 10.18632/oncotarget.17893.

Ziegenhain, C., Vieth, B., Parekh, S., Reinius, B., Guillaumet-Adkins, A., Smets, M., Leonhardt, H., Heyn, H., Hellmann, I. and Enard, W. (2017) 'Comparative Analysis of Single-Cell RNA Sequencing Methods', *Molecular Cell*, 65(4), pp. 631-643.e4. doi: 10.1016/j.molcel.2017.01.023.

Zucha, D., Androvic, P., Kubista, M. and Valihrach, L. (2020) 'Performance Comparison of Reverse Transcriptases for Single-Cell Studies', *Clinical Chemistry*, 66(1), pp. 217–228. doi: 10.1373/clinchem.2019.307835.

10 Attachments

Attachment 1 - Extended information on material quality, protocols and data sets